NASA Technical Paper 3411

Static Performance Investigation of a Skewed-Throat Multiaxis Thrust-Vectoring Nozzle Concept

David J. Wing

April 1994

NASA Technical Paper 3411

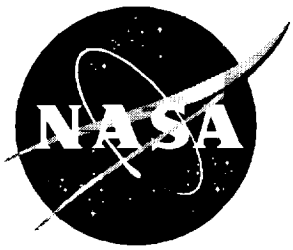

Static Performance Investigation of a Skewed-Throat Multiaxis Thrust-Vectoring Nozzle Concept

David J. Wing
Langley Research Center • Hampton, Virginia

National Aeronautics and Space Administration
Langley Research Center • Hampton, Virginia 23681-0001

April 1994

Abstract

The static performance of a jet exhaust nozzle which achieves multiaxis thrust vectoring by physically skewing the geometric throat has been characterized in the static test facility of the 16-Foot Transonic Tunnel at NASA Langley Research Center. The nozzle has an asymmetric internal geometry defined by four surfaces: a convergent-divergent upper surface with its ridge perpendicular to the nozzle centerline, a convergent-divergent lower surface with its ridge skewed relative to the nozzle centerline, an outwardly deflected sidewall, and a straight sidewall. The primary goal of the concept is to provide efficient yaw thrust vectoring by forcing the sonic plane (nozzle throat) to form at a yaw angle defined by the skewed ridge of the lower surface contour. A secondary goal is to provide multiaxis thrust vectoring by combining the skewed-throat yaw-vectoring concept with upper and lower pitch flap deflections. The geometric parameters varied in this investigation included lower surface ridge skew angle, nozzle expansion ratio (divergence angle), aspect ratio, pitch flap deflection angle, and sidewall deflection angle. Nozzle pressure ratio was varied from 2 to a high of 11.5 for some configurations. The results of the investigation indicate that efficient, substantial multiaxis thrust vectoring was achieved by the skewed-throat nozzle concept. However, certain control surface deflections destabilized the internal flow field, which resulted in substantial shifts in the position and orientation of the sonic plane and had an adverse effect on thrust-vectoring and weight flow characteristics. By increasing the expansion ratio, the location of the sonic plane was stabilized. The asymmetric design resulted in interdependent pitch and yaw thrust vectoring as well as nonzero thrust-vector angles with undeflected control surfaces. By skewing the ridges of both the upper and lower surface contours, the interdependency between pitch and yaw thrust vectoring may be eliminated and the location of the sonic plane may be further stabilized.

Introduction

To maintain air superiority, future fighter airplanes will most likely incorporate thrust-vectoring capability into their nozzle designs. Studies have shown the following advantages of thrust vectoring, particularly, multiaxis thrust vectoring on fighter airplane performance: increased maneuverability (refs. 1-5), reduced drag and weight (refs. 4 and 6), and improved survivability (refs. 2, 4, and 7). Thrust vectoring will also permit airplanes to operate in flight regimes where conventional airplanes cannot operate: at the low speeds which occur during vertical or short takeoffs and landings (refs. 2, 3, and 7) and at the high angles of attack which occur during supermaneuvers or poststall maneuvers (refs. 1, 4, and 5).

To provide thrust-vectoring capability with minimal adverse impact on airplane performance, many thrust-vectoring concepts have been considered. (See refs. 8–22.) Early thrust-vectoring nozzle concepts incorporated single-axis thrust vectoring usually in the pitch plane. More recent nozzle studies have expanded the scope to include development of multiaxis (pitch and yaw) thrust-vectoring capability. Both axisymmetric and rectangular (two-dimensional (2D)) nozzles have been the focus of thrust-vectoring research; more emphasis has been placed on the latter because the flat surfaces of a rectangular nozzle are more easily actuated.

Exhaust nozzles of current design maximize thrust by accelerating the exhaust flow to supersonic speeds with a convergent-divergent (CD) internal geometry. However, achieving vectored thrust by deflecting supersonic flow results in significant losses attributable to oblique shocks. A more efficient method turns the exhaust flow at the subsonic condition upstream of the minimum geometric flow area (geometric throat) of the nozzle. Research of 2D-CD nozzles has shown that when the divergent surfaces of the nozzle were deflected in the direction of desired vectored thrust, the sonic plane deflected in the same

direction, which indicated that most of the flow directional change occurred subsonically. Oblique shock losses were eliminated and efficient pitch thrust vectoring was achieved (refs. 8 10).

A vectoring concept has been proposed to take advantage of the efficiency of subsonic flow directional change in producing yaw thrust vectoring. The design goal is to alter the internal geometry of a 2D-CD nozzle so that the sonic plane would be pivoted in the yaw direction relative to the nozzle primary centerline. By designing the lower convergent-divergent contour of the nozzle with the ridge skewed in relation to the primary nozzle centerline, a skewed minimum-area flow plane (throat) would result. With sufficient sidewall ventilation, the exhaust should exit the nozzle perpendicular to the skewed throat and produce yaw thrust vectoring. Because the flow is turned before it accelerates to supersonic speed, the vectoring should be efficient; significant vector angles should be achieved with minimal losses in resultant thrust.

The nozzle concept installed on a generic fighter airplane is shown in figure 1. The sketch shows the nozzle in a twin-engined arrangement with oppositely oriented nozzles which cancel any inherent yaw thrust vectoring during unvectored cruise operation. Minimum vectoring for each nozzle is achieved with the sidewalls closed as shown on the right nozzle; some vectoring remains because of the asymmetric geometry of the nozzle. When yaw thrust vectoring is desired, the sidewall is deflected outward as shown on the left nozzle, which ventilates the exhaust passage and permits the flow to expand at an angle relative to the primary nozzle centerline. The amount of vectoring is controlled by varying the sidewall deflection angle.

Although the sketch in figure 1 shows a fixed geometry except for the sidewalls, the concept could include a pitch-vectoring capability as well. Deflection of the upper and lower divergent surfaces (flaps) up or down in tandem would produce pitch vectoring in a manner similar to that of a classical 2D-CD nozzle. Some pitch vectoring should be incorporated in the design to compensate for residual pitching moments caused by the nozzle vertical asymmetry.

The skewed-throat nozzle concept originated as a convertible design in which a nozzle with classical 2D-CD cruise geometry could be transformed into the skewed-throat geometry for yaw vectoring. This conversion is facilitated by placing a hinge along the skewed crest of the lower convergent-divergent surface. By deflecting the entire lower flap upward about a lateral upstream hinge and simultaneously deflecting the aft portion of the flap downward about the skewed hinge, the nozzle converts to the skewed-throat geometry described above. A nozzle with this convertible design combines the advantages of efficient yaw-vectoring and cruise performance. The disadvantages of the nozzle include increased weight and complexity because of the extra hinges and actuators required for in-flight transformation.

A static test of internal performance was conducted to assess the thrust-vectoring ability and to define the flow characteristics of a skewed-throat nozzle. The test was conducted in the static test facility of the Langley 16-Foot Transonic Tunnel using high-pressure, room temperature air as the test medium. Parameters obtained from measured test data included axial and resultant gross thrust efficiencies, nozzle discharge coefficient, and surface static pressure distributions on the upper and lower flaps and sidewalls. Parameters chosen as geometric variables were hinge line skew angle, nozzle expansion ratio (upper and lower flap divergence angle), sidewall deflection angle, upper and lower flap deflection angle (pitch vectoring), and nozzle aspect ratio. However, a complete matrix of all parameters was not tested. The nozzle pressure ratio of the simulated exhaust flow was varied from 2 to a high of 11.5 for some configurations.

Acknowledgments

The research presented in this report is the result of the cooperative effort of the Flight Dynamics Lab of the United States Air Force (Wright-Patterson Air Force Base); Pratt & Whitney, Government Engines & Space Propulsion Division of United Technologies Corporation; the McDonnell Aircraft Company, subsidiary of McDonnell Douglas Corporation; and the NASA Langley Research Center. Program funding was provided by the United States Air Force. The design and development of the nozzle concept and test hardware were accomplished by Pratt & Whitney with the support of the McDonnell Aircraft Company. The test was conducted by the staff of the Propulsion Aerodynamics Branch at the NASA Langley Research Center.

Symbols

A	length of upper flap from hinge to trailing edge, in. (fig. 4(a))
A_t	nozzle throat area, in^2
B	width of upper flap, in. (fig. 4(a))
C	angle between undeflected upper flap and nozzle axis, deg (fig. 4(a))

D linear vertical dimension from upper surface of transition section to lowest point on undeflected upper flap, in. (fig. 4(a))

E linear vertical dimension from lower surface of transition section to lower flap lateral hinge, in. (fig. 4(b))

F angle between nozzle axis and lower flap upstream of skewed hinge line, deg (fig. 4(b))

F_A measured axial thrust component, lb

F_i ideal isentropic thrust, $w_p\sqrt{\frac{R_j T_{t,j}}{g^2}\,\frac{2\gamma}{\gamma-1}\left[1-\left(\frac{p_a}{p_{t,j}}\right)^{(\gamma-1)/\gamma}\right]}$, lb

F_N measured normal thrust component, lb

F_r resultant gross thrust, $\sqrt{F_A^2+F_N^2+F_S^2}$, lb

F_S measured side thrust component, lb

G angle between nozzle axis and lower flap downstream of skewed hinge line, deg (fig. 4(b))

g gravitational acceleration, 32.174 ft/sec^2

J linear dimension measured along left side of lower flap from lateral hinge to skewed hinge line, in. (fig. 4(b))

K width of lower flap, in. (fig. 4(b))

L length of undeflected lower flap from lateral hinge to trailing edge, measured along nozzle axis, in. (fig. 4(b))

M length of undeflected sidewall from transition section to trailing edge, in. (fig. 4(c))

N height of undeflected sidewall, in. (fig. 4(c))

NPR nozzle pressure ratio, $\frac{p_{t,j}}{p_a}$

P length of deflected sidewall, in. (fig. 4(c))

p internal static pressure, psi

p_a atmospheric pressure, psi

$p_{t,j}$ jet total pressure, psi

Q convergence half-angle in horizontal plane of transition section, deg (fig. 4(d))

R width of transition section at nozzle connect station, in. (fig. 4(d))

R_j gas constant for air, (γ = 1.3997), 1716 ft^2/sec^2-°R

$T_{t,j}$ jet total temperature, °R

w_i ideal weight flow, $A_t p_{t,j}\left(\frac{2}{\gamma+1}\right)^{\frac{\gamma+1}{2(\gamma-1)}}\sqrt{\frac{\gamma g^2}{T_{t,j}R_j}}$, lb/sec

w_p measured air weight flow, lb/sec

x distance downstream from lateral hinge along nozzle axis, in. (figs. 4(a) and 4(b))

y lateral distance from flap centerline, in. (figs. 4(a) and 4(b))

δ_p resultant pitch thrust-vector angle, $\tan^{-1}\frac{F_N}{F_A}$, deg

$\delta_{v,p}$ pitch flap deflection angle, positive deflection downward, deg

$\delta_{v,s}$ deflection angle of left sidewall, positive deflection outward, deg

δ_y resultant yaw thrust-vector angle, $\tan^{-1}\frac{F_S}{F_A}$, deg

γ ratio of specific heats, 1.3997 for air

θ_{skew} angle between nozzle lateral axis and skewed hinge line, measured in plane of lower flap upstream of skewed hinge line, deg (fig. 4(b))

Abbreviations:

AR aspect ratio (flow passage width divided by height at upstream hinge station) or throat aspect ratio of a 2D-CD nozzle with an unskewed lower flap

2D two dimensional

CD convergent-divergent

Sta. model station

Apparatus and Methods

Static Test Facility

The nozzle test was conducted in the static test facility of the Langley 16-Foot Transonic Tunnel by using the jet from the single engine propulsion simulation system, which exhausts to the atmosphere through an acoustically treated passage. The static test facility has an air control system that is similar to that of the Langley 16-Foot Transonic Tunnel and is described in detail in reference 23.

Single Engine Propulsion Simulation System

A sketch of the air-powered, single engine propulsion simulation system on which the nozzle configurations were statically tested is presented in figure 2. The propulsion simulation system is shown with a typical skewed-throat nozzle installation.

An external high-pressure air system with a heat exchanger provided a continuous flow of clean dry air at a controlled temperature of about 80°F. The pressure of the air entering the nozzle was a test variable and was set as high as 170 psi during jet simulation. The pressurized air was supplied to a high-pressure plenum by the six air lines integral with the dolly-mounted support strut. The air was then discharged into a low-pressure plenum through eight sonic radial nozzles equally spaced around the high-pressure plenum. (See fig. 2.) The airflow system was designed to minimize any forces imposed by the transfer of axial momentum as the air passes from the nonmetric high-pressure plenum to the metric low-pressure plenum (i.e., attached to the force balance). Two metal bellows bridged the metric and nonmetric plenums compensating for axial forces caused by pressurization and sealing the air system from the atmosphere. The air then passed from the low-pressure plenum through a rectangular choke plate and instrumentation section, both of which were common to all nozzle test configurations. All test configurations were attached to the instrumentation section at model station 41.13. The air was then discharged through the nozzle to sea level atmospheric conditions.

Nozzle Conceptual Design

A three-view sketch of a typical skewed-throat nozzle configuration is presented in figure 3(a). Several surfaces in the sketches are shaded for clarity. The nozzle shape is defined by a transition section, two flaps (upper and lower surfaces), and two sidewalls. The downstream transition section joins the instrumentation section exit with the nozzle entrance and initiates convergence of the nozzle. The upper flap is a hinged flat plate and is identical to that of a classical 2D-CD pitch-vectoring nozzle. The flap divergence angle and pitch-vectoring deflection angle are set by pinning the flap at the appropriate holes in a pin bar. The lower flap is a 2D-CD flap which is modified to provide the nozzle skewed-throat geometry. Internally, the flap consists of two flat surfaces, one convergent to and one divergent from the primary nozzle centerline, joined at a ridge which is skewed in relation to the ridge of the upper CD surface. Viewed from the rear (fig. 3(a)), the divergent surface slopes downward to the left, which establishes the direction of vectoring. Although this report refers to the skewed ridge as a hinge line, the CD lower surfaces are modeled by a one-piece flap. The lower flap is hinged upstream of the skewed ridge at the same location as the upper flap hinge; the lower flap divergence and deflection angles are also set with a pin bar.

The right sidewall was fixed in the closed position for all test configurations. The left sidewall was tested in the closed position and at several deflection angles to permit flow expansion in the yaw direction. The nozzle sidewalls extend aft to the trailing edges of the divergent flaps and above and below the pitch flaps to sufficiently contain the exhaust flow in all pitch-vectored configurations except those with a deflected sidewall.

Geometric variables in this investigation included hinge line skew angle, nozzle expansion ratio, sidewall deflection angle, upper and lower flap deflection angles (pitch vectoring), and nozzle aspect ratio AR. Several configurations are shown in figure 3(b) with the left sidewall removed for clarity.

Hinge line skew angles θ_{skew} of 35° and 50° relative to the lateral upstream hinges were tested. Note in figure 3(b) that a longer nozzle was required to accommodate the hinge line skew angle of 50°. For each skew angle, the nozzle was tested at a subsonic and a supersonic expansion ratio, corresponding to typical on-design operating pressure ratios for subsonic and supersonic cruise flight configurations. The terms subsonic and supersonic will be used instead of numerical values because the three-dimensional skewed-throat nozzle configuration complicates the numerical definition of the nozzle expansion ratio, which is normally defined as the exit plane area divided by the throat area. The primary difference between the subsonic and supersonic configurations is that the divergence angle between the upper flap

and the aft portion of the lower flap of the supersonic configuration is greater than that of the subsonic configuration.

Twenty-five configurations were tested. (See table 1 for the complete list.) The hinge line angle of $\theta_{\text{skew}} = 35°$ was tested with sidewall deflection angles of $\delta_{v,s} = 0°$, 12°, 24°, and 35° in combination with upper and lower pitch flap deflection angles of $\delta_{v,p} = 0°$. Additionally, multiaxis thrust-vectoring configurations were tested with a fixed sidewall angle of $\delta_{v,s} = 35°$ and pitch flap deflection angles of $\delta_{v,p} = 7°$, 20°, and 25°. The AR of all configurations described thus far was 1.748 based on the geometry at the upstream hinge station. The supersonic configuration for $\theta_{\text{skew}} = 35°$ was also tested with AR = 3.500. The test configurations for AR = 3.500 and $\theta_{\text{skew}} = 50°$ included only the following combinations of pitch flap $\delta_{v,p}$ and sidewall $\delta_{v,s}$ deflection angles: 0°/0°, 0°/35°, and 25°/35°. The intermediate pitch flap and sidewall deflection angles were not tested because of test schedule constraints. As shown in table 1, two additional test configurations included the supersonic nozzle with a skewed hinge line of 50° assembled with the two short sidewalls designed for the nozzle configuration with a skewed hinge line of 35° and the supersonic nozzle with one short and one long sidewall. Photographs of two typical skewed-throat nozzle configurations are shown in figure 3(c). Geometric details of the model components are tabulated in figure 4.

Instrumentation

A six-component strain gauge balance was used to measure forces and moments on the model. Jet total pressure was calculated by averaging total pressure measurements from nine individual pitot probes located at a fixed station in the instrumentation section. A thermocouple was also positioned in the instrumentation section to measure jet total temperature. The weight flow w_p of the high-pressure air supplied to the nozzle was measured by two critical flow venturis located in the air system upstream of the model.

The internal jet flow static pressure distribution was measured for each test configuration. Static pressure orifice locations are shown in figure 4 and are tabulated in table 2. Each upper and lower flap had three rows of orifices: one on the nozzle centerline and one on either side of the centerline at one-half the distance to the sidewalls. Each sidewall had a single row of orifices on the nozzle centerline.

Data Reduction

Every data point used in the computations was the average of 50 frames of data recorded at a rate of 10 frames per second. With the exception of resultant gross thrust F_r, all thrust data in this report are coincident with the model centerline. Five basic performance parameters are used in the presentation of results: resultant thrust ratio F_r/F_i, axial thrust ratio F_A/F_i, discharge coefficient w_p/w_i, resultant pitch thrust-vector angle δ_p, and resultant yaw thrust-vector angle δ_y. Reference 24 presents a detailed description of the data reduction procedures used for the current investigation.

The resultant thrust ratio F_r/F_i is the resultant gross thrust divided by the ideal isentropic thrust. Resultant gross thrust is obtained from the axial, normal, and side components of the jet thrust measured by the force balance. Ideal thrust F_i is based on measured weight flow w_p, jet total pressure $p_{t,j}$, and jet total temperature $T_{t,j}$ and assumes full isentropic expansion of the flow. (See "Symbols" for the equation.)

The axial thrust ratio F_A/F_i is the ratio of the measured nozzle thrust along the model centerline to the ideal nozzle thrust. From the definitions of F_A and F_r, the thrust F_A along the model centerline reflects the geometric loss that results from turning the exhaust vector away from the axial direction; the resultant gross thrust F_r does not.

Corrections are applied to all balance force and moment measurements before they are used in the calculation of performance parameters. Each balance component is initially corrected for model weight tares and isolated balance interactions. Because the bellows create a restraint on the balance, the balance is recalibrated after installation in the model and the additional component interaction corrections are computed. Besides providing a set of assembly interaction corrections, the recalibration accounts for the effects of pressurization (blowing the jet) and momentum (varying nozzle throat area). The bellows in the air pressurization system were designed to eliminate pressure and momentum interactions with the balance. However, residual tares still exist and result from a small pressure differential between the ends of the bellows when air system internal velocities are great and from small differences in the spring constants of the forward and aft bellows when pressurized. The residual tares were determined by testing a set of reference calibration nozzles with known performance over a range of expected internal pressures and external forces and moments. The procedures for

determining and computing the tares are discussed in detail in references 23 and 24.

The nozzle discharge coefficient w_p/w_i is the ratio of measured weight flow to ideal weight flow and reflects the nozzle flow efficiency. The discharge coefficient is reduced by any momentum and *vena contracta* losses (effective throat area less than A_t); nozzle throat area A_t is the measured geometric minimum area in the nozzle. The nozzles in the current investigation were designed so that the minimum area would occur along the skewed hinge line. The skewed-throat areas used in the ideal weight flow calculation are tabulated in table 1.

The angles δ_p and δ_y are the calculated angles in the pitch- and yaw-vector planes at which the resultant gross thrust is deflected from the nozzle axis. As indicated in the symbols section, these angles are calculated from the measured normal, side, and axial forces produced by the jet and will increase with either an increase in normal or side forces or a decrease in axial force.

Discussion of Results

The basic thrust and weight flow performance of the skewed-throat nozzle, which includes static pressure distributions for selected configurations, is presented graphically in figures 5–19. The static pressure measurements are tabulated in table 3; the thrust and weight flow performance is tabulated in table 4. Performance data are shown as functions of nozzle pressure ratio (NPR).

Results will be discussed in the following manner. An analysis of the nozzle configuration with a skewed hinge line of $\theta_{\text{skew}} = 35°$ and AR = 1.748 will be presented in detail to define the basic flow characteristics of the skewed-throat nozzle concept. The internal flow field will be described; the thrust performance, discharge performance, and vectoring characteristics will be defined; and the overall nozzle performance as affected by variations in expansion ratio will be determined.

A brief discussion of the basic data for the configurations of $\theta_{\text{skew}} = 50°$ with AR = 1.748 and $\theta_{\text{skew}} = 35°$ with AR = 3.500 will then be presented. The discussion will not be as detailed as that referred to in the previous paragraph because data at the intermediate pitch flap and sidewall deflection angles were not acquired, and the data that were acquired will be discussed again in the comparisons of parameters that follow. Separate comparisons of the effects of expansion ratio, aspect ratio, and hinge line skew angle variations on basic nozzle performance will conclude the "Discussion of Results."

Analysis of Basic Nozzle Data

Skewed Hinge Line of 35°, AR = 1.748, and Subsonic Expansion Ratio

The thrust and weight flow performance of the skewed-throat nozzle with $\theta_{\text{skew}} = 35°$ with subsonic expansion ratio and AR = 1.748 is presented in figure 5 in two segments: the first shows nozzle performance with a fixed pitch flap angle $\delta_{v,p} = 0°$ and varied sidewall deflection $\delta_{v,s}$ (fig. 5(a)) and the second shows nozzle performance with a fixed sidewall deflection angle $\delta_{v,s} = 35°$ and varied pitch flap deflection $\delta_{v,p}$ (fig. 5(b)).

No sidewall or pitch flap deflections. As shown in figure 5(a), the unvectored skewed-throat nozzle thrust performance ($\delta_{v,p} = 0°$, $\delta_{v,s} = 0°$: circle symbol) is excellent despite the complex three-dimensional geometry. The maximum measured resultant thrust ratio of $F_r/F_i = 0.9859$ is comparable with the thrust efficiency of nozzles having unskewed throats.

Small pitch and yaw thrust-vector angles are generated from nozzle asymmetry in this configuration ($\delta_{v,p} = 0°$, $\delta_{v,s} = 0°$). The relatively constant positive value of δ_p between 1° and 3° is consistent in direction for a lower pitch flap turned downward about the skewed hinge line. (See fig. 3(a).) A yaw thrust-vector angle δ_y of nearly 4° is generated at NPR = 2 but decreases almost to 0° at NPR = 4. The yaw thrust-vector angles are low because the sidewall is undeflected; the vectored flow from the skewed throat is unvectored by the closed sidewall.

The discharge coefficient of the unvectored skewed-throat nozzle is low (fig. 5(a)); the values were between 0.83 and 0.84. However, the ideal weight flow was calculated using a value of A_t (see definition of w_i in "Symbols") obtained by assuming the nozzle throat forms along the skewed hinge line. The static pressure distributions shown in figure 6 assist in locating sonic flow in the nozzle and in mapping the location of the throat. Examination of the unvectored nozzle pressure distributions indicates that sonic flow ($p/p_{t,j} = 0.528$) along the upper flap occurs approximately between $x/L = 0.42$ and 0.50 and that the sonic line is roughly perpendicular to the nozzle axis for $\delta_{v,s} = 0°$. However, the sonic line along the lower flap is highly skewed in relation to the sonic line along the upper flap; the sonic flow appears to occur along the hinge line represented by the vertical dashed lines. The nozzle throat, therefore, tends to be warped rather than planar; the low

value of discharge coefficient is probably the result of the deformed throat and an inaccurate value of A_t used in the calculation of w_i.

Sidewall deflections only. As the left sidewall is deflected outward to $\delta_{v,s} = 12°$ (fig. 5(a)), maximum F_r/F_i decreases in value and occurs at a higher NPR. The NPR shift indicates an increase in the effective expansion ratio (equivalent exit area divided by throat area) of the nozzle. As the left sidewall is deflected, the entire left side of the divergent passage is ventilated; the results are an increase in the effective exit area and in the capability of the nozzle to fully expand flow at higher pressure. Peak nozzle efficiency as indicated by F_r/F_i generally occurs near the NPR for fully expanded flow. As the sidewall is deflected beyond 12°, maximum F_r/F_i continues to shift to higher NPR's, but the maximum value of F_r/F_i remains relatively constant at about 0.97. (See fig. 5(a).)

With an initial sidewall deflection of $\delta_{v,s} = 12°$ (fig. 5(a)), pitch thrust-vector angle δ_p increases to values between 4° and 7° for NPR > 3; δ_p is not affected by further increases in $\delta_{v,s}$. Yaw thrust-vector angle δ_y increases with increasing sidewall deflection and for $\delta_{v,s} = 12°$ and NPR > 2 equals the sidewall deflection angle. However, yaw thrust-vectoring capability is degraded at the higher sidewall deflection angles with only a 1.6° increase in δ_y at NPR = 8 as the sidewall deflection is increased from 24° to 35°. The skewed-throat nozzle with $\theta_{skew} = 35°$ does not fully turn the flow because δ_y does not approach 35° even for the left sidewall deflection of $\delta_{v,s} = 35°$. In fact, 35° of yaw vectoring would not be expected because the right sidewall is not deflected into the flow. However, a skewed hinge line with $\theta_{skew} = 35°$ results in more that 12° of yaw vectoring at NPR $\geq$ 4; the sidewall deflection of 12° limits the magnitude of δ_y to a constant value. That is, the flow is unvectored somewhat by the 12° of sidewall deflection at the test NPR's. For comparison, a 2D-CD nozzle with one sidewall deflected outward 20° about a hinge at the throat station provided only 7° of yaw vectoring for NPR > 3. (See ref. 22.) For given NPR's precise yaw thrust-vector angles of up to approximately 20° can be set with a single sidewall deflection. (See fig. 5(a).) The skewed-throat geometry does provide increased yaw vectoring of the exhaust flow.

When the left sidewall is initially deflected outward at $\delta_{v,s} = 12°$, the discharge coefficient increases to values between 0.87 and 0.89 and is not affected by further increases in $\delta_{v,s}$. (See fig. 5(a).) The pressure distributions in figure 6 show that the throat is oriented approximately along the skewed hinge line on both the lower and upper flaps with the sidewall deflected and is more planar than with the sidewall closed. However, the magnitude of w_p/w_i (fig. 5(a)), is still less than values normally measured for high-performance nozzles. (See ref. 21.) As indicated by the flat pressure distribution downstream of the hinge line, the sharp edge along the skewed hinge line of the lower flap probably caused flow separation from the divergent surface of the flap. (See fig. 6.) Small radii at the nozzle throat have demonstrated an adverse effect on discharge coefficient. (See ref. 25.) Improved discharge performance may result from a larger radius at the lower flap skewed hinge line.

Sidewall and pitch flap deflections. The effect on thrust performance by increasing $\delta_{v,p}$ with $\delta_{v,s} = 35°$ is presented in figure 5(b). Resultant thrust ratio F_r/F_i remains fairly constant as $\delta_{v,p}$ changes for NPR > 4. However, significant pitch-vectoring effects on δ_p and δ_y are noted. Although the increase in δ_p (<2°) when increasing $\delta_{v,p}$ from 0° to 7° is small because of the inherent δ_p in the configuration of $\delta_{v,p} = 0°$, the increase in δ_p when increasing $\delta_{v,p}$ from 7° to 20° is more significant throughout the NPR test range; the increase in δ_p as $\delta_{v,p}$ is increased to 25° is dramatic with pitch thrust-vector angles significantly exceeding the flap deflection angle. The characteristic is indicative of instability in the internal flow field. The large variation in incremental δ_p with increasing $\delta_{v,p}$ is caused by large shifts in throat location and orientation as indicated by the pressure distributions shown in figure 7. The pressure distributions are discussed below.

The effect on δ_y of varying $\delta_{v,p}$ with the sidewall deflected 35° further indicates an unstable flow field. (See fig. 5(b).) As pitch flap deflection is increased from 0° to 20°, yaw thrust-vector angle decreases by approximately 6° for all NPR's. The decrease in δ_y appears to be offset by an increase in δ_p because the axial thrust ratio F_A/F_i and resultant thrust ratio F_r/F_i are relatively unaffected by changes in $\delta_{v,p}$ up to 20°. However, increasing $\delta_{v,p}$ to 25° reverses the trend in δ_y and results in a substantial increase in δ_y. Axial thrust is significantly reduced, but F_r/F_i is still relatively unaffected. The change in thrust performance indicates a strong coupling between pitch and yaw thrust-vector angle, which is an undesirable characteristic. Linear uncoupled thrust vectoring is preferable for airplane control.

Flow field changes are further indicated by the discharge coefficient data. (See fig. 5(b).) As $\delta_{v,p}$ is increased from 0° to 20°, w_p/w_i increases dramatically from approximately 0.88 to 1.07. As $\delta_{v,p}$ is

further increased to 25°, w_p/w_i decreases to approximately 0.95, a level similar to that for $\delta_{v,p} = 7°$. Ideal weight flow was computed by assuming a throat area equal to the area of a plane passing through the skewed hinge line and perpendicular to the upper flap. The data for w_p/w_i suggest that the actual throat position is significantly relocated during pitch thrust vectoring. The following discussion of pressure distributions shown in figure 7 will support this hypothesis.

The change in pressure distributions in the nozzle as $\delta_{v,p}$ is increased from 0° to 25° is shown in figure 7. As $\delta_{v,p}$ is increased from 0° to 20°, the sonic plane ($p/p_{t,j} = 0.528$) moves upstream of the skewed hinge line and becomes less skewed relative to the upper and lower flaps. At $\delta_{v,p} = 20°$, the sonic line is upstream of all pressure taps on the lower flap and sidewalls and of most taps on the upper flap. The cross-sectional area at the upstream location is larger than the area used in the w_i calculation, which results in a greater than unity discharge coefficient at $\delta_{v,p} = 20°$. (See fig. 5(b).) Increasing $\delta_{v,p}$ from 20° to 25° has a dramatic effect on the throat location in the nozzle. The throat shifts back to the skewed hinge line on the lower flap and moves significantly aft of this location on the upper flap, which deflects the throat significantly in both pitch and yaw. The shift results in large values of δ_p and δ_y, a reduced level of axial thrust, and a reasonable value of discharge coefficient relative to the configuration for $\delta_{v,p} = 20°$. The results for this configuration indicate that the attempt to force the location of the sonic plane to coincide with the skewed hinge line was unsuccessful. A nozzle with such vectoring characteristics would be unacceptable because of the nonlinear-vectoring response with flap deflections and the effect of the unstable internal flow field on discharge coefficient.

Skewed Hinge Line of 35°, AR = 1.748, and Supersonic Expansion Ratio

Data are presented in figure 8 for the skewed-throat nozzle with $\theta_{skew} = 35°$ and AR = 1.748 in a supersonic configuration (greater expansion ratio than the subsonic nozzle). For the unvectored configuration (circle symbol), the peak $F_r/F_i = 0.9792$ (fig. 8(a)) is slightly less than the corresponding peak F_r/F_i for the subsonic expansion ratio. (See fig. 5(a).) As expected for a greater expansion ratio nozzle, the peak resultant thrust ratio occurs at a higher value of NPR than for the subsonic expansion ratio configuration. Pitch thrust-vector angles of 4° to 6° for the unvectored configuration are relatively constant; yaw thrust-vector angles of 2° to 4° are also relatively constant throughout the NPR test range.

The data trends with increasing sidewall deflection are similar to those of the subsonic expansion ratio configuration. Deflecting the sidewall for yaw thrust vectoring ($\delta_{v,s} > 0°$) causes δ_p to vary by as much as 5°. All undesired pitch thrust vectoring needs to be compensated for by appropriate deflections of the upper and lower pitch flaps. Alternatively, an upper flap with a skewed hinge design would restore vertical symmetry to the nozzle which should eliminate the coupling between pitch and yaw thrust vectoring. As was true for the subsonic configuration, full yaw control capability is established up to $\delta_y = 12°$. Sidewall deflections greater than 12° again produce yaw vector angles less than $\delta_{v,s}$ which results in smaller increases in control capability at the greater sidewall deflection angles. The discharge coefficient characteristics are also similar to those of the subsonic configuration with the exception of a decrease in w_p/w_i as $\delta_{v,s}$ was increased from 24° to 35°. Again, the data suggest a sensitivity of internal flow characteristics to nozzle surface deflections. Relocation of the sidewall hinge could possibly improve discharge coefficient performance.

However, the pitch flap deflection effect on the supersonic expansion ratio configuration data trends (fig. 8(b)) do not follow those of the subsonic expansion ratio configuration. The data for the subsonic nozzle discussed earlier showed an erratic response of δ_p and δ_y with increases in $\delta_{v,p}$. As the pitch flaps were deflected up to 20°, δ_p increased by a small amount and δ_y decreased in magnitude; a further increase in $\delta_{v,p}$ to 25° resulted in a dramatic flow field change accompanied by significant increases in δ_p and δ_y. However, for the supersonic configuration, δ_p and δ_y appear to have consistent responses to increases in $\delta_{v,p}$.

A summary of the thrust-vectoring performance of both nozzles (subsonic and supersonic expansion ratios) as the pitch flap angle is varied at fixed NPR and $\delta_{v,s}$ is presented in figure 9. The abrupt change in the thrust-vector angles discussed earlier for the subsonic nozzle as $\delta_{v,p}$ is increased from 20° to 25° can be clearly seen. In fact, a comparison of the subsonic expansion ratio data with the supersonic expansion ratio data suggests that the configurations for $\delta_{v,p} = 7°$ and $\delta_{v,p} = 20°$ of the former deviate from the expected results as indicated by the dashed lines. After $\delta_{v,p}$ is increased to 25°, the results return to the expected flow field and vectoring levels. The supersonic expansion ratio configuration avoids a similar deviation for reasons not fully understood. A possible explanation is that the lower flap convergence angle of the supersonic expansion ratio nozzle

is slightly greater than that of the subsonic expansion ratio nozzle.

Similar to the subsonic configuration, pitch thrust-vector angles of the supersonic configuration exceed the flap deflection angles at NPR > 5. (See fig. 8(b).) The discharge coefficient also increases with pitch flap deflection but does not exceed a value of unity as occurred with the subsonic nozzle. The pressure distributions in figure 10 show that the sonic line along the lower flap nearly coincides with the skewed hinge line for all test pitch flap deflections. The sonic line along the upper flap moves less than 20 percent in longitudinal position with variations of $\delta_{v,p}$; the sonic line for the subsonic nozzle moves more than 40 percent. (See fig. 7.) Increasing the expansion ratio of the skewed-throat nozzle has a mitigating effect on the unstable flow field of the subsonic configurations with a low expansion ratio.

Skewed Hinge Line of 50°, AR = 1.748

The thrust and weight flow performance data for the skewed-throat nozzle with $\theta_{skew} = 50°$ and AR = 1.748 are presented in figure 11. The intermediate settings of pitch flap angle and sidewall deflection angle were not tested for this configuration due to test facility schedule constraints. Instead, the thrust-vectoring envelope was defined by testing an unvectored skewed-throat nozzle with a fully deployed sidewall and a full multiaxis thrust-vectoring configuration ($\delta_{v,p} = 25°$, $\delta_{v,s} = 35°$). The increase in $\delta_{v,p}$ or $\delta_{v,s}$ from 0° to 25° and 35°, respectively, results in significant increases in δ_p, δ_y, and w_p/w_i with a corresponding decrease in F_A/F_i. However, the vectoring characteristics at intermediate flap and sidewall settings cannot be determined from the limited data. As noted in the results of the skewed-throat nozzle with $\theta_{skew} = 35°$, an increase in $\delta_{v,p}$ likewise does not significantly affect the resultant thrust ratio F_r/F_i for NPR > 2 for the subsonic configuration. (See fig. 11(a).) For the supersonic configuration (fig. 11(b)), more significant effects on F_r/F_i are observed for NPR < 6. Moreover, very large multiaxis thrust-vectoring angles are produced by this configuration with minimal losses in thrust. For example, at NPR = 7, pitch and yaw thrust-vector angles of 35° and 31° are produced with only a 4-percent loss in resultant gross thrust, which demonstrates the efficiency of subsonic flow turning of the design.

The discharge coefficient of the skewed-throat nozzle with $\theta_{skew} = 50°$ increases almost linearly with increasing NPR. The pressure distributions for the yaw thrust-vectoring configuration ($\delta_{v,p} = 0°$, $\delta_{v,s} = 35°$) in figure 12 do not suggest a reason for this characteristic as throat location does not appear to be a function of NPR > 2. Although an engine can operate in spite of inefficiencies at $w_p/w_i = 0.84$ (fig. 5(a)), operation is probably not possible with $w_p/w_i = 0.67$ to 0.75 (figs. 11(a) and 11(b)) without oversizing the throat.

The effect of sidewall length was investigated for the skewed-throat configuration with $\theta_{skew} = 50°$ and the results are presented in figure 13. Shortening one or both sidewalls by approximately 40 percent generally increases the values of δ_p and δ_y. The effect of shortening the sidewall is similar to that of deflecting the sidewall outward; internal flow turned by the skewed throat can escape the nozzle without being redirected aft by a solid sidewall. As shown in figure 13, the resultant thrust ratio is generally reduced 1 to 3 percent by these modifications. This loss is slightly greater than the 0.5-percent loss typically measured for 2D-CD nozzles with both sidewalls shortened. (See refs. 21 and 22.)

Skewed Hinge Line of 35°, AR = 3.500, and Supersonic Expansion Ratio

A supersonic expansion ratio skewed-throat nozzle with $\theta_{skew} = 35°$ was also tested with AR = 3.500; its performance is presented in figure 14. The data trends for the nozzle at AR = 3.500 are similar to those presented in figure 8 for the nozzle with AR = 1.748. Specific effects of aspect ratio will be discussed in "Comparison of Aspect Ratio."

Comparison of Expansion Ratio

A comparison of subsonic versus supersonic expansion ratio on the skewed-throat nozzle with $\theta_{skew} = 35°$ and AR = 1.748 is presented in figure 15. Because the nozzle lengths are equal, the configurations differ from one another mainly in divergence angle. (See fig. 4 for dimensions.) A comparison of the resultant thrust ratios at equivalent pitch flap and sidewall deflection angles indicates that variation of the expansion ratio does not adversely affect nozzle thrust efficiency. As expected, the predominant effect of increasing the expansion ratio is to shift the most efficient operating condition to a higher NPR. Additionally, as the sidewall is deflected outward, the effective exit area for flow expansion is increased which results in a further shift in NPR.

With the pitch flaps undeflected and the sidewall closed ($\delta_{v,p} = \delta_{v,s} = 0°$, fig. 15(a)), both configurations have some residual vectoring as a result of nozzle asymmetry. The supersonic expansion ratio

configuration develops greater pitch and yaw thrust-vector angles because as expansion ratio is increased, the aft portion of the lower flap is deflected downward through a greater angle than the upper flap is deflected upward; the net effect is that more flow is directed down and to the left. Any residual vectoring would need to be either compensated for or eliminated by adding symmetry to the skewed-throat nozzle design.

As the sidewall is deflected outward, the supersonic expansion ratio configurations produce a greater variation in pitch thrust-vector angle δ_p across the NPR test range. Variations of up to 15° were measured for the supersonic expansion ratio configurations compared with approximately 8° for the subsonic expansion ratio. Increases in δ_p as NPR is increased have been previously documented (ref. 21) for pitch-vectoring 2D-CD nozzles. The increase generally occurs in the regime where the nozzle is highly overexpanded (i.e., at NPR's below the design point). The supersonic expansion ratio configurations of the skewed-throat nozzle have highly overexpanded flow fields throughout the NPR test range. In contrast, the subsonic expansion ratio configurations have either reached or nearly reached peak thrust efficiency F_r/F_i by the maximum test NPR. This large variation in δ_p is an adverse characteristic of high expansion ratio nozzles and is why most vectoring-nozzle concepts incorporate the ability to vary expansion ratio as the flight conditions warrant. A similar ability would be beneficial for a skewed-throat nozzle concept.

The subsonic and supersonic expansion ratio nozzles provide approximately the same yaw thrust-vector angles (generally within $\approx 1°$) at all positive sidewall deflection angles ($\delta_{v,s} > 0°$). A maximum yaw vector angle of nearly 20° was obtained within the NPR test range. Greater angles appear attainable at higher NPR's.

Comparisons between the subsonic and supersonic expansion ratio configurations with $\delta_{v,p} > 0°$ are presented in figures 15(e) 15(g). An earlier section of this report concluded that as $\delta_{v,p}$ of the subsonic expansion ratio configuration is increased to 20°, the sonic plane moves upstream of the skewed hinge line, which markedly changed the nozzle vectoring and weight flow characteristics; the corresponding supersonic expansion ratio configuration parameters were not affected. As $\delta_{v,p}$ is increased to 25°, the sonic plane shifts back to the skewed hinge line, which results in similar vectoring and weight flow characteristics for both the subsonic and supersonic expansion ratio configurations.

Although the reasons for the difference in performance are not fully understood, one possibility is that the slightly greater convergence angle on the lower flap of the supersonic expansion ratio configuration (18.55° versus 15.35°) forced the sonic plane to remain in the vicinity of the skewed hinge line.

At $\delta_{v,p} = 25°$ and $\delta_{v,s} = 35°$ (fig. 15(g)), the subsonic and supersonic expansion ratio configurations reach essentially equal magnitudes of pitch thrust vectoring; because of the overexpansion effect discussed earlier, the supersonic expansion ratio configuration produces lower pitch thrust vectoring at lower NPR's.

A comparison of expansion ratios for the skewed hinge line configurations with $\theta_{\text{skew}} = 50°$ is presented in figure 16. Data were not taken at the intermediate settings of sidewall and pitch flap deflections; therefore, the adverse performance of the subsonic expansion ratio configuration of the skewed-throat nozzle with $\theta_{\text{skew}} = 35°$ was not verified as a characteristic of the skewed-throat nozzle with $\theta_{\text{skew}} = 50°$.

For $\delta_{v,p} = 0°$, thrust efficiency, discharge performance, and thrust-vector angles show little variation as expansion ratio is varied. The result is expected because the geometric variations needed to increase expansion ratio were small due to the long nozzle length. As $\delta_{v,p}$ is increased to 25° (with $\delta_{v,s} = 35°$), differences in resultant thrust ratio and pitch thrust-vector angle are evident as a result of the overexpansion effect on performance discussed earlier.

Comparison of Aspect Ratio

A comparison of the effect of AR = 1.748 and AR = 3.500 on the performance of the skewed-throat nozzle concept is presented in figure 17. Both configurations in the comparison have skewed hinge lines of 35° and supersonic expansion ratios. Once again, the aspect ratio is based on the throat dimensions of the unskewed cruise configuration geometry. Although neither of the test aspect ratios was particularly high, they are referred to as low and high AR's in this section for the purpose of discussion.

The resultant thrust ratio and discharge coefficient levels of the two aspect ratio configurations are similar, with the high-AR nozzle developing a slightly greater weight flow when $\delta_{v,p} = 0°$. The high-AR nozzle in the unvectored skewed-throat configuration produces more positive pitch and yaw thrust-vector angles. In the yaw thrust-vectoring ($\delta_{v,s} = 35°$, fig. 17(b)) and multiaxis thrust-vectoring ($\delta_{v,p} = 25°$, $\delta_{v,s} = 35°$, fig. 17(c)) configurations, the low-AR nozzle produces greater values of δ_y and the high-AR

nozzle produces greater values of δ_p, which would be expected. As aspect ratio increases, pitch vectoring becomes more effective because the relative size of the pitch-vectoring mechanism increases; yaw vectoring becomes less effective because the relative size of the yaw-vectoring mechanism decreases.

Comparison of Skew Angle

A comparison of nozzle performance at subsonic and supersonic expansion ratios for configurations with skewed hinge angles of 35° and 50° with AR = 1.748 is presented in figures 18 and 19. At $\delta_{v,p} = 0°$ and $\delta_{v,s} = 0°$, the resultant thrust ratio is approximately the same throughout most of the NPR test range for both nozzle expansion ratios. (See figs. 18(a) and 19(a).) In the yaw thrust-vectoring ($\delta_{v,s} = 35°$) and multiaxis thrust-vectoring ($\delta_{v,p} = 25°$, $\delta_{v,s} = 35°$) configurations, the skewed-throat nozzle with $\theta_{skew} = 50°$ has a 2- to 3-percent decrease in resultant thrust ratio for NPR > 2. The loss appears to be primarily in axial thrust.

At positive pitch and yaw deflection angles, the skewed-throat nozzle with $\theta_{skew} = 50°$ develops greater pitch and yaw thrust-vector angles than the skewed-throat nozzle with $\theta_{skew} = 35°$, but at the expense of axial force and resultant gross thrust. Greater yaw thrust-vector angles for the skewed-throat configurations with $\theta_{skew} = 50°$ are expected because the greater skew angle at the throat turns the exhaust flow more in the yaw direction than do the skewed-throat configurations with $\theta_{skew} = 35°$. The greater pitch thrust-vector angles of the skewed-throat configurations with $\theta_{skew} = 50°$ result from pitch flaps that have longer lengths and larger areas than the corresponding pitch flaps of the skewed-throat configurations with $\theta_{skew} = 35°$. (See fig. 4.)

A comparison of discharge coefficient shows that the skewed-throat nozzle with $\theta_{skew} = 50°$ has greater shifts with thrust vectoring than does the skewed-throat nozzle with $\theta_{skew} = 35°$. The variations make regulation of weight flow from the engine more difficult. Reasons for discharge coefficient variations have been discussed in previous sections.

Conclusions

An experimental investigation has been conducted in the static test facility of the Langley 16-Foot Transonic Tunnel of a multiaxis thrust-vectoring nonaxisymmetric nozzle which provides yaw thrust vectoring by physically skewing the throat plane and pitch thrust vectoring by deflecting the divergent pitch flaps. Geometric parameters that were investigated include skewed hinge line angle, nozzle expansion ratio, aspect ratio, pitch flap deflection angle, and sidewall deflection angle. Nozzle pressure ratio was varied from 2 to 11.5. The following conclusions are based on the results obtained in this investigation:

1. In most of the test configurations, the skewed-throat nozzle successfully develops efficient thrust vectoring by forcing the sonic plane to form along a skewed hinge line. However, with certain deflections of the pitch flaps and sidewall, the sonic plane shifts well upstream of the hinge line, which results in adverse-vectoring and weight flow characteristics; by increasing the expansion ratio of these configurations, the sonic plane shifts back to the expected position.

2. As a consequence of nozzle asymmetry, pitch and yaw thrust vectoring are interdependent and nonzero thrust-vector angles are produced in the unvectored configurations.

3. Simultaneous pitch and yaw thrust-vector angles of 35° and 31°, respectively, are obtained with only a 4-percent loss in resultant gross thrust, which demonstrates that efficient and substantial thrust vectoring results from the skewed-throat nozzle concept.

4. An increase in nozzle aspect ratio results in greater pitch thrust-vector angles both in the pitch-vectored and unvectored configurations regardless of sidewall deflection. The greater pitch thrust-vector angles probably result from an increase in the pitch flap area as the aspect ratio increases.

5. An increase in the skew hinge line angle generally results in greater pitch and yaw thrust-vector angles during vectoring, but at the expense of axial thrust. The increased angles probably result from an increase in both throat skew angle and pitch flap surface area.

As designed for this investigation, the skewed-throat nozzle is not likely to be a viable thrust-vectoring concept. Although efficient vectoring was demonstrated by some configurations, severe adverse flow field instabilities were observed with certain control surface deflections. The nozzle was designed with skewed geometry only on the lower flap. The two-dimensional contour of the upper flap may have been counterproductive to the concept goal of providing a fixed location for the sonic plane. Additionally, the asymmetric design resulted in coupled pitch and yaw thrust vectoring as well as nonzero thrust-vector angles in the unvectored configuration.

A symmetrically designed skewed-throat nozzle with skewed geometry added to the upper flap would decouple pitch and yaw thrust vectoring and enhance the stability of throat location; the skewed-throat concept would then be a more viable candidate for an efficient thrust-vectoring nozzle.

NASA Langley Research Center
Hampton, VA 23681-0001
December 6, 1993

References

1. Herbst, W. B.: Future Fighter Technologies. *J. Aircr.*, vol. 17, no. 8, Aug. 1980, pp. 561 566.

2. Nelson, B. D.; and Nicolai, L. M.: Application of Multi-Function Nozzles to Advanced Fighters. AIAA-81-2618, Dec. 1981.

3. Richey, G. K.; Surber, L. E.; and Berrier, B. L.: Airframe-Propulsion Integration for Fighter Aircraft. AIAA-83-0084, Jan. 1983.

4. Herrick, Paul W.: Propulsion Influences on Air Combat. AIAA-85-1457, July 1985.

5. Gallaway, C. R.; and Osborn, R. F.: Aerodynamics Perspective of Supermaneuverability. AIAA-85-4068, Oct. 1985.

6. Frassinelli, Mark C.; and Carson, George T., Jr.: *Effect of Tail Size Reductions on Longitudinal Aerodynamic Characteristics of a Three-Surface F-15 Model With Nonaxisymmetric Nozzles.* NASA TP-3036, 1990.

7. *F-15 2-D Nozzle System Integration Study. V.I - Technical Report.* NASA CR-145,295, 1978.

8. Berrier, Bobby L.: *Results From NASA Langley Experimental Studies of Multiaxis Thrust Vectoring Nozzles.* SAE Tech. Paper Ser. 881481, Oct. 1988.

9. Leavitt, Laurence D.: Summary of Nonaxisymmetric Nozzle Internal Performance From the NASA Langley Static Test Facility. AIAA-85-1347, July 1985.

10. Capone, Francis J.: *Static Performance of Five Twin-Engine Nonaxisymmetric Nozzles With Vectoring and Reversing Capability.* NASA TP-1224, 1978.

11. Capone, Francis J.; Mason, Mary L.; and Leavitt, Laurence D.: *An Experimental Investigation of Thrust Vectoring Two-Dimensional Convergent-Divergent Nozzles Installed in a Twin-Engine Fighter Model at High Angles of Attack.* NASA TM-4155, 1990.

12. Mason, Mary L.; Capone, Francis J.; and Asbury, Scott C.: *A Static Investigation of the Thrust Vectoring System of the F/A-18 High-Alpha Research Vehicle.* NASA TM-4359, 1992.

13. Willard, C. M.; Capone, F. J.; Konarski, M.; and Stevens, H. L.: Static Performance of Vectoring/Reversing Non-Axisymmetric Nozzles. AIAA Paper 77-840, July 1977.

14. Lacey, David W.; and Murphy, Richard D.: Jet Engine Thrust Turning by the Use of Small Externally Mounted Vanes. DTNSRDC-82/080, U.S. Navy, Jan. 1983. (Available from DTIC as AD B070 970L.)

15. Wing, David J.; and Asbury, Scott C.: *Static Performance of a Cruciform Nozzle With Multiaxis Thrust-Vectoring and Reverse-Thrust Capabilities.* NASA TP-3188, 1992.

16. Capone, Francis J.; and Bare, E. Ann: *Multiaxis Control Power From Thrust Vectoring for a Supersonic Fighter Aircraft Model at Mach 0.20 to 2.47.* NASA TP-2712, 1987.

17. Capone, Francis J.; and Schirmer, Alberto W: *Static Internal Performance of a Single Expansion Ramp Nozzle with Multiaxis Thrust Vectoring Capability.* NASA TM-4450, 1993.

18. Taylor, John G.: *Static Investigation of a Two-Dimensional Convergent-Divergent Exhaust Nozzle With Multiaxis Thrust-Vectoring Capability.* NASA TP-2973, 1990.

19. Asbury, Scott C.; and Capone, Francis J.: Thrust Vectoring Characteristics of the F-18 High Alpha Research Vehicle at Angles of Attack From 0° to 70°. AIAA-92-3095, July 1992.

20. Berrier, Bobby L.; and Taylor, John G.: *Internal Performance of Two Nozzles Utilizing Gimbal Concepts for Thrust Vectoring.* NASA TP-2991, 1990.

21. Re, Richard J.; and Leavitt, Laurence D.: *Static Internal Performance Including Thrust Vectoring and Reversing of Two-Dimensional Convergent-Divergent Nozzles.* NASA TP-2253, 1984.

22. Mason, Mary L.; and Berrier, Bobby L.: *Static Investigation of Several Yaw Vectoring Concepts on Nonaxisymmetric Nozzles.* NASA TP-2432, 1985.

23. *A User's Guide to the Langley 16-Foot Transonic Tunnel Complex, Revision 1.* NASA TM-102750, 1990.

24. Mercer, Charles E.; Berrier, Bobby L.; Capone, Francis J.; and Grayston, Alan M.: *Data Reduction Formulas for the 16-Foot Transonic Tunnel NASA Langley Research Center, Revision 2.* NASA TM-107646, 1992.

25. Mason Mary L.; Putnam, Lawrence E.; and Re, Richard J.: *The Effect of Throat Contouring on Two-Dimensional Converging-Diverging Nozzles at Static Conditions.* NASA TP-1704, 1980.

Table 1. Nozzle Geometric Data Summary

[Configuration list]

θ_{skew}	AR	Expansion ratio	$\delta_{v,s}$	$\delta_{v,p}$			
				0°	7°	20°	25°
35°	1.748	Subsonic	0°	x			
↓	↓	↓	12°	x			
↓	↓	↓	24°	x			
↓	↓	↓	35°	x	x	x	x
↓	↓	Supersonic	0°	x			
↓	↓	↓	12°	x			
↓	↓	↓	24°	x			
↓	↓	↓	35°	x	x	x	x
↓	3.500	Supersonic	0°	x			
↓	3.500	Supersonic	35°	x			x
50°	1.748	Subsonic	0°	x			
↓	↓	Subsonic	35°	x			x
↓	↓	Supersonic	0°	x			
↓	↓	Supersonic	35°	x			x

[Additional configurations]

θ_{skew}	AR	Expansion ratio	$\delta_{v,s}$	$\delta_{v,p}$	Left sidewall length, in.	Right sidewall length, in.
50°	1.748	Supersonic	0°	0°	3.658	5.718
50°	1.748	Supersonic	0°	0°	3.658	3.658

[Throat areas for ideal weight flow calculations]

θ_{skew}	AR	Expansion ratio	A_t (in^2)			
			$\delta_{v,p} = 0°$	7°	20°	25°
35°	1.748	Subsonic	3.505	3.481	3.208	3.027
35°	1.748	Supersonic	3.506	3.525	3.334	3.183
35°	3.500	Supersonic	3.501			3.116
50°	1.748	Subsonic	3.506			2.871
50°	1.748	Supersonic	3.507			2.923

Table 2. Static Pressure Tap Locations x/L (Fig. 4)

(a) $\theta_{\text{skew}} = 35°$, subsonic expansion ratio, AR = 1.748

$[\delta_{v,p} = 0°, \delta_{v,s} = 0°]$

Upper flap x/L			Lower flap x/L			Sidewall x/L	
Left	Center	Right	Left	Center	Right	Left	Right
0.128	0.086		0.176	0.115	0.176	0.131	0.131
.289	.141	0.289	.335	.189	.335	.262	.262
.465	.227	.465	.496	.271	.496	.394	.394
.644	.321	.644	.657	.355	.657	.525	.525
.823	.417	.823	.820	.452	.820	.656	.656
	.514			.540		.788	.788
	.611			.628			
	.709			.716			
	.807			.805			
	.905			.893			
			Skew line location x/L				
			0.244	0.375	0.508		

$[\delta_{v,p} = 0°, \delta_{v,s} = 12°]$

Upper flap x/L			Lower flap x/L			Sidewall x/L	
Left	Center	Right	Left	Center	Right	Left	Right
0.128	0.086		0.176	0.115	0.176	0.128	0.131
.289	.141	0.289	.335	.189	.335	.256	.262
.465	.227	.465	.496	.271	.496	.384	.394
.644	.321	.644	.657	.355	.657	.512	.525
.823	.417	.823	.820	.452	.820	.641	.656
	.514			.540		.769	.788
	.611			.628			
	.709			.716			
	.807			.805			
	.905			.893			
			Skew line location x/L				
			0.244	0.375	0.508		

Table 2. Continued

(a) Continued

$[\delta_{v,p} = 0°, \delta_{v,s} = 24°]$

Upper flap x/L			Lower flap x/L			Sidewall x/L	
Left	Center	Right	Left	Center	Right	Left	Right
0.128	0.086		0.176	0.115	0.176	0.120	0.131
.289	.141	0.289	.335	.189	.335	.239	.262
.465	.227	.465	.496	.271	.496	.359	.394
.644	.321	.644	.657	.355	.657	.479	.525
.823	.417	.823	.820	.452	.820	.598	.656
	.514			.540		.718	.788
	.611			.628			
	.709			.716			
	.807			.805			
	.905			.893			
			Skew line location x/L				
			0.244	0.375	0.508		

$[\delta_{v,p} = 0°, \delta_{v,s} = 35°]$

Upper flap x/L			Lower flap x/L			Sidewall x/L	
Left	Center	Right	Left	Center	Right	Left	Right
0.128	0.086		0.176	0.115	0.176	0.108	0.131
.289	.141	0.289	.335	.189	.335	.215	.262
.465	.227	.465	.496	.271	.496	.323	.394
.644	.321	.644	.657	.355	.657	.430	.525
.823	.417	.823	.820	.452	.820	.538	.656
	.514			.540		.645	.788
	.611			.628			
	.709			.716			
	.807			.805			
	.905			.893			
			Skew line location x/L				
			0.244	0.375	0.508		

Table 2. Continued

(a) Continued

$[\delta_{v,p} = 7°, \delta_{v,s} = 35°]$

Upper flap x/L			Lower flap x/L			Sidewall x/L	
Left	Center	Right	Left	Center	Right	Left	Right
0.127	0.085		0.181	0.118	0.181	0.108	0.131
.288	.140	0.288	.330	.194	.335	.215	.262
.463	.226	.463	.497	.278	.495	.323	.394
.641	.320	.641	.663	.364	.661	.430	.525
.820	.415	.820	.829	.450	.827	.538	.656
	.512			.541		.645	.788
	.609			.631			
	.706			.722			
	.804			.813			
	.901			.903			
			Skew line location x/L				
			0.250	0.385	0.522		

$[\delta_{v,p} = 20°, \delta_{v,s} = 35°]$

Upper flap x/L			Lower flap x/L			Sidewall x/L	
Left	Center	Right	Left	Center	Right	Left	Right
0.121	0.081		0.182	0.119	0.182	0.108	0.131
.275	.134	0.275	.329	.195	.338	.215	.262
.441	.216	.441	.491	.280	.499	.323	.394
.611	.304	.611	.654	.367	.658	.430	.525
.781	.395	.781	.817	.449	.820	.538	.656
	.487			.537		.645	.788
	.580			.626			
	.673			.715			
	.766			.804			
	.859			.892			
			Skew line location x/L				
			0.252	0.388	0.526		

Table 2. Continued

(a) Concluded

$[\delta_{v,p} = 25°, \delta_{v,s} = 35°]$

Upper flap x/L			Lower flap x/L			Sidewall x/L	
Left	Center	Right	Left	Center	Right	Left	Right
0.117	0.079		0.180	0.117	0.180	0.108	0.131
.266	.129	0.266	.327	.193	.334	.215	.262
.427	.209	.427	.486	.277	.494	.323	.394
.591	.294	.591	.645	.363	.655	.430	
.755	.382	.755	.804	.447	.814	.538	
	.471			.534		.645	
	.561			.621			
	.650			.708			
	.740			.794			
	.830			.881			
			Skew line location x/L				
			0.249	0.383	0.520		

Table 2. Continued

(b) $\theta_{skew} = 35°$, supersonic expansion ratio, AR = 1.748

$[\delta_{v,p} = 0°, \delta_{v,s} = 0°]$

Upper flap x/L			Lower flap x/L			Sidewall x/L	
Left	Center	Right	Left	Center	Right	Left	Right
0.128	0.086		0.169	0.111	0.169	0.131	0.131
	.140	0.288	.329	.182	.329	.262	.262
	.227	.464	.485	.260	.485	.394	.394
.641	.320	.641	.644	.340	.644	.525	.525
.820		.820	.802	.442	.802	.656	.656
				.528		.788	.788
	.609			.615			
	.706			.701			
	.804			.788			
	.902			.875			
			Skew line location x/L				
			0.244	0.377	0.513		

$[\delta_{v,p} = 0°, \delta_{v,s} = 12°]$

Upper flap x/L			Lower flap x/L			Sidewall x/L	
Left	Center	Right	Left	Center	Right	Left	Right
0.128	0.086		0.169	0.111	0.169	0.128	0.131
.288	.140	0.288	.329	.182	.329	.256	.262
.464	.227	.464	.485	.260	.485	.384	.394
.641	.320	.641	.644	.340	.644	.512	.525
.820	.415	.820	.802	.442	.802	.641	.656
	.512			.528		.769	.788
	.609			.615			
	.706			.701			
	.804			.788			
	.902			.875			
			Skew line location x/L				
			0.244	0.377	0.513		

Table 2. Continued

(b) Continued

$[\delta_{v,p} = 0°, \delta_{v,s} = 24°]$

Upper flap x/L			Lower flap x/L			Sidewall x/L	
Left	Center	Right	Left	Center	Right	Left	Right
0.128	0.086		0.169	0.111	0.169	0.120	0.131
.288	.140	0.288	.329	.182	.329	.239	.262
.464	.227	.464	.485	.260	.485	.359	.394
.641	.320	.641	.644	.340	.644	.479	.525
.820	.415	.820	.802	.442	.802	.598	.656
	.512			.528		.718	.788
	.609			.615			
	.706			.701			
	.804			.788			
	.902			.875			
			Skew line location x/L				
			0.244	0.377	0.513		

$[\delta_{v,p} = 0°, \delta_{v,s} = 35°]$

Upper flap x/L			Lower flap x/L			Sidewall x/L	
Left	Center	Right	Left	Center	Right	Left	Right
0.128	0.086		0.169	0.111	0.169	0.108	0.131
.288	.140	0.288	.329	.182	.329	.215	.262
.464	.227	.464	.485	.260	.485	.323	.394
.641	.320	.641	.644	.340	.644	.430	.525
.820	.415	.820	.802	.442	.802	.538	.656
	.512			.528		.645	.788
	.609			.615			
	.706			.701			
	.804			.788			
	.902			.875			
			Skew line location x/L				
			0.244	0.377	0.513		

Table 2. Continued

(b) Continued

$[\delta_{v,p} = 7°, \delta_{v,s} = 35°]$

Upper flap x/L			Lower flap x/L			Sidewall x/L	
Left	Center	Right	Left	Center	Right	Left	Right
0.128	0.086		0.175	0.115	0.175	0.108	0.131
.289	.141	0.289	.323	.188	.324	.215	.262
.465	.227	.465	.488	.268	.478	.323	.394
.644	.321	.644	.652	.351	.645	.430	.525
.823	.417	.823	.817	.439	.809	.538	.656
	.514			.529		.645	.788
	.611			.618			
	.709			.708			
	.807			.798			
	.905			.888			
			Skew line location x/L				
			0.252	0.390	0.530		

$[\delta_{v,p} = 20°, \delta_{v,s} = 35°]$

Upper flap x/L			Lower flap x/L			Sidewall x/L	
Left	Center	Right	Left	Center	Right	Left	Right
0.124	0.083		0.178	0.117	0.178	0.108	0.131
.280	.136	0.280	.320	.192	.330	.215	.262
.450	.220	.450	.480	.274	.487	.323	.394
.622	.310	.622	.639	.359	.641	.430	.525
.796	.403	.796	.799	.437	.801	.538	.656
	.497			.524		.645	.788
	.591			.611			
	.685			.698			
	.780			.785			
	.875			.872			
			Skew line location x/L				
			0.257	0.398	0.541		

Table 2. Continued

(b) Concluded

$[\delta_{v,p} = 25°, \delta_{v,s} = 35°]$

Upper flap x/L			Lower flap x/L			Sidewall x/L	
Left	Center	Right	Left	Center	Right	Left	Right
0.120	0.081		0.177	0.117	0.177	0.108	0.131
.272	.132	0.272	.318	.190	.328	.215	.262
.438	.214	.438	.474	.272	.485	.323	.394
.606	.302	.606	.629	.356	.638	.430	.525
.774	.392	.774	.784	.436	.794	.538	.656
	.483			.521		.645	
	.575			.605			
	.667			.690			
	.759			.775			
	.851			.859			
			Skew line location x/L				
			0.256	0.396	0.538		

Table 2. Continued

(c) $\theta_{\text{skew}} = 50°$, subsonic and supersonic expansion ratios, AR = 1.748

[$\delta_{v,p} = 0°$, $\delta_{v,s} = 0°$, subsonic expansion ratio]

Upper flap x/L			Lower flap x/L			Sidewall x/L	
Left	Center	Right	Left	Center	Right	Left	Right
0.135	0.067		0.162	0.096	0.162	0.131	0.131
.305	.150	0.305	.326	.176	.316	.262	.262
.478	.243	.478	.487	.260	.471	.393	.393
.652	.336	.652	.647	.344	.652	.524	
.827	.431	.827	.808	.445	.813	.655	
	.526			.533		.786	
	.621			.621			
	.716			.708			
	.811			.796			
	.906			.884			
			Skew line location x/L				
			0.221	0.356	0.492		

[$\delta_{v,p} = 0°$, $\delta_{v,s} = 35°$, subsonic expansion ratio]

Upper flap x/L			Lower flap x/L			Sidewall x/L	
Left	Center	Right	Left	Center	Right	Left	Right
	0.067		0.162	0.096	0.162	0.107	0.131
0.305	.150	0.305	.326	.176	.316	.215	.262
.478	.243	.478	.487	.260	.471	.322	.393
.652	.336	.652	.647	.344	.652	.429	
.827	.431	.827	.808	.445	.813	.537	
	.526			.533		.644	
	.621			.621			
	.716			.708			
	.811			.796			
	.906			.884			
			Skew line location x/L				
			0.221	0.356	0.492		

Table 2. Continued

(c) Continued

[$\delta_{v,p} = 25°$, $\delta_{v,s} = 35°$, subsonic expansion ratio]

Upper flap x/L			Lower flap x/L			Sidewall x/L	
Left	Center	Right	Left	Center	Right	Left	Right
	0.062		0.168	0.099	0.168	0.107	0.131
0.279	.137	0.279	.325	.183	.328	.215	.262
.437	.222	.437	.485	.269	.489	.322	.393
.596	.307	.596	.646	.357	.652	.429	
.755	.394	.755	.806	.445	.812	.537	
	.480			.532		.644	
	.567			.620			
	.654			.707			
	.741			.794			
	.828			.882			
			Skew line location x/L				
			0.230	0.369	0.510		

[$\delta_{v,p} = 0°$, $\delta_{v,s} = 0°$, supersonic expansion ratio]

Upper flap x/L			Lower flap x/L			Sidewall x/L	
Left	Center	Right	Left	Center	Right	Left	Right
0.135	0.067		0.161	0.095	0.161	0.131	0.131
.305	.150	0.305	.324	.174	.312	.262	.262
.478	.242	.478	.485	.257	.466	.393	.393
.652	.336	.652	.645	.340	.649	.524	
.826	.431	.826	.806	.443	.809	.655	
	.525			.530		.786	
	.620			.618			
	.715			.705			
	.810			.793			
	.905			.880			
			Skew line location x/L				
			0.222	0.357	0.493		

Table 2. Continued

(c) Continued

[$\delta_{v,p} = 0°$, $\delta_{v,s} = 35°$, supersonic expansion ratio]

Upper flap x/L			Lower flap x/L			Sidewall x/L	
Left	Center	Right	Left	Center	Right	Left	Right
0.135	0.067		0.161	0.095	0.161	0.107	0.131
.305	.150	0.305	.324	.174	.312	.215	.262
.478	.242	.478	.485	.257	.466	.322	.393
.652	.336	.652	.645	.340	.649	.429	
.826	.431	.826	.806	.443	.809	.537	
	.525			.530		.644	
	.620			.618			
	.715			.705			
	.810			.793			
	.905			.880			
			Skew line location x/L				
			0.222	0.357	0.493		

[$\delta_{v,p} = 25°$, $\delta_{v,s} = 35°$, supersonic expansion ratio]

Upper flap x/L			Lower flap x/L			Sidewall x/L	
Left	Center	Right	Left	Center	Right	Left	Right
0.125	0.062		0.168	0.099	0.168	0.107	0.131
.281	.138	0.281	.323	.182	.326	.215	.262
.440	.223	.440	.482	.268	.487	.322	
.600	.310	.600	.642	.355	.648	.429	
.761	.397	.761	.801	.442	.807	.537	
	.484			.529		.644	
	.571			.616			
	.659			.703			
	.746			.789			
	.834			.876			
			Skew line location x/L				
			0.232	0.373	0.516		

Table 2. Continued

(c) Concluded

[$\delta_{v,p} = 0°$, $\delta_{v,s} = 0°$, short left and right sidewalls]

Upper flap x/L			Lower flap x/L			Sidewall x/L	
Left	Center	Right	Left	Center	Right	Left	Right
0.135	0.067		0.161	0.095	0.161	0.077	0.077
.305	.150	0.305	.324	.174	.312	.154	.154
.478	.242	.478	.485	.257	.466	.231	.231
.652	.336	.652	.645	.340	.649	.308	.308
.826	.431	.826	.806	.443	.809	.385	.385
	.525			.530		.463	
	.620			.618			
	.715			.705			
	.810			.793			
	.905			.880			
			Skew line location x/L				
			0.222	0.357	0.493		

[$\delta_{v,p} = 0°$, $\delta_{v,s} = 0°$, short left sidewall]

Upper flap x/L			Lower flap x/L			Sidewall x/L	
Left	Center	Right	Left	Center	Right	Left	Right
0.135	0.067		0.161	0.095	0.161	0.077	0.131
.305	.150	0.305	.324	.174	.312	.154	.262
.478	.242	.478	.485	.257	.466	.231	.393
.652	.336	.652	.645	.340	.649	.308	
.826	.431	.826	.806	.443	.809	.385	
	.525			.530		.463	
	.620			.618			
	.715			.705			
	.810			.793			
	.905			.880			
			Skew line location x/L				
			0.222	0.357	0.493		

Table 2. Continued

(d) $\theta_{\text{skew}} = 35°$, supersonic expansion ratio, AR = 3.500

$[\delta_{v,p} = 0°,\ \delta_{v,s} = 0°]$

Upper flap x/L			Lower flap x/L			Sidewall x/L	
Left	Center	Right	Left	Center	Right	Left	Right
0.128	0.086		0.178	0.117	0.178	0.131	0.131
	.140	0.289	.330	.192	.331	.262	.262
.464	.227	.464	.500	.275	.490	.394	.394
.642	.320		.669	.360		.525	.525
.821		.821	.839		.827	.656	.656
				.540		.788	.788
	.610			.633			
	.707			.725			
	.805			.818			
	.903			.910			
			Skew line location x/L				
			0.290	0.480	0.672		

$[\delta_{v,p} = 0°,\ \delta_{v,s} = 35°]$

Upper flap x/L			Lower flap x/L			Sidewall x/L	
Left	Center	Right	Left	Center	Right	Left	Right
0.128	0.086		0.178	0.117	0.178	0.108	0.131
	.140	0.289	.330	.192	.331	.215	.262
.464	.227	.464	.500	.275	.490	.323	.394
.642	.320		.669	.360	.649	.430	.525
.821		.821	.839	.446	.827	.538	.656
				.540		.645	.788
	.610			.633			
	.707			.725			
	.805			.818			
	.903			.910			
			Skew line location x/L				
			0.290	0.480	0.672		

Table 2. Concluded

(d) Concluded

$[\delta_{v,p} = 25°, \delta_{v,s} = 35°]$

Upper flap x/L			Lower flap x/L			Sidewall x/L	
Left	Center	Right	Left	Center	Right	Left	Right
0.120	0.080		0.177	0.116	0.177	0.108	0.131
.271	.132	0.271	.325	.190	.329	.215	.262
.436	.213	.436	.476	.273	.486	.323	.394
.603	.301	.603	.626	.357	.645	.430	
.772	.391	.772	.777	.443	.811	.538	
	.482			.534		.645	
	.573			.616			
	.664			.698			
	.756			.780			
	.848			.862			
			Skew line location x/L				
			0.288	0.476	0.667		

Table 3. Skewed-Throat Nozzle Static Pressure Ratios, $p/p_{t,j}$

(a) $\delta_{v,p} = 0°$, $\delta_{v,s} = 0°$, $\theta_{\text{skew}} = 35°$, AR = 1.748, subsonic expansion ratio

[Upper flap]

	$p/p_{t,j}$ for center row x/L of –									
NPR	0.086	0.141	0.227	0.321	0.417	0.514	0.611	0.709	0.807	0.905
2.005	0.672	0.712	0.678	0.627	0.570	0.524	0.481	0.452	0.446	0.471
4.010	.664	.708	.672	.621	.557	.485	.4097	.349	.312	.290
5.006	.662	.706	.671	.620	.556	.485	.409	.348	.310	.290
5.900	.661	.706	.670	.620	.555	.483	.408	.347	.309	.289
7.011	.659	.705	.669	.619	.555	.483	.409	.347	.309	.289
7.820	.657	.705	.668	.619	.555	.483	.408	.346	.308	.289

	$p/p_{t,j}$ for left row x/L of—					$p/p_{t,j}$ for right row x/L of—			
NPR	0.128	0.289	0.465	0.644	0.823	0.289	0.465	0.644	0.823
2.005	0.694	0.616	0.535	0.484	0.450	0.678	0.579	0.469	0.436
4.010	.687	.608	.502	.414	.356	.673	.570	.418	.255
5.006	.686	.608	.501	.412	.355	.672	.570	.417	.255
5.900	.683	.607	.500	.412	.354	.672	.571	.417	.255
7.011	.682	.607	.500	.410	.353	.671	.570	.418	.256
7.820	.681	.607	.501	.410	.353	.671	.570	.417	.257

[Lower flap]

	$p/p_{t,j}$ for center row x/L of -									
NPR	0.115	0.189	0.271	0.355	0.449	0.539	0.629	0.719	0.808	0.898
2.005	0.787	0.745	0.683	0.567	0.399	0.435	0.437	0.448	0.460	0.475
4.010	.781	.737	.681	.565	.217	.386	.411	.383	.347	.319
5.006	.781	.735	.680	.565	.206	.378	.412	.384	.348	.320
5.900	.780	.734	.679	.565	.203	.370	.414	.385	.349	.321
7.011	.778	.732	.678	.565	.224	.360	.412	.386	.350	.322
7.820	.777	.731	.677	.564	.210	.353	.414	.386	.351	.321

	$p/p_{t,j}$ for left row x/L of—					$p/p_{t,j}$ for right row x/L of—				
NPR	0.176	0.330	0.494	0.658	0.823	0.176	0.327	0.483	0.659	0.824
2.005	0.696	0.466	0.514	0.475	0.458	0.772	0.697	0.560	0.433	0.445
4.010	.693	.466	.460	.411	.355	.766	.688	.556	.180	.295
5.006	.691	.469	.458	.409	.354	.764	.687	.555	.183	.287
5.900	.690	.465	.457	.408	.353	.763	.685	.555	.187	.283
7.011	.689	.430	.459	.410	.354	.760	.684	.554	.200	.278
7.820	.688	.432	.457	.409	.354	.759	.683	.554	.207	.275

Table 3. Continued

(a) Concluded

[Sidewalls]

NPR	$p/p_{t,j}$ for left sidewall centerline x/L of—					
	0.131	0.262	0.394	0.525	0.656	0.788
2.005	0.673	0.577	0.532	0.508	0.475	0.449
4.010	.668	.564	.502	.458	.413	.376
5.006	.667	.561	.501	.456	.412	.376
5.900	.666	.560	.500	.455	.411	.375
7.011	.666	.559	.499	.454	.411	.375
7.820	.665	.558	.499	.453	.411	.375
NPR	$p/p_{t,j}$ for right sidewall centerline x/L of—					
	0.131	0.262	0.394	0.525	0.656	0.788
2.005	0.764	0.711	0.644	0.550	0.446	0.402
4.010	.761	.708	.641	.545	.247	.170
5.006	.760	.707	.640	.545	.250	.088
5.900	.759	.706	.639	.545	.252	.088
7.011	.757	.704	.638	.544	.255	.089
7.820	.756	.704	.638	.544	.257	.090

Table 3. Continued

(b) $\delta_{v,p} = 0°$, $\delta_{v,s} = 12°$, $\theta_{\text{skew}} = 35°$, AR = 1.748, subsonic expansion ratio

[Upper flap]

	$p/p_{t,j}$ for center row x/L of—									
NPR	0.086	0.141	0.227	0.321	0.417	0.514	0.611	0.709	0.807	0.905
2.003	0.625	0.671	0.637	0.588	0.527	0.453	0.479	0.457	0.468	0.502
4.006	.615	.665	.624	.568	.514	.438	.356	.278	.213	.162
5.020	.614	.664	.622	.568	.513	.438	.355	.277	.213	.162
5.906	.612	.663	.621	.567	.511	.438	.355	.277	.214	.162
7.001	.609	.661	.619	.566	.507	.437	.355	.277	.214	.163
8.224	.606	.660	.618	.564	.503	.437	.355	.277	.215	.163
8.586	.606	.660	.617	.564	.502	.437	.355	.277	.215	.163

	$p/p_{t,j}$ for left row x/L of—					$p/p_{t,j}$ for right row x/L of—			
NPR	0.128	0.289	0.465	0.644	0.823	0.289	0.465	0.644	0.823
2.003	0.615	0.545	0.442	0.483	0.489	0.652	0.554	0.442	0.482
4.006	.605	.471	.398	.268	.172	.645	.546	.400	.237
5.020	.604	.468	.396	.267	.171	.643	.544	.399	.237
5.906	.603	.467	.397	.266	.171	.642	.543	.399	.237
7.001	.602	.465	.397	.265	.171	.640	.542	.398	.237
8.224	.601	.464	.397	.265	.170	.638	.540	.397	.238
8.586	.601	.464	.397	.265	.170	.637	.540	.397	.238

[Lower flap]

	$p/p_{t,j}$ for center row x/L of—									
NPR	0.115	0.189	0.271	0.355	0.449	0.539	0.629	0.719	0.808	0.898
2.003	0.762	0.715	0.654	0.547	0.386	0.432	0.424	0.427	0.439	0.457
4.006	.758	.707	.648	.543	.162	.184	.195	.204	.199	.210
5.020	.756	.704	.648	.543	.162	.182	.192	.202	.196	.185
5.906	.754	.703	.647	.542	.162	.181	.190	.201	.195	.183
7.001	.753	.701	.646	.542	.161	.180	.188	.197	.192	.181
8.224	.751	.699	.644	.540	.159	.178	.186	.192	.191	.179
8.586	.751	.699	.643	.540	.159	.178	.185	.191	.190	.179

	$p/p_{t,j}$ for left row x/L of—					$p/p_{t,j}$ for right row x/L of—				
NPR	0.176	0.330	0.494	0.658	0.823	0.176	0.327	0.483	0.659	0.824
2.003	0.655	0.352	0.464	0.495	0.493	0.747	0.669	0.545	0.433	0.439
4.006	.652	.183	.215	.266	.235	.740	.663	.538	.160	.219
5.020	.651	.182	.200	.246	.215	.739	.659	.538	.158	.164
5.906	.650	.181	.198	.239	.206	.737	.658	.537	.156	.163
7.001	.649	.180	.195	.229	.201	.735	.657	.536	.155	.162
8.224	.648	.179	.193	.218	.198	.733	.654	.535	.153	.160
8.586	.647	.179	.192	.216	.197	.732	.653	.534	.152	.160

Table 3. Continued

(b) Concluded

[Sidewalls]

NPR	$p/p_{t,j}$ for left sidewall centerline x/L of—					
	0.128	0.256	0.384	0.512	0.641	0.769
2.003	0.430	0.494	0.493	0.507	0.496	0.493
4.006	.427	.369	.292	.248	.224	.198
5.020	.421	.367	.283	.227	.202	.182
5.906	.417	.366	.276	.221	.194	.175
7.001	.412	.365	.271	.220	.187	.170
8.224	.407	.363	.267	.219	.183	.166
8.586	.405	.363	.266	.219	.182	.165

NPR	$p/p_{t,j}$ for right sidewall centerline x/L of—					
	0.131	0.262	0.394	0.525	0.656	0.788
2.003	0.739	0.687	0.623	0.535	0.442	0.421
4.006	.736	.682	.619	.528	.249	.196
5.020	.734	.680	.617	.528	.251	.098
5.906	.733	.679	.616	.527	.254	.097
7.001	.731	.677	.615	.525	.258	.095
8.224	.729	.675	.612	.522	.263	.105
8.586	.728	.674	.611	.521	.265	.105

Table 3. Continued

(c) $\delta_{v,p} = 0°$, $\delta_{v,s} = 24°$, $\theta_{\text{skew}} = 35°$, AR = 1.748, subsonic expansion ratio

[Upper flap]

	$p/p_{t,j}$ for center row x/L of—									
NPR	0.086	0.141	0.227	0.321	0.417	0.514	0.611	0.709	0.807	0.905
2.010	0.624	0.671	0.636	0.584	0.522	0.447	0.405	0.466	0.505	0.491
4.003	.613	.664	.623	.568	.504	.427	.344	.266	.202	.152
5.005	.612	.664	.622	.567	.504	.426	.343	.266	.202	.153
5.908	.610	.663	.621	.567	.504	.426	.343	.266	.203	.153
7.009	.608	.661	.620	.566	.503	.426	.342	.266	.203	.153
8.202	.605	.660	.618	.567	.503	.426	.342	.267	.204	.154

	$p/p_{t,j}$ for left row x/L of—					$p/p_{t,j}$ for right row x/L of—				
NPR	0.128	0.289	0.465	0.644	0.823		0.289	0.465	0.644	0.823
2.010	0.616	0.530	0.446	0.473	0.501		0.650	0.552	0.424	0.502
4.003	.604	.467	.344	.228	.145		.643	.545	.398	.235
5.005	.603	.466	.344	.227	.145		.643	.544	.399	.234
5.908	.602	.466	.344	.227	.145		.642	.543	.399	.235
7.009	.601	.465	.344	.226	.144		.640	.543	.399	.235
8.202	.600	.464	.343	.226	.145		.638	.544	.399	.235

[Lower flap]

	$p/p_{t,j}$ for center row x/L of—									
NPR	0.115	0.189	0.271	0.355	0.449	0.539	0.629	0.719	0.808	0.898
2.010	0.762	0.714	0.655	0.546	0.370	0.393	0.427	0.444	0.443	0.455
4.003	.756	.706	.649	.544	.157	.184	.192	.190	.179	.174
5.005	.756	.705	.648	.543	.159	.183	.190	.188	.177	.160
5.908	.753	.703	.647	.543	.160	.182	.189	.187	.176	.159
7.009	.752	.701	.647	.542	.161	.180	.188	.186	.174	.158
8.202	.751	.699	.645	.541	.160	.179	.186	.185	.173	.157

	$p/p_{t,j}$ for left row x/L of—					$p/p_{t,j}$ for right row x/L of—				
NPR	0.176	0.330	0.494	0.658	0.823	0.176	0.327	0.483	0.659	0.824
2.010	0.655	0.333	0.428	0.506	0.499	0.753	0.671	0.542	0.428	0.430
4.003	.651	.179	.177	.207	.221	.742	.661	.538	.160	.217
5.005	.651	.180	.176	.152	.155	.740	.659	.537	.158	.161
5.908	.650	.179	.175	.152	.129	.738	.658	.537	.157	.162
7.009	.649	.178	.174	.151	.129	.736	.656	.536	.155	.160
8.202	.648	.176	.172	.150	.128	.734	.654	.536	.153	.159

Table 3. Continued

(c) Concluded

[Sidewalls]

NPR	$p/p_{t,j}$ for left sidewall centerline x/L of—					
	0.120	0.239	0.359	0.479	0.598	0.718
2.010	0.421	0.474	0.498	0.498	0.496	0.497
4.003	.211	.258	.253	.259	.233	.246
5.005	.211	.256	.185	.191	.185	.170
5.908	.212	.255	.181	.149	.150	.143
7.009	.213	.253	.179	.135	.124	.117
8.202	.212	.251	.177	.131	.105	.101

NPR	$p/p_{t,j}$ for right sidewall centerline x/L of—					
	0.131	0.262	0.394	0.525	0.656	0.788
2.010	0.740	0.687	0.623	0.533	0.439	0.422
4.003	.735	.683	.617	.528	.247	.205
5.005	.735	.681	.617	.528	.247	.108
5.908	.733	.680	.616	.527	.250	.107
7.009	.731	.678	.613	.525	.254	.110
8.202	.729	.676	.613	.524	.258	.117

Table 3. Continued

(d) $\delta_{v,p} = 0°$, $\delta_{v,s} = 35°$, $\theta_{\text{skew}} = 35°$, AR = 1.748, subsonic expansion ratio

[Upper flap]

	$p/p_{t,j}$ for center row x/L of—									
NPR	0.086	0.141	0.227	0.321	0.417	0.514	0.611	0.709	0.807	0.905
2.006	0.629	0.677	0.643	0.593	0.529	0.454	0.379	0.454	0.535	0.498
4.004	.612	.664	.623	.570	.505	.427	.344	.267	.203	.153
5.007	.611	.663	.621	.568	.503	.426	.344	.267	.202	.153
5.901	.609	.662	.620	.567	.503	.426	.343	.267	.203	.153
7.002	.607	.661	.619	.567	.503	.426	.344	.267	.204	.154
7.998	.606	.660	.618	.566	.502	.426	.344	.268	.204	.154

	$p/p_{t,j}$ for left row x/L of—					$p/p_{t,j}$ for right row x/L of				
NPR	0.128	0.289	0.465	0.644	0.823		0.289	0.465	0.644	0.823
2.006	0.629	0.546	0.452	0.463	0.521		0.653	0.555	0.411	0.542
4.004	.603	.465	.345	.228	.145		.643	.544	.400	.236
5.007	.602	.464	.344	.227	.145		.640	.543	.399	.236
5.901	.601	.463	.343	.227	.145		.640	.543	.399	.236
7.002	.601	.462	.343	.227	.145		.639	.543	.401	.237
7.998	.600	.462	.343	.226	.145		.637	.542	.401	.237

[Lower flap]

	$p/p_{t,j}$ for center row x/L of									
NPR	0.115	0.189	0.271	0.355	0.449	0.539	0.629	0.719	0.808	0.898
2.006	0.762	0.717	0.658	0.549	0.332	0.351	0.384	0.417	0.451	0.477
4.004	.755	.705	.648	.542	.157	.183	.190	.188	.176	.160
5.007	.753	.703	.647	.541	.158	.181	.188	.186	.174	.158
5.901	.752	.702	.646	.541	.159	.180	.187	.185	.174	.158
7.002	.752	.701	.646	.541	.159	.179	.186	.184	.173	.157
7.998	.751	.699	.645	.540	.158	.178	.184	.183	.172	.156

	$p/p_{t,j}$ for left row x/L of—					$p/p_{t,j}$ for right row x/L of				
NPR	0.176	0.330	0.494	0.658	0.823	0.176	0.327	0.483	0.659	0.824
2.006	0.660	0.341	0.483	0.506	0.505	0.752	0.672	0.546	0.407	0.439
4.004	.650	.177	.173	.215	.226	.741	.660	.538	.158	.196
5.007	.649	.177	.171	.148	.147	.739	.657	.536	.157	.163
5.901	.649	.176	.170	.148	.127	.737	.656	.535	.156	.162
7.002	.648	.175	.169	.147	.126	.735	.655	.535	.154	.162
7.998	.647	.174	.168	.146	.126	.733	.654	.534	.153	.161

Table 3. Continued

(d) Concluded

[Sidewalls]

NPR	$p/p_{t,j}$ for left sidewall centerline x/L of—					
	0.108	0.215	0.323	0.430	0.538	0.645
2.006	0.497	0.497	0.498	0.498	0.498	0.498
4.004	.110	.233	.286	.257	.257	.254
5.007	.109	.160	.236	.217	.203	.205
5.901	.109	.155	.163	.195	.170	.174
7.002	.109	.154	.128	.163	.147	.136
7.998	.109	.152	.116	.130	.132	.118
NPR	$p/p_{t,j}$ for right sidewall centerline x/L of—					
	0.131	0.262	0.394	0.525	0.656	0.788
2.006	0.741	0.689	0.625	0.538	0.448	0.423
4.004	.735	.680	.617	.528	.261	.196
5.007	.733	.678	.614	.527	.263	.119
5.901	.733	.677	.613	.526	.264	.118
7.002	.732	.677	.614	.528	.267	.116
7.998	.730	.676	.612	.527	.270	.116

Table 3. Continued

(e) $\delta_{v,p} = 7°$, $\delta_{v,s} = 35°$, $\theta_{\text{skew}} = 35°$, AR = 1.748, subsonic expansion ratio

[Upper flap]

	$p/p_{t,j}$ for center row x/L of—									
NPR	0.085	0.140	0.226	0.320	0.415	0.512	0.609	0.706	0.804	0.901
2.004	0.477	0.612	0.583	0.546	0.500	0.452	0.404	0.392	0.544	0.517
4.001	.421	.595	.553	.504	.451	.399	.342	.282	.227	.182
5.000	.423	.595	.552	.502	.450	.398	.341	.281	.227	.182
5.905	.421	.594	.551	.501	.449	.398	.341	.280	.227	.182
6.999	.414	.593	.549	.501	.448	.397	.341	.280	.227	.182
8.202	.373	.591	.548	.499	.447	.396	.340	.280	.227	.182
8.424	.369	.591	.548	.499	.447	.396	.340	.280	.227	.182

	$p/p_{t,j}$ for left row x/L of—						$p/p_{t,j}$ for right row x/L of—			
NPR	0.127	0.288	0.463	0.641	0.820		0.288	0.463	0.641	0.820
2.004	0.582	0.521	0.465	0.443	0.526		0.584	0.513	0.414	0.543
4.001	.559	.409	.313	.232	.161		.564	.488	.390	.275
5.000	.559	.408	.313	.230	.159		.562	.487	.389	.274
5.905	.558	.408	.312	.230	.158		.561	.486	.389	.274
6.999	.558	.407	.311	.229	.158		.559	.484	.388	.274
8.202	.558	.406	.310	.228	.158		.557	.482	.387	.274
8.424	.558	.406	.310	.228	.158		.557	.482	.386	.274

[Lower flap]

	$p/p_{t,j}$ for center row x/L of—									
NPR	0.118	0.194	0.278	0.364	0.450	0.541	0.631	0.722	0.813	0.903
2.004	0.659	0.623	0.576	0.484	0.289	0.291	0.347	0.495	0.525	0.519
4.001	.648	.605	.556	.471	.123	.129	.128	.201	.241	.247
5.000	.646	.602	.554	.472	.124	.129	.127	.123	.118	.123
5.905	.646	.601	.553	.471	.125	.128	.126	.122	.116	.106
6.999	.645	.599	.552	.471	.126	.127	.125	.121	.115	.106
8.202	.643	.597	.550	.470	.126	.126	.125	.120	.114	.106
8.424	.642	.596	.550	.470	.126	.126	.124	.120	.114	.106

	$p/p_{t,j}$ for left row x/L of—					$p/p_{t,j}$ for right row x/L of—				
NPR	0.181	0.330	0.497	0.663	0.829	0.181	0.335	0.495	0.661	0.827
2.004	0.578	0.267	0.498	0.501	0.498	0.649	0.585	0.482	0.415	0.445
4.001	.559	.128	.213	.217	.224	.635	.562	.467	.116	.209
5.000	.558	.128	.120	.169	.167	.632	.560	.465	.116	.155
5.905	.558	.128	.114	.141	.146	.630	.558	.465	.115	.110
6.999	.556	.128	.113	.096	.129	.627	.557	.463	.113	.109
8.202	.556	.127	.112	.094	.081	.625	.555	.462	.112	.109
8.424	.555	.127	.112	.094	.081	.624	.554	.462	.112	.109

Table 3. Continued

(e) Concluded

[Sidewalls]

NPR	$p/p_{t,j}$ for left sidewall centerline x/L of—					
	0.108	0.215	0.323	0.430	0.538	0.645
2.004	0.497	0.499	0.498	0.499	0.498	0.499
4.001	.100	.227	.250	.251	.251	.251
5.000	.092	.120	.228	.222	.206	.207
5.905	.092	.103	.171	.202	.179	.173
6.999	.092	.100	.121	.172	.158	.149
8.202	.092	.099	.107	.129	.137	.126
8.424	.093	.098	.107	.122	.133	.123

NPR	$p/p_{t,j}$ for right sidewall centerline x/L of—					
	0.131	0.262	0.394	0.525	0.656	0.788
2.004	0.653	0.608	0.555	0.493	0.452	0.451
4.001	.642	.591	.535	.475	.375	.202
5.000	.639	.590	.533	.473	.374	.200
5.905	.638	.587	.532	.472	.373	.201
6.999	.635	.586	.530	.471	.374	.200
8.202	.633	.584	.529	.469	.374	.201
8.424	.632	.583	.528	.469	.374	.201

Table 3. Continued

(f) $\delta_{v,p} = 20°$, $\delta_{v,s} = 35°$, $\theta_{\text{skew}} = 35°$, AR = 1.748, subsonic expansion ratio

[Upper flap]

	$p/p_{t,j}$ for center row x/L of									
NPR	0.081	0.134	0.216	0.304	0.395	0.487	0.580	0.673	0.766	0.859
2.001	0.557	0.570	0.499	0.426	0.523	0.505	0.487	0.477	0.494	0.514
4.006	.550	.567	.491	.405	.324	.376	.333	.291	.256	.218
5.006	.549	.567	.491	.405	.324	.375	.332	.290	.255	.217
5.913	.548	.567	.491	.405	.323	.369	.331	.289	.255	.216
7.011	.547	.567	.490	.405	.323	.356	.329	.288	.255	.216
8.212	.546	.566	.490	.404	.323	.351	.329	.287	.254	.217
9.023	.546	.566	.490	.405	.324	.352	.325	.286	.253	.216
9.628	.546	.566	.490	.405	.324	.352	.324	.286	.252	.216

	$p/p_{t,j}$ for left row x/L of –						$p/p_{t,j}$ for right row x/L of—			
NPR	0.121	0.275	0.441	0.611	0.781		0.275	0.441	0.611	0.781
2.001	0.569	0.457	0.507	0.486	0.498		0.453	0.515	0.478	0.503
4.006	.560	.370	.224	.249	.254		.449	.453	.372	.301
5.006	.559	.370	.223	.228	.181		.449	.450	.372	.300
5.913	.559	.369	.222	.228	.180		.448	.443	.372	.298
7.011	.559	.369	.222	.224	.179		.448	.426	.371	.297
8.212	.559	.369	.221	.217	.179		.446	.399	.369	.297
9.023	.559	.369	.222	.214	.178		.447	.397	.366	.296
9.628	.559	.369	.221	.214	.178		.447	.394	.365	.296

[Lower flap]

	$p/p_{t,j}$ for center row x/L of—									
NPR	0.119	0.195	0.280	0.367	0.449	0.537	0.626	0.715	0.804	0.892
2.001	0.400	0.539	0.508	0.458	0.457	0.450	0.456	0.467	0.478	0.485
4.006	.388	.490	.466	.398	.200	.216	.222	.228	.233	.237
5.006	.383	.485	.465	.398	.100	.101	.161	.167	.175	.185
5.913	.381	.480	.465	.398	.101	.092	.089	.141	.151	.162
7.011	.381	.476	.464	.397	.101	.092	.085	.078	.103	.127
8.212	.379	.473	.462	.395	.100	.091	.084	.078	.070	.073
9.023	.380	.475	.461	.391	.099	.091	.084	.077	.070	.062
9.628	.379	.473	.461	.391	.099	.091	.084	.077	.070	.062

	$p/p_{t,j}$ for left row x/L of– –					$p/p_{t,j}$ for right row x/L of—				
NPR	0.182	0.329	0.491	0.654	0.817	0.182	0.338	0.499	0.658	0.820
2.001	0.515	0.472	0.488	0.493	0.496	0.510	0.500	0.472	0.471	0.478
4.006	.441	.236	.241	.244	.245	.470	.470	.382	.196	.222
5.006	.436	.175	.187	.190	.193	.461	.469	.382	.082	.189
5.913	.435	.097	.153	.156	.160	.462	.467	.382	.082	.149
7.011	.434	.096	.127	.126	.124	.461	.466	.381	.082	.074
8.212	.431	.095	.081	.110	.109	.462	.464	.381	.081	.070
9.023	.432	.095	.072	.098	.097	.458	.461	.381	.081	.070
9.628	.431	.095	.072	.091	.093	.457	.460	.381	.081	.069

Table 3. Continued

(f) Concluded

[Sidewalls]

NPR	$p/p_{t,j}$ for left sidewall centerline x/L of—					
	0.108	0.215	0.323	0.430	0.538	0.645
2.001	0.497	0.498	0.499	0.498	0.499	0.499
4.006	.239	.241	.244	.246	.247	.248
5.006	.103	.188	.196	.199	.203	.204
5.913	.086	.153	.168	.171	.175	.177
7.011	.087	.086	.144	.148	.149	.150
8.212	.087	.079	.113	.130	.136	.132
9.023	.087	.079	.070	.112	.119	.139
9.628	.087	.079	.068	.101	.107	.125

NPR	$p/p_{t,j}$ for right sidewall centerline x/L of—					
	0.131	0.262	0.394	0.525	0.656	0.788
2.001	0.511	0.498	0.516	0.497	0.461	0.514
4.006	.509	.427	.446	.413	.364	.339
5.006	.509	.427	.445	.410	.365	.336
5.913	.508	.424	.445	.406	.365	.335
7.011	.507	.422	.444	.399	.366	.334
8.212	.506	.419	.442	.392	.366	.325
9.023	.508	.414	.440	.390	.365	.324
9.628	.508	.412	.438	.387	.365	.323

Table 3. Continued

(g) $\delta_{v,p} = 25°$, $\delta_{v,s} = 35°$, $\theta_{\text{skew}} = 35°$, AR = 1.748, subsonic expansion ratio

[Upper flap]

	$p/p_{t,j}$ for center row x/L of									
NPR	0.079	0.129	0.209	0.294	0.382	0.471	0.561	0.650	0.740	0.830
2.001	0.859	0.819	0.769	0.720	0.672	0.623	0.563	0.489	0.439	0.427
4.001	.850	.808	.750	.694	.642	.595	.536	.463	.374	.282
5.003	.848	.807	.749	.692	.641	.592	.535	.462	.374	.283
5.901	.848	.805	.746	.691	.639	.591	.534	.462	.374	.284
6.793	.847	.805	.744	.689	.637	.589	.532	.462	.374	.284

	$p/p_{t,j}$ for left row x/L of—					$p/p_{t,j}$ for right row x/L of—				
NPR	0.117	0.266	0.427	0.591	0.755		0.266	0.427	0.591	0.755
2.001	0.798	0.675	0.581	0.482	0.471		0.764	0.690	0.603	0.473
4.001	.783	.627	.508	.393	.252		.748	.671	.589	.454
5.003	.781	.625	.506	.392	.252		.747	.669	.587	.454
5.901	.781	.623	.504	.391	.252		.745	.667	.586	.454
6.793	.779	.821	.502	.391	.252		.742	.665	.584	.454

[Lower flap]

	$p/p_{t,j}$ for center row x/L of—									
NPR	0.117	0.193	0.277	0.363	0.447	0.534	0.621	0.708	0.794	0.881
2.001	0.686	0.672	0.633	0.540	0.403	0.407	0.410	0.417	0.427	0.451
4.001	.662	.646	.609	.528	.155	.168	.174	.172	.165	.193
5.003	.658	.642	.607	.527	.154	.167	.172	.171	.162	.145
5.901	.656	.640	.604	.527	.152	.165	.171	.169	.161	.145
6.793	.653	.638	.603	.526	.151	.164	.169	.168	.160	.145

	$p/p_{t,j}$ for left row x/L of—					$p/p_{t,j}$ for right row x/L of—				
NPR	0.180	0.327	0.486	0.645	0.804	0.180	0.334	0.494	0.655	0.814
2.001	0.598	0.361	0.449	0.490	0.496	0.709	0.660	0.543	0.416	0.425
4.001	.554	.143	.239	.243	.230	.689	.641	.534	.157	.214
5.003	.553	.140	.147	.193	.182	.686	.639	.533	.155	.156
5.901	.551	.140	.141	.140	.147	.683	.636	.532	.154	.156
6.793	.550	.138	.140	.137	.123	.680	.634	.530	.152	.156

Table 3. Continued

(g) Concluded

[Sidewalls]

NPR	$p/p_{t,j}$ for left sidewall centerline x/L of—					
	0.108	0.215	0.323	0.430	0.538	0.645
2.001	0.481	0.481	0.501	0.505	0.502	0.501
4.001	.118	.287	.323	.275	.228	.257
5.003	.118	.268	.231	.248	.193	.177
5.901	.118	.256	.207	.212	.182	.138
6.793	.117	.246	.194	.182	.160	.142

NPR	$p/p_{t,j}$ for right sidewall centerline x/L of—					
	0.131	0.262	0.394			
2.001	0.782	0.737	0.686			
4.001	.768	.721	.670			
5.003	.766	.720	.666			
5.901	.764	.717	.663			
6.793	.761	.714	.660			

Table 3. Continued

(h) $\delta_{v,p} = 0°$, $\delta_{v,s} = 0°$, $\theta_{\text{skew}} = 35°$, AR = 1.748, supersonic expansion ratio

[Upper flap]

NPR	$p/p_{t,j}$ for center row x/L of							
	0.086	0.140	0.227	0.320	0.609	0.706	0.804	0.902
4.004	0.620	0.674	0.646	0.594	0.365	0.292	0.232	0.187
5.998	.618	.674	.645	.594	.365	.292	.233	.187
8.024	.616	.672	.644	.595	.366	.293	.234	.188
9.006	.616	.674	.644	.595	.366	.294	.235	.188
9.902	.615	.674	.644	.595	.367	.295	.236	.189
11.002	.615	.675	.638	.595	.368	.296	.235	.187
11.373	.615	.675	.617	.595	.368	.296	.237	.189

NPR	$p/p_{t,j}$ for left row x/L of—				$p/p_{t,j}$ for right row x/L of—			
	0.128	0.641	0.820		0.288	0.464	0.641	0.820
4.004	0.658	0.330	0.243		0.650	0.544	0.391	0.231
5.998	.658	.329	.242		.649	.544	.392	.232
8.024	.657	.330	.242		.648	.544	.393	.232
9.006	.658	.330	.242		.648	.544	.394	.233
9.902	.658	.331	.242		.647	.544	.394	.234
11.002	.658	.328	.240		.646	.544	.395	.235
11.373	.658	.332	.243		.646	.544	.395	.235

[Lower flap]

NPR	$p/p_{t,j}$ for center row x/L of—									
	0.111	0.182	0.260	0.340	0.439	0.528	0.618	0.707	0.796	0.886
4.004	0.793	0.744	0.686	0.590	0.095	0.181	0.200	0.230	0.262	0.268
5.998	.792	.743	.684	.589	.086	.118	.214	.226	.266	.249
8.024	.791	.741	.683	.588	.086	.118	.208	.220	.257	.250
9.006	.790	.740	.681	.587	.086	.120	.206	.218	.253	.250
9.902	.789	.739	.681	.586	.087	.124	.205	.216	.250	.250
11.002	.788	.738	.680	.586	.087	.129	.204	.214	.246	.250
11.373	.788	.738	.679	.585	.087	.130	.203	.214	.246	.250

NPR	$p/p_{t,j}$ for left row x/L of—					$p/p_{t,j}$ for right row x/L of—				
	0.169	0.323	0.487	0.651	0.814	0.169	0.313	0.462	0.644	0.808
4.004	0.705	0.149	0.344	0.320	0.274	0.773	0.692	0.575	0.190	0.207
5.998	.703	.177	.348	.304	.260	.771	.690	.573	.090	.178
8.024	.701	.198	.350	.304	.260	.769	.689	.572	.089	.152
9.006	.700	.203	.350	.304	.260	.768	.688	.571	.089	.154
9.902	.699	.204	.349	.304	.260	.767	.688	.571	.088	.155
11.002	.698	.206	.348	.304	.260	.767	.687	.570	.088	.155
11.373	.698	.205	.347	.304	.260	.766	.686	.570	.087	.155

Table 3. Continued

(h) Concluded

[Sidewalls]

NPR	$p/p_{t,j}$ for left sidewall centerline x/L of—					
	0.131	0.262	0.394	0.525	0.656	0.788
4.004	0.641	0.494	0.398	0.343	0.303	0.269
5.998	.641	.493	.397	.341	.302	.266
8.024	.641	.493	.396	.339	.301	.264
9.006	.641	.493	.396	.338	.300	.263
9.902	.641	.493	.396	.338	.299	.262
11.002	.641	.493	.396	.432	.314	.258
11.373	.641	.493	.395	.337	.298	.261
NPR	$p/p_{t,j}$ for right sidewall centerline x/L of—					
	0.131	0.262	0.394	0.525	0.656	0.788
4.004	0.754	0.699	0.633	0.542	0.228	0.219
5.998	.753	.698	.632	.543	.102	.126
8.024	.751	.696	.632	.542	.099	.056
9.006	.751	.696	.632	.541	.102	.056
9.902	.750	.695	.631	.541	.104	.056
11.002	.749	.694	.630	.540	.107	.056
11.373	.749	.694	.630	.540	.108	.056

Table 3. Continued

(i) $\delta_{v,p} = 0°$, $\delta_{v,s} = 12°$, $\theta_{\text{skew}} = 35°$, AR = 1.748, supersonic expansion ratio

[Upper flap]

	$p/p_{t,j}$ for center row x/L of									
NPR	0.086	0.140	0.227	0.320	0.415	0.512	0.609	0.706	0.804	0.902
2.006	0.604	0.657	0.635	0.597	0.554	0.520	0.505	0.508	0.507	0.502
4.012	.588	.641	.605	.552	.484	.416	.336	.261	.200	.153
5.995	.581	.640	.604	.552	.483	.414	.334	.261	.200	.152
8.012	.574	.638	.603	.552	.482	.412	.334	.261	.201	.153
9.065	.570	.637	.602	.551	.482	.411	.334	.262	.201	.154

	$p/p_{t,j}$ for left row x/L of—					$p/p_{t,j}$ for right row x/L of—				
NPR	0.128	0.288	0.464	0.641	0.820		0.288	0.464	0.641	0.820
2.006	0.605	0.558	0.513	0.505	0.505		0.647	0.568	0.510	0.506
4.012	.585	.445	.378	.248	.161		.626	.526	.380	.223
5.995	.584	.443	.376	.245	.160		.625	.525	.380	.223
8.012	.584	.442	.376	.245	.160		.623	.524	.381	.223
9.065	.584	.442	.376	.245	.160		.622	.524	.381	.222

[Lower flap]

	$p/p_{t,j}$ for center row x/L of—									
NPR	0.111	0.182	0.260	0.340	0.439	0.528	0.618	0.707	0.796	0.886
2.006	0.783	0.735	0.675	0.592	0.496	0.495	0.494	0.494	0.494	0.493
4.012	.773	.722	.660	.566	.194	.200	.215	.220	.222	.221
5.995	.773	.719	.657	.565	.079	.098	.106	.109	.109	.131
8.012	.771	.717	.655	.563	.079	.096	.104	.108	.107	.101
9.065	.769	.716	.654	.562	.079	.095	.104	.107	.107	.101

	$p/p_{t,j}$ for left row x/L of—					$p/p_{t,j}$ for right row x/L of—				
NPR	0.169	0.323	0.487	0.651	0.814	0.169	0.313	0.462	0.644	0.808
2.006	0.681	0.493	0.492	0.494	0.496	0.767	0.688	0.586	0.495	0.493
4.012	.672	.179	.208	.215	.229	.754	.671	.559	.229	.225
5.995	.670	.101	.112	.147	.155	.752	.668	.556	.083	.132
8.012	.668	.099	.110	.126	.125	.750	.667	.555	.082	.090
9.065	.667	.099	.108	.122	.122	.749	.666	.554	.082	.089

Table 3. Continued

(i) Concluded

[Sidewalls]

NPR	$p/p_{t,j}$ for left sidewall centerline x/L of—					
	0.128	0.256	0.384	0.512	0.641	0.769
2.006	0.546	0.515	0.499	0.495	0.498	0.501
4.012	.434	.341	.248	.224	.240	.220
5.995	.425	.338	.238	.198	.153	.128
8.012	.416	.337	.236	.197	.152	.122
9.065	.411	.336	.235	.196	.152	.122
NPR	$p/p_{t,j}$ for right sidewall centerline x/L of					
	0.131	0.262	0.394	0.525	0.656	0.788
2.006	0.745	0.692	0.636	0.559	0.499	0.494
4.012	.735	.679	.615	.529	.223	.209
5.995	.733	.677	.614	.530	.127	.125
8.012	.730	.675	.613	.529	.132	.051
9.065	.729	.674	.612	.529	.136	.050

Table 3. Continued

(j) $\delta_{v,p} = 0°$, $\delta_{v,s} = 24°$, $\theta_{\text{skew}} = 35°$, AR = 1.748, supersonic expansion ratio

[Upper flap]

	$p/p_{t,j}$ for center row x/L of—									
NPR	0.086	0.140	0.227	0.320	0.415	0.512	0.609	0.706	0.804	0.902
2.001	0.603	0.661	0.629	0.594	0.553	0.523	0.510	0.510	0.510	0.505
3.996	.587	.645	.606	.552	.483	.404	.323	.250	.189	.143
6.011	.581	.644	.605	.552	.482	.404	.323	.250	.190	.144
7.997	.573	.642	.603	.551	.482	.403	.323	.251	.191	.144
9.021	.568	.642	.601	.551	.481	.403	.323	.251	.192	.145

	$p/p_{t,j}$ for left row x/L of—					$p/p_{t,j}$ for right row x/L of—				
NPR	0.128	0.288	0.464	0.641	0.820		0.288	0.464	0.641	0.820
2.001	0.597	0.551	0.516	0.508	0.508		0.644	0.567	0.514	0.509
3.996	.585	.444	.322	.212	.138		.626	.525	.378	.220
6.011	.584	.443	.321	.211	.136		.625	.525	.378	.220
7.997	.584	.442	.321	.210	.136		.623	.524	.379	.221
9.021	.584	.442	.321	.210	.136		.621	.523	.380	.221

[Lower flap]

	$p/p_{t,j}$ for center row x/L of—									
NPR	0.111	0.182	0.260	0.340	0.439	0.528	0.618	0.707	0.796	0.886
2.001	0.783	0.732	0.672	0.588	0.498	0.497	0.497	0.497	0.496	0.495
3.996	.774	.721	.659	.567	.166	.196	.206	.223	.224	.218
6.011	.773	.719	.657	.565	.079	.097	.106	.108	.106	.125
7.997	.770	.717	.655	.563	.079	.096	.104	.107	.105	.096
9.021	.769	.715	.653	.562	.079	.095	.103	.106	.104	.096

	$p/p_{t,j}$ for left row x/L of—					$p/p_{t,j}$ for right row x/L of—				
NPR	0.169	0.323	0.487	0.651	0.814	0.169	0.313	0.462	0.644	0.808
2.001	0.681	0.495	0.495	0.497	0.498	0.768	0.687	0.583	0.496	0.495
3.996	.672	.097	.231	.231	.233	.755	.671	.557	.230	.225
6.011	.670	.099	.105	.146	.144	.752	.669	.555	.083	.131
7.997	.668	.099	.104	.089	.097	.749	.666	.553	.082	.090
9.021	.667	.098	.103	.089	.076	.748	.665	.551	.081	.089

Table 3. Continued

(j) Concluded

[Sidewalls]

NPR	$p/p_{t,j}$ for left sidewall centerline x/L of—					
	0.120	0.239	0.359	0.479	0.598	0.718
2.001	0.384	0.512	0.519	0.506	0.502	0.501
3.996	.212	.242	.246	.264	.238	.257
6.011	.214	.240	.157	.139	.148	.146
7.997	.213	.238	.155	.113	.092	.094
9.021	.211	.236	.154	.111	.088	.076
NPR	$p/p_{t,j}$ for right sidewall centerline x/L of—					
	0.131	0.262	0.394	0.525	0.656	0.788
2.001	0.743	0.690	0.633	0.558	0.501	0.498
3.996	.734	.677	.614	.530	.220	.210
6.011	.732	.677	.613	.533	.122	.124
7.997	.730	.674	.612	.532	.125	.051
9.021	.728	.673	.611	.532	.130	.051

Table 3. Continued

(k) $\delta_{v,p} = 0°$, $\delta_{v,s} = 35°$, $\theta_{\text{skew}} = 35°$, AR = 1.748, supersonic expansion ratio

[Upper flap]

NPR	$p/p_{t,j}$ for center row x/L of—									
	0.086	0.140	0.227	0.320	0.415	0.512	0.609	0.706	0.804	0.902
2.004	0.598	0.655	0.622	0.572	0.506	0.441	0.412	0.485	0.515	0.492
3.999	.582	.644	.602	.549	.482	.404	.324	.251	.190	.143
6.005	.576	.643	.600	.548	.481	.403	.323	.251	.190	.143
8.599	.566	.641	.597	.547	.480	.403	.323	.251	.191	.144

NPR	$p/p_{t,j}$ for left row x/L of—						$p/p_{t,j}$ for right row x/L of—			
	0.128	0.288	0.464	0.641	0.820		0.288	0.464	0.641	0.820
2.004	0.607	0.528	0.439	0.492	0.514		0.634	0.535	0.431	0.521
3.999	.582	.443	.323	.212	.136		.624	.524	.378	.222
6.005	.581	.444	.323	.211	.136		.623	.524	.378	.221
8.599	.580	.442	.322	.210	.136		.621	.522	.379	.225

[Lower flap]

NPR	$p/p_{t,j}$ for center row x/L of—									
	0.111	0.182	0.260	0.340	0.439	0.528	0.618	0.707	0.796	0.886
2.004	0.780	0.730	0.665	0.576	0.373	0.349	0.368	0.415	0.459	0.475
3.999	.772	.720	.656	.565	.203	.201	.201	.201	.203	.206
6.005	.771	.717	.656	.564	.079	.097	.105	.107	.105	.133
8.599	.769	.715	.653	.562	.078	.095	.103	.105	.103	.095

NPR	$p/p_{t,j}$ for left row x/L of—					$p/p_{t,j}$ for right row x/L of—				
	0.169	0.323	0.487	0.651	0.814	0.169	0.313	0.462	0.644	0.808
2.004	0.681	0.211	0.529	0.500	0.498	0.762	0.683	0.566	0.434	0.440
3.999	.672	.169	.223	.205	.218	.753	.670	.557	.221	.219
6.005	.670	.098	.105	.139	.139	.750	.667	.555	.082	.136
8.599	.668	.098	.103	.089	.077	.746	.664	.552	.081	.091

Table 3. Continued

(k) Concluded

[Sidewalls]

NPR	$p/p_{t,j}$ for left sidewall centerline x/L of—					
	0.108	0.215	0.323	0.430	0.538	0.645
2.004	0.497	0.498	0.499	0.499	0.498	0.499
3.999	.108	.223	.292	.262	.255	.253
6.005	.107	.149	.142	.191	.168	.174
8.599	.106	.145	.098	.102	.119	.113

NPR	$p/p_{t,j}$ for right sidewall centerline x/L of—					
	0.131	0.262	0.394	0.525	0.656	0.788
2.004	0.737	0.684	0.617	0.533	0.484	0.461
3.999	.732	.676	.611	.527	.220	.217
6.005	.730	.674	.609	.526	.117	.143
8.599	.727	.671	.608	.522	.117	.105

Table 3. Continued

(l) $\delta_{v,p} = 7°$, $\delta_{v,s} = 35°$, $\theta_{\text{skew}} = 35°$, AR = 1.748, supersonic expansion ratio

[Upper flap]

NPR	$p/p_{t,j}$ for center row x/L of—									
	0.086	0.141	0.227	0.321	0.417	0.514	0.611	0.709	0.807	0.905
2.002	0.652	0.689	0.655	0.610	0.552	0.486	0.419	0.441	0.531	0.488
4.007	.634	.674	.634	.584	.526	.460	.381	.302	.232	.177
6.002	.631	.673	.631	.583	.525	.459	.380	.302	.233	.178
7.994	.628	.671	.628	.581	.524	.458	.380	.303	.233	.177

NPR	$p/p_{t,j}$ for left row x/L of—					$p/p_{t,j}$ for right row x/L of—			
	0.128	0.289	0.465	0.644	0.823	0.289	0.465	0.644	0.823
2.002	0.646	0.562	0.471	0.460	0.513	0.664	0.578	0.464	0.520
4.007	.621	.483	.371	.254	.164	.651	.565	.438	.283
6.002	.619	.482	.370	.253	.163	.650	.564	.438	.283
7.994	.618	.480	.368	.252	.163	.647	.563	.438	.286

[Lower flap]

NPR	$p/p_{t,j}$ for center row x/L of—									
	0.115	0.188	0.268	0.351	0.439	0.529	0.618	0.708	0.798	0.888
2.002	0.740	0.703	0.650	0.566	0.315	0.320	0.370	0.432	0.472	0.490
4.007	.730	.689	.635	.553	.188	.199	.205	.214	.225	.233
6.002	.728	.686	.634	.551	.077	.092	.098	.100	.118	.181
7.994	.725	.684	.632	.549	.077	.091	.096	.098	.096	.090

NPR	$p/p_{t,j}$ for left row x/L of					$p/p_{t,j}$ for right row x/L of—				
	0.175	0.323	0.488	0.652	0.817	0.175	0.324	0.478	0.645	0.809
2.002	0.647	0.264	0.478	0.496	0.497	0.735	0.669	0.560	0.449	0.455
4.007	.631	.215	.223	.241	.244	.723	.654	.549	.218	.227
6.002	.630	.087	.148	.152	.154	.720	.652	.547	.080	.134
7.994	.628	.087	.089	.102	.116	.717	.649	.545	.079	.088

Table 3. Continued

(l) Concluded

[Sidewalls]

NPR	$p/p_{t,j}$ for left sidewall centerline x/L of—					
	0.108	0.215	0.323	0.430	0.538	0.645
2.002	0.497	0.497	0.498	0.499	0.498	0.498
4.007	.108	.248	.300	.262	.257	.260
6.002	.107	.149	.161	.194	.171	.161
7.994	.107	.146	.135	.121	.124	.114

NPR	$p/p_{t,j}$ for right sidewall centerline x/L of—					
	0.131	0.262	0.394	0.525	0.656	0.788
2.002	0.737	0.686	0.629	0.552	0.485	0.485
4.007	.729	.676	.618	.542	.409	.223
6.002	.727	.675	.616	.540	.409	.191
7.994	.724	.672	.614	.539	.412	.191

Table 3. Continued

(m) $\delta_{v,p} = 20°$, $\delta_{v,s} = 35°$, $\theta_{\text{skew}} = 35°$, AR = 1.748, supersonic expansion ratio

[Upper flap]

	$p/p_{t,j}$ for center row x/L of—									
NPR	0.083	0.136	0.220	0.310	0.403	0.497	0.591	0.685	0.780	0.875
2.006	0.781	0.766	0.723	0.681	0.639	0.597	0.556	0.523	0.513	0.505
3.999	.764	.748	.696	.645	.595	.544	.480	.402	.321	.244
6.020	.762	.746	.693	.643	.593	.542	.479	.401	.321	.245
7.394	.760	.744	.691	.641	.591	.541	.478	.401	.321	.245

	$p/p_{t,j}$ for left row x/L of –					$p/p_{t,j}$ for right row x/L of—				
NPR	0.124	0.280	0.450	0.622	0.796		0.280	0.450	0.622	0.796
2.006	0.735	0.632	0.565	0.519	0.511		0.726	0.657	0.579	0.521
3.999	.711	.558	.454	.339	.220		.703	.628	.535	.390
6.020	.710	.557	.452	.338	.219		.701	.625	.533	.391
7.394	.708	.555	.451	.337	.219		.699	.623	.531	.390

[Lower flap]

	$p/p_{t,j}$ for center row x/L of—									
NPR	0.117	0.192	0.274	0.359	0.437	0.524	0.611	0.698	0.785	0.872
2.006	0.698	0.682	0.644	0.579	0.497	0.496	0.496	0.496	0.495	0.495
3.999	.671	.652	.612	.541	.247	.247	.247	.247	.247	.247
6.020	.668	.647	.608	.539	.075	.087	.091	.096	.129	.178
7.394	.665	.645	.606	.537	.075	.086	.090	.092	.090	.084

	$p/p_{t,j}$ for left row x/L of-					$p/p_{t,j}$ for right row x/L of—				
NPR	0.178	0.320	0.480	0.639	0.799	0.178	0.330	0.487	0.641	0.801
2.006	0.617	0.495	0.495	0.496	0.497	0.717	0.670	0.579	0.495	0.495
3.999	.572	.246	.246	.248	.249	.691	.641	.545	.247	.247
6.020	.570	.074	.142	.146	.145	.686	.638	.542	.079	.130
7.394	.568	.075	.107	.120	.119	.684	.635	.539	.079	.088

Table 3. Continued

(m) Concluded

[Sidewalls]

NPR	$p/p_{t,j}$ for left sidewall centerline x/L of—					
	0.108	0.215	0.323	0.430	0.538	0.645
2.006	0.494	0.495	0.496	0.497	0.497	0.498
3.999	.108	.290	.322	.259	.239	.262
6.020	.107	.172	.213	.206	.172	.146
7.394	.108	.166	.202	.173	.140	.118

NPR	$p/p_{t,j}$ for right sidewall centerline x/L of—					
	0.131	0.262	0.394	0.525	0.656	0.788
2.006	0.758	0.715	0.670	0.615	0.550	0.548
3.999	.740	.692	.642	.584	.505	.448
6.020	.738	.692	.640	.580	.506	.422
7.394	.735	.689	.638	.577	.505	.407

Table 3. Continued

(n) $\delta_{v,p} = 25°$, $\delta_{v,s} = 35°$, $\theta_{\text{skew}} = 35°$, AR = 1.748, supersonic expansion ratio

[Upper flap]

	$p/p_{t,j}$ for center row x/L of—									
NPR	0.081	0.132	0.214	0.302	0.392	0.483	0.575	0.667	0.759	0.851
1.996	0.823	0.794	0.746	0.699	0.659	0.619	0.576	0.539	0.517	0.507
3.999	.812	.780	.723	.668	.619	.571	.514	.441	.358	.274
6.010	.810	.778	.720	.666	.616	.569	.513	.440	.358	.275
7.110	.809	.776	.717	.664	.614	.567	.512	.440	.358	.276

	$p/p_{t,j}$ for left row x/L of—					$p/p_{t,j}$ for right row x/L of—				
NPR	0.120	0.272	0.438	0.606	0.774		0.272	0.438	0.606	0.774
1.996	0.769	0.653	0.581	0.530	0.514		0.746	0.678	0.603	0.528
3.999	.750	.592	.481	.372	.243		.726	.649	.566	.437
6.010	.748	.590	.479	.370	.242		.723	.647	.564	.437
7.110	.747	.588	.477	.370	.242		.720	.644	.562	.437

[Lower flap]

	$p/p_{t,j}$ for center row x/L of—									
NPR	0.117	0.190	0.272	0.356	0.436	0.521	0.605	0.690	0.775	0.859
1.996	0.683	0.675	0.642	0.577	0.499	0.498	0.498	0.497	0.497	0.496
3.999	.656	.644	.608	.539	.246	.246	.246	.246	.247	.247
6.010	.653	.639	.604	.537	.077	.087	.091	.114	.139	.164
7.110	.650	.637	.602	.536	.078	.086	.090	.092	.091	.091

	$p/p_{t,j}$ for left row x/L of					$p/p_{t,j}$ for right row x/L of—				
NPR	0.177	0.318	0.474	0.629	0.784	0.177	0.328	0.485	0.638	0.794
1.996	0.607	0.497	0.497	0.498	0.499	0.710	0.667	0.581	0.497	0.497
3.999	.557	.246	.246	.248	.249	.685	.638	.547	.246	.246
6.010	.554	.104	.151	.157	.158	.681	.636	.544	.080	.114
7.110	.552	.073	.128	.130	.129	.678	.633	.542	.079	.086

Table 3. Continued

(n) Concluded

[Sidewalls]

NPR	$p/p_{t,j}$ for left sidewall centerline x/L of—					
	0.108	0.215	0.323	0.430	0.538	0.645
1.996	0.480	0.478	0.497	0.502	0.501	0.502
3.999	.111	.310	.316	.250	.237	.256
6.010	.109	.223	.209	.209	.174	.148
7.110	.109	.213	.194	.183	.150	.129

NPR	$p/p_{t,j}$ for right sidewall centerline x/L of—					
	0.131	0.262	0.394	0.525	0.656	
1.996	0.769	0.726	0.682	0.632	0.589	
3.999	.751	.704	.657	.602	.544	
6.010	.747	.701	.654	.598	.541	
7.110	.745	.698	.651	.597	.511	

Table 3. Continued

(o) $\delta_{v,p} = 0°$, $\delta_{v,s} = 0°$, $\theta_{\text{skew}} = 50°$, AR = 1.748, subsonic expansion ratio

[Upper flap]

	$p/p_{t,j}$ for center row x/L of—									
NPR	0.067	0.150	0.243	0.336	0.431	0.526	0.621	0.716	0.811	0.906
2.004	0.826	0.799	0.742	0.659	0.552	0.449	0.411	0.393	0.402	0.467
4.006	.815	.790	.730	.648	.544	.446	.380	.333	.284	.238
5.003	.804	.780	.720	.639	.538	.442	.376	.329	.283	.239
5.899	.799	.774	.715	.635	.536	.441	.374	.327	.282	.240
7.006	.791	.767	.708	.630	.533	.439	.371	.325	.283	.242
8.207	.782	.758	.700	.624	.529	.436	.368	.323	.283	.242
8.343	.782	.757	.699	.623	.528	.436	.368	.323	.283	.242

	$p/p_{t,j}$ for left row x/L of—					$p/p_{t,j}$ for right row x/L of—			
NPR	0.135	0.305	0.478	0.652	0.827	0.305	0.478	0.652	0.827
2.004	0.785	0.661	0.521	0.429	0.392	0.736	0.557	0.320	0.443
4.006	.772	.651	.515	.408	.315	.726	.549	.247	.191
5.003	.762	.643	.508	.405	.314	.716	.543	.254	.189
5.899	.757	.638	.505	.403	.314	.711	.541	.257	.188
7.006	.750	.632	.501	.401	.314	.704	.538	.262	.188
8.207	.741	.625	.496	.399	.314	.695	.534	.267	.187
8.343	.740	.624	.495	.399	.313	.694	.533	.268	.186

[Lower flap]

	$p/p_{t,j}$ for center row x/L of—									
NPR	0.096	0.176	0.260	0.344	0.445	0.533	0.621	0.708	0.796	0.884
2.004	0.865	0.814	0.750	0.595	0.426	0.467	0.436	0.397	0.411	0.463
4.006	.852	.801	.737	.587	.530	.472	.410	.357	.300	.256
5.003	.843	.791	.726	.579	.511	.463	.405	.355	.300	.258
5.899	.839	.786	.721	.575	.472	.459	.404	.355	.301	.259
7.006	.833	.778	.713	.569	.406	.455	.405	.357	.304	.261
8.207	.825	.769	.704	.562	.375	.446	.407	.360	.307	.263
8.343	.825	.768	.703	.561	.372	.445	.407	.360	.307	.263

	$p/p_{t,j}$ for left row x/L of					$p/p_{t,j}$ for right row x/L of—				
NPR	0.162	0.326	0.487	0.647	0.808	0.162	0.316	0.471	0.652	0.813
2.004	0.777	0.629	0.522	0.422	0.360	0.845	0.756	0.565	0.332	0.417
4.006	.766	.613	.512	.407	.309	.831	.740	.553	.309	.221
5.003	.754	.600	.505	.404	.309	.820	.728	.546	.298	.222
5.899	.748	.594	.502	.402	.309	.814	.722	.542	.298	.220
7.006	.741	.577	.498	.401	.308	.806	.714	.536	.294	.221
8.207	.731	.571	.491	.399	.309	.797	.706	.530	.290	.223
8.343	.730	.568	.491	.398	.309	.796	.704	.529	.289	.223

Table 3. Continued

(o) Concluded

[Sidewalls]

NPR	$p/p_{t,j}$ for left sidewall centerline x/L of—					
	0.131	0.262	0.393	0.524	0.655	0.786
2.004	0.762	0.660	0.574	0.490	0.419	0.360
4.006	.752	.648	.563	.480	.411	.336
5.003	.742	.636	.553	.474	.407	.340
5.899	.737	.631	.548	.471	.405	.340
7.006	.729	.624	.541	.467	.403	.339
8.207	.721	.615	.533	.462	.402	.338
8.343	.720	.613	.532	.461	.401	.338

NPR	$p/p_{t,j}$ for right sidewall centerline x/L of—					
	0.131	0.262	0.393			
2.004	0.843	0.786	0.705			
4.006	.833	.775	.694			
5.003	.824	.765	.683			
5.899	.819	.760	.678			
7.006	.811	.752	.671			
8.207	.803	.744	.663			
8.343	.802	.743	.662			

Table 3.. Continued

(p) $\delta_{v,p} = 0°$, $\delta_{v,s} = 35°$, $\theta_{\text{skew}} = 50°$, AR = 1.748, subsonic expansion ratio

[Upper flap]

NPR	$p/p_{t,j}$ for center row x/L of—									
	0.067	0.150	0.243	0.336	0.431	0.526	0.621	0.716	0.811	0.906
2.006	0.743	0.712	0.654	0.573	0.449	0.298	0.325	0.445	0.474	0.490
3.997	.716	.680	.619	.546	.432	.283	.163	.242	.244	.246
5.005	.712	.675	.614	.543	.430	.284	.164	.158	.194	.196
5.905	.708	.672	.611	.540	.429	.285	.166	.093	.163	.165
7.000	.702	.664	.604	.534	.427	.287	.168	.095	.133	.138
7.343	.700	.662	.602	.533	.426	.287	.168	.096	.123	.131

NPR	$p/p_{t,j}$ for left row x/L of—					$p/p_{t,j}$ for right row x/L of—				
	0.305	0.478	0.652	0.827		0.305	0.478	0.652	0.827	
2.006	0.502	0.385	0.503	0.504		0.677	0.521	0.289	0.463	
3.997	.435	.230	.229	.243		.654	.510	.196	.242	
5.005	.433	.230	.100	.194		.649	.506	.199	.192	
5.905	.431	.231	.101	.163		.644	.503	.202	.159	
7.000	.427	.231	.102	.132		.636	.500	.204	.134	
7.343	.426	.231	.102	.123		.633	.497	.206	.126	

[Lower flap]

NPR	$p/p_{t,j}$ for center row x/L of—									
	0.096	0.176	0.260	0.344	0.445	0.533	0.621	0.708	0.796	0.884
2.006	0.798	0.734	0.666	0.533	0.271	0.265	0.283	0.409	0.560	0.509
3.997	.775	.705	.638	.516	.124	.150	.146	.121	.227	.278
5.005	.772	.701	.635	.514	.124	.148	.144	.120	.108	.189
5.905	.769	.697	.630	.512	.123	.146	.143	.120	.088	.087
7.000	.764	.690	.624	.507	.121	.143	.141	.119	.089	.064
7.343	.763	.689	.622	.506	.120	.142	.140	.119	.089	.064

NPR	$p/p_{t,j}$ for left row x/L of—					$p/p_{t,j}$ for right row x/L of—				
	0.162	0.326	0.487	0.647	0.808	0.162	0.316	0.471	0.652	0.813
2.006	0.652	0.265	0.502	0.506	0.498	0.780	0.691	0.531	0.333	0.414
3.997	.616	.124	.217	.186	.342	.755	.665	.518	.140	.220
5.005	.613	.122	.136	.115	.199	.751	.659	.514	.138	.085
5.905	.610	.120	.134	.110	.104	.747	.654	.510	.136	.086
7.000	.605	.118	.131	.109	.070	.740	.646	.505	.133	.088
7.343	.604	.117	.130	.108	.070	.738	.643	.502	.132	.089

Table 3. Continued

(p) Concluded

[Sidewalls]

NPR	$p/p_{t,j}$ for left sidewall centerline x/L of—					
	0.107	0.215	0.322	0.429	0.537	0.644
2.006	0.468	0.496	0.498	0.496	0.497	0.497
3.997	.197	.308	.237	.260	.255	.254
5.005	.185	.245	.179	.193	.217	.208
5.905	.180	.200	.176	.142	.191	.169
7.000	.174	.165	.147	.115	.119	.217
7.343	.172	.158	.139	.111	.108	.216

NPR	$p/p_{t,j}$ for right sidewall centerline x/L of—					
	0.131	0.262	0.393			
2.006	0.781	0.726	0.656			
3.997	.763	.703	.638			
5.005	.758	.697	.630			
5.905	.754	.692	.622			
7.000	.748	.683	.616			
7.343	.746	.680	.619			

Table 3. Continued

(q) $\delta_{v,p} = 25°$, $\delta_{v,s} = 35°$, $\theta_{\text{skew}} = 50°$, AR = 1.748, subsonic expansion ratio

[Upper flap]

NPR	$p/p_{t,j}$ for center row x/L of—									
	0.062	0.137	0.222	0.307	0.394	0.480	0.567	0.654	0.741	0.828
2.009	0.863	0.803	0.749	0.705	0.652	0.574	0.507	0.499	0.498	0.495
3.998	.844	.773	.704	.656	.606	.509	.337	.178	.240	.243
5.011	.840	.766	.696	.649	.599	.506	.338	.182	.141	.195
5.907	.836	.760	.689	.642	.595	.503	.341	.186	.097	.163
7.007	.830	.752	.680	.634	.588	.501	.344	.191	.100	.134
7.245	.829	.750	.678	.632	.587	.500	.344	.192	.101	.127

NPR	$p/p_{t,j}$ for left row x/L of—					$p/p_{t,j}$ for right row x/L of—				
	0.279	0.437	0.596	0.755		0.279	0.437	0.596	0.755	
2.009	0.638	0.528	0.499	0.497		0.767	0.698	0.556	0.502	
3.998	.554	.400	.170	.237		.730	.660	.475	.230	
5.011	.547	.399	.172	.192		.721	.652	.472	.113	
5.907	.539	.399	.174	.153		.715	.646	.470	.120	
7.007	.530	.398	.176	.070		.705	.640	.469	.126	
7.245	.528	.398	.177	.071		.703	.638	.468	.127	

[Lower flap]

NPR	$p/p_{t,j}$ for center row x/L of—									
	0.099	0.183	0.269	0.357	0.445	0.532	0.620	0.707	0.794	0.882
2.009	0.754	0.728	0.683	0.573	0.488	0.488	0.487	0.488	0.489	0.491
3.998	.712	.678	.640	.532	.128	.152	.138	.209	.268	.285
5.011	.705	.670	.632	.527	.127	.149	.137	.103	.184	.287
5.907	.698	.662	.626	.523	.125	.147	.137	.105	.072	.136
7.007	.689	.653	.618	.517	.123	.145	.137	.106	.073	.087
7.245	.687	.651	.616	.516	.123	.145	.136	.107	.074	.049

NPR	$p/p_{t,j}$ for left row x/L of—					$p/p_{t,j}$ for right row x/L of—				
	0.168	0.325	0.485	0.646	0.806	0.168	0.328	0.489	0.652	0.812
2.009	0.637	0.487	0.488	0.489	0.493	0.775	0.719	0.584	0.487	0.485
3.998	.559	.242	.244	.214	.230	.735	.677	.540	.143	.298
5.011	.551	.128	.181	.137	.220	.727	.669	.534	.141	.150
5.907	.544	.112	.133	.099	.159	.719	.662	.529	.140	.066
7.007	.535	.109	.131	.100	.058	.709	.654	.524	.138	.069
7.245	.533	.109	.130	.100	.059	.707	.652	.522	.137	.070

Table 3. Continued

(q) Concluded

[Sidewalls]

NPR	$p/p_{t,j}$ for left sidewall centerline x/L of—					
	0.107	0.215	0.322	0.429	0.537	0.644
2.009	0.448	0.508	0.502	0.500	0.499	0.498
3.998	.314	.335	.206	.267	.268	.229
5.011	.286	.285	.204	.192	.244	.190
5.907	.269	.229	.188	.137	.218	.170
7.007	.253	.204	.169	.121	.151	.176
7.245	.250	.200	.165	.121	.142	.179

NPR	$p/p_{t,j}$ for right sidewall centerline x/L of—					
	0.131	0.262	0.393			
2.009	0.816	0.776	0.485			
3.998	.789	.740	.288			
5.011	.782	.732	.277			
5.907	.775	.725	.480			
7.007	.764	.714	.447			
7.245	.762	.711	.449			

Table 3. Continued

(r) $\delta_{v,p} = 0°$, $\delta_{v,s} = 0°$, $\theta_{\text{skew}} = 50°$, AR = 1.748, supersonic expansion ratio

[Upper flap]

	$p/p_{t,j}$ for center row x/L of—									
NPR	0.067	0.150	0.242	0.336	0.431	0.525	0.620	0.715	0.810	0.905
2.005	0.814	0.787	0.727	0.640	0.523	0.401	0.387	0.459	0.502	0.501
3.993	.805	.779	.717	.631	.516	.399	.321	.276	.243	.223
6.002	.791	.765	.704	.621	.511	.397	.320	.273	.241	.206
8.009	.778	.752	.692	.611	.505	.397	.319	.272	.239	.210
8.754	.773	.746	.687	.607	.503	.397	.318	.271	.237	.210

	$p/p_{t,j}$ for left row x/L of						$p/p_{t,j}$ for right row x/L of—			
NPR	0.135	0.305	0.478	0.652	0.826		0.305	0.478	0.652	0.826
2.005	0.769	0.634	0.480	0.421	0.520		0.724	0.543	0.373	0.480
3.993	.759	.625	.475	.364	.278		.715	.537	.219	.203
6.002	.745	.615	.468	.358	.280		.702	.530	.231	.133
8.009	.733	.605	.466	.358	.280		.689	.523	.238	.128
8.754	.728	.601	.463	.358	.279		.685	.521	.242	.125

[Lower flap]

	$p/p_{t,j}$ for center row x/L of —									
NPR	0.095	0.174	0.257	0.340	0.443	0.530	0.618	0.705	0.793	0.880
2.005	0.860	0.806	0.740	0.593	0.331	0.381	0.471	0.466	0.503	0.500
3.993	.851	.795	.729	.587	.319	.373	.402	.336	.274	.228
6.002	.839	.780	.715	.575	.309	.365	.391	.337	.279	.234
8.009	.827	.767	.700	.565	.305	.374	.368	.328	.281	.239
8.754	.822	.762	.695	.561	.303	.367	.363	.328	.282	.241

	$p/p_{t,j}$ for left row x/L of—					$p/p_{t,j}$ for right row x/L of—				
NPR	0.161	0.324	0.485	0.645	0.806	0.161	0.312	0.466	0.649	0.809
2.005	0.764	0.603	0.480	0.409	0.514	0.838	0.744	0.571	0.372	0.450
3.993	.756	.585	.470	.377	.283	.827	.731	.563	.249	.157
6.002	.741	.554	.462	.376	.286	.814	.715	.551	.234	.162
8.009	.727	.519	.457	.373	.290	.800	.701	.540	.228	.169
8.754	.721	.505	.455	.372	.293	.796	.696	.536	.224	.170

Table 3. Continued

(r) Concluded

[Sidewalls]

NPR	$p/p_{t,j}$ for left sidewall centerline x/L of—					
	0.131	0.262	0.393	0.524	0.655	0.786
2.005	0.743	0.626	0.536	0.452	0.385	0.533
3.993	.733	.613	.524	.442	.376	.312
6.002	.720	.598	.511	.433	.372	.310
8.009	.707	.583	.500	.429	.370	.308
8.754	.702	.578	.495	.427	.369	.307

NPR	$p/p_{t,j}$ for right sidewall centerline x/L of—					
	0.131	0.262	0.393			
2.005	0.835	0.776	0.704			
3.993	.827	.769	.698			
6.002	.815	.755	.676			
8.009	.802	.742	.660			
8.754	. .797	.737	.654			

Table 3. Continued

(s) $\delta_{v,p} = 0°$, $\delta_{v,s} = 35°$, $\theta_{\text{skew}} = 50°$, AR = 1.748, supersonic expansion ratio

[Upper flap]

	$p/p_{t,j}$ for center row x/L of—									
NPR	0.067	0.150	0.242	0.336	0.431	0.525	0.620	0.715	0.810	0.905
2.001	0.737	0.708	0.649	0.571	0.452	0.322	0.272	0.467	0.452	0.486
4.008	.710	.675	.612	.541	.426	.276	.160	.233	.236	.240
6.004	.703	.666	.603	.534	.423	.279	.162	.093	.160	.162
7.430	.696	.658	.596	.528	.421	.281	.166	.094	.111	.127

	$p/p_{t,j}$ for left row x/L of—					$p/p_{t,j}$ for right row x/L of—			
NPR	0.135	0.305	0.478	0.652	0.826	0.305	0.478	0.652	0.826
2.001	0.633	0.504	0.384	0.488	0.502	0.672	0.515	0.363	0.453
4.008	.567	.430	.224	.213	.234	.648	.502	.191	.235
6.004	.558	.426	.226	.099	.160	.639	.496	.205	.158
7.430	.552	.423	.227	.101	.116	.629	.491	.207	.116

[Lower flap]

	$p/p_{t,j}$ for center row x/L of—									
NPR	0.095	0.174	0.257	0.340	0.443	0.530	0.618	0.705	0.793	0.880
2.001	0.798	0.735	0.663	0.542	0.305	0.291	0.298	0.354	0.471	0.542
4.008	.778	.704	.634	.523	.103	.186	.195	.191	.276	.253
6.004	.772	.695	.626	.517	.101	.122	.123	.106	.083	.126
7.430	.766	.688	.619	.511	.098	.119	.120	.105	.081	.063

	$p/p_{t,j}$ for left row x/L of—					$p/p_{t,j}$ for right row x/L of—				
NPR	0.161	0.324	0.485	0.645	0.806	0.161	0.312	0.466	0.649	0.809
2.001	0.652	0.329	0.423	0.489	0.502	0.783	0.692	0.543	0.339	0.389
4.008	.617	.187	.216	.234	.249	.758	.661	.528	.118	.216
6.004	.612	.099	.112	.122	.130	.749	.649	.519	.115	.081
7.430	.607	.097	.109	.094	.064	.742	.638	.511	.111	.084

Table 3. Continued

(s) Concluded

[Sidewalls]

NPR	$p/p_{t,j}$ for left sidewall centerline x/L of –					
	0.107	0.215	0.322	0.429	0.537	0.644
2.001	0.472	0.495	0.498	0.497	0.498	0.498
4.008	.211	.311	.243	.256	.254	.253
6.004	.192	.185	.179	.141	.175	.164
7.430	.187	.146	.139	.110	.111	.208

NPR	$p/p_{t,j}$ for right sidewall centerline x/L of—					
	0.131	0.262	0.393			
2.001	0.779	0.722	0.626			
4.008	.760	.700	.613			
6.004	.752	.689	.607			
7.430	.746	.679	.594			

Table 3. Continued

(t) $\delta_{v,p} = 25°$, $\delta_{v,s} = 35°$, $\theta_{\text{skew}} = 50°$, AR = 1.748, supersonic expansion ratio

[Upper flap]

	$p/p_{t,j}$ for center row x/L of—									
NPR	0.062	0.138	0.223	0.310	0.397	0.484	0.571	0.659	0.746	0.834
2.013	0.860	0.802	0.747	0.703	0.645	0.550	0.452	0.444	0.480	0.472
4.004	.841	.772	.703	.660	.609	.510	.338	.179	.234	.237
6.007	.833	.759	.689	.645	.598	.505	.343	.188	.097	.159
7.251	.826	.749	.676	.632	.586	.500	.345	.194	.101	.125

	$p/p_{t,j}$ for left row x/L of—					$p/p_{t,j}$ for right row x/L of—			
NPR	0.125	0.281	0.440	0.600	0.761	0.281	0.440	0.600	0.761
2.013	0.749	0.633	0.493	0.453	0.464	0.767	0.694	0.531	0.483
4.004	.706	.556	.400	.176	.224	.734	.666	.480	.215
6.007	.694	.542	.400	.175	.148	.719	.651	.475	.126
7.251	.685	.529	.398	.178	.072	.704	.637	.471	.134

[Lower flap]

	$p/p_{t,j}$ for center row x/L of—									
NPR	0.099	0.182	0.268	0.355	0.442	0.529	0.616	0.703	0.789	0.876
2.013	0.755	0.726	0.681	0.571	0.425	0.426	0.435	0.448	0.460	0.475
4.004	.716	.680	.642	.545	.231	.240	.243	.242	.257	.267
6.007	.701	.663	.628	.534	.102	.126	.121	.096	.111	.149
7.251	.690	.649	.614	.524	.099	.123	.120	.095	.067	.049

	$p/p_{t,j}$ for left row x/L of—					$p/p_{t,j}$ for right row x/L of—				
NPR	0.168	0.323	0.482	0.642	0.801	0.168	0.326	0.487	0.648	0.807
2.013	0.634	0.418	0.419	0.454	0.479	0.778	0.719	0.590	0.458	0.467
4.004	.561	.240	.241	.244	.246	.743	.682	.559	.126	.245
6.007	.547	.098	.149	.120	.164	.727	.666	.548	.122	.062
7.251	.533	.090	.110	.090	.057	.713	.650	.538	.116	.072

Table 3. Continued

(t) Concluded

[Sidewalls]

NPR	$p/p_{t,j}$ for left sidewall centerline x/L of—					
	0.107	0.215	0.322	0.429	0.537	0.644
2.013	0.456	0.508	0.501	0.498	0.498	0.497
4.004	.310	.329	.206	.270	.275	.227
6.007	.260	.248	.181	.132	.221	.169
7.251	.238	.204	.163	.120	.145	.186

NPR	$p/p_{t,j}$ for right sidewall centerline x/L of—					
	0.131	0.262				
2.013	0.817	0.779				
4.004	.790	.750				
6.007	.776	.737				
7.251	.764	.714				

Table 3. Continued

(u) $\delta_{v,p} = 0°$, $\delta_{v,s} = 0°$, short sidewalls, $\theta_{\text{skew}} = 50°$, AR = 1.748, supersonic expansion ratio

[Upper flap]

	$p/p_{t,j}$ for center row x/L of—									
NPR	0.067	0.150	0.242	0.336	0.431	0.525	0.620	0.715	0.810	0.905
2.007	0.811	0.784	0.721	0.634	0.517	0.399	0.509	0.498	0.509	0.509
4.030	.799	.775	.711	.625	.511	.393	.310	.244	.173	.205
6.011	.786	.763	.700	.617	.506	.391	.310	.243	.173	.119
8.004	.773	.750	.688	.608	.500	.387	.302	.237	.174	.118
8.814	.768	.744	.683	.603	.498	.386	.299	.236	.172	.118

	$p/p_{t,j}$ for left row x/L of—					$p/p_{t,j}$ for right row x/L of—			
NPR	0.135	0.305	0.478	0.652	0.826	0.305	0.478	0.652	0.826
2.007	0.764	0.628	0.472	0.527	0.515	0.720	0.538	0.507	0.501
4.030	.753	.619	.467	.310	.170	.710	.533	.180	.305
6.011	.742	.610	.462	.309	.142	.699	.528	.183	.160
8.004	.730	.599	.452	.303	.144	.687	.523	.190	.086
8.814	.725	.594	.449	.303	.144	.681	.519	.193	.084

[Lower flap]

	$p/p_{t,j}$ for center row x/L of—									
NPR	0.095	0.174	0.257	0.340	0.443	0.530	0.618	0.705	0.793	0.880
2.007	0.856	0.801	0.733	0.590	0.322	0.399	0.529	0.497	0.508	0.511
4.030	.845	.789	.723	.582	.309	.376	.391	.300	.197	.122
6.011	.835	.777	.711	.573	.310	.355	.375	.302	.198	.124
8.004	.824	.764	.697	.562	.301	.321	.363	.306	.201	.126
8.814	.818	.759	.692	.558	.293	.326	.357	.305	.203	.127

	$p/p_{t,j}$ for left row x/L of—					$p/p_{t,j}$ for right row x/L of—				
NPR	0.161	0.324	0.485	0.645	0.806	0.161	0.312	0.466	0.649	0.809
2.007	0.758	0.600	0.481	0.507	0.510	0.836	0.741	0.566	0.390	0.487
4.030	.749	.565	.473	.271	.182	.821	.726	.557	.198	.166
6.011	.737	.544	.464	.269	.107	.809	.713	.548	.202	.140
8.004	.723	.533	.448	.271	.108	.796	.699	.538	.201	.133
8.814	.717	.517	.443	.273	.109	.791	.693	.533	.199	.130

Table 3. Continued

(u) Concluded

[Sidewalls]

NPR	$p/p_{t,j}$ for left sidewall centerline x/L of –					
	0.077	0.154	0.231	0.308	0.385	0.463
2.007	0.789	0.709	0.640	0.587	0.536	0.477
4.030	.781	.697	.629	.576	.526	.468
6.011	.771	.686	.615	.563	.515	.461
8.004	.759	.671	.599	.547	.499	.451
8.814	.753	.665	.591	.540	.494	.447

NPR	$p/p_{t,j}$ for right sidewall centerline x/L of—					
	0.077	0.154	0.231	0.308	0.385	
2.007	0.849	0.821	0.784	0.744	0.697	
4.030	.843	.814	.776	.736	.692	
6.011	.833	.803	.763	.725	.682	
8.004	.821	.790	.750	.713	.669	
8.814	.815	.784	.744	.707	.665	

Table 3. Continued

(v) $\delta_{v,p} = 0°$, $\delta_{v,s} = 0°$, short left sidewall, $\theta_{\text{skew}} = 50°$, AR = 1.748, supersonic expansion ratio

[Upper flap]

	$p/p_{t,j}$ for center row x/L of—									
NPR	0.067	0.150	0.242	0.336	0.431	0.525	0.620	0.715	0.810	0.905
2.005	0.802	0.779	0.719	0.632	0.516	0.394	0.366	0.502	0.494	0.504
3.994	.790	.767	.704	.619	.506	.386	.308	.254	.195	.143
6.016	.770	.749	.685	.603	.494	.374	.289	.245	.194	.145
8.010	.750	.730	.669	.590	.485	.370	.283	.227	.192	.146
9.008	.740	.720	.660	.582	.481	.368	.279	.219	.191	.151
9.216	.737	.718	.657	.580	.480	.368	.278	.219	.191	.148

	$p/p_{t,j}$ for left row x/L of					$p/p_{t,j}$ for right row x/L of—			
NPR	0.135	0.305	0.478	0.652	0.826	0.305	0.478	0.652	0.826
2.005	0.759	0.624	0.471	0.524	0.512	0.718	0.540	0.312	0.471
3.994	.745	.610	.459	.312	.175	.705	.533	.212	.179
6.016	.726	.590	.440	.304	.152	.688	.525	.220	.105
8.010	.707	.574	.429	.292	.152	.671	.516	.231	.098
9.008	.698	.566	.420	.292	.156	.662	.513	.235	.089
9.216	.695	.564	.418	.291	.154	.660	.512	.237	.086

[Lower flap]

	$p/p_{t,j}$ for center row x/L of—									
NPR	0.095	0.174	0.257	0.340	0.443	0.530	0.618	0.705	0.793	0.880
2.005	0.854	0.801	0.730	0.587	0.318	0.367	0.448	0.501	0.513	0.510
3.994	.841	.783	.716	.577	.309	.348	.379	.311	.210	.139
6.016	.824	.764	.697	.562	.280	.307	.350	.312	.214	.143
8.010	.808	.746	.679	.549	.276	.289	.319	.304	.217	.147
9.008	.799	.736	.669	.542	.290	.295	.305	.290	.217	.148
9.216	.796	.734	.667	.540	.299	.299	.298	.282	.215	.147

	$p/p_{t,j}$ for left row x/L of—					$p/p_{t,j}$ for right row x/L of—				
NPR	0.161	0.324	0.485	0.645	0.806	0.161	0.312	0.466	0.649	0.809
2.005	0.753	0.596	0.479	0.524	0.504	0.831	0.740	0.566	0.350	0.444
3.994	.742	.548	.464	.276	.188	.816	.721	.552	.202	.174
6.016	.722	.493	.432	.281	.117	.796	.702	.538	.205	.155
8.010	.702	.443	.420	.283	.120	.777	.683	.525	.212	.160
9.008	.693	.425	.423	.283	.120	.768	.674	.519	.199	.163
9.216	.690	.422	.418	.282	.120	.766	.671	.517	.197	.164

Table 3. Continued

(v) Concluded

[Sidewalls]

	$p/p_{t,j}$ for left sidewall centerline x/L of—					
NPR	0.077	0.154	0.231	0.308	0.385	0.463
2.005	0.785	0.705	0.634	0.582	0.531	0.477
3.994	.772	.687	.616	.564	.514	.463
6.016	.753	.662	.584	.537	.494	.442
8.010	.733	.641	.567	.515	.472	.416
9.008	.724	.630	.556	.509	.460	.408
9.216	.722	.627	.551	.507	.460	.406

	$p/p_{t,j}$ for right sidewall centerline x/L of—					
NPR	0.131	0.262	0.393			
2.005	0.828	0.768	0.700			
3.994	.817	.759	.678			
6.016	.799	.739	.674			
8.010	.782	.720	.654			
9.008	.772	.710	.645			
9.216	.769	.708	.649			

Table 3. Continued

(w) $\delta_{v,p} = 0°$, $\delta_{v,s} = 0°$, $\theta_{\text{skew}} = 35°$, AR = 3.500, supersonic expansion ratio

[Upper flap]

	$p/p_{t,j}$ for center row x/L of—							
NPR	0.086	0.140	0.227	0.320	0.610	0.707	0.805	0.903
1.995	0.662	0.699	0.676	0.631	0.493	0.488	0.498	0.487
4.010	.645	.691	.662	.615	.384	.290	.213	.157
6.001	.637	.689	.659	.614	.384	.291	.214	.159
8.013	.631	.684	.657	.612	.386	.293	.216	.160
9.011	.629	.683	.655	.611	.386	.294	.217	.161
9.908	.628	.682	.654	.609	.387	.295	.218	.162
10.996	.626	.682	.646	.610	.388	.297	.219	.162
11.412	.627	.681	.622	.610	.388	.297	.219	.163

	$p/p_{t,j}$ for left row x/L of—				$p/p_{t,j}$ for right row x/L of—		
NPR	0.128	0.464	0.642	0.821	0.289	0.464	0.821
1.995	0.664	0.505	0.493	0.499	0.692	0.623	0.490
4.010	.646	.393	.255	.177	.681	.611	.325
6.001	.643	.394	.255	.176	.678	.609	.327
8.013	.641	.394	.255	.176	.675	.607	.328
9.011	.639	.394	.256	.176	.673	.606	.329
9.908	.639	.395	.256	.176	.672	.605	.330
10.996	.638	.395	.257	.176	.670	.604	.331
11.412	.637	.395	.257	.176	.669	.603	.332

[Lower flap]

	$p/p_{t,j}$ for center row x/L of—								
NPR	0.117	0.192	0.275	0.360	0.540	0.633	0.725	0.818	0.910
1.995	0.764	0.725	0.683	0.640	0.478	0.479	0.480	0.481	0.482
4.010	.752	.711	.674	.626	.117	.134	.141	.145	.244
6.001	.747	.706	.671	.624	.118	.132	.139	.141	.178
8.013	.744	.702	.668	.621	.118	.131	.138	.140	.177
9.011	.743	.701	.666	.620	.118	.130	.137	.139	.176
9.908	.741	.699	.664	.619	.118	.130	.137	.138	.175
10.996	.740	.698	.663	.617	.118	.129	.136	.138	.174
11.412	.739	.697	.662	.617	.117	.129	.136	.138	.174

	$p/p_{t,j}$ for left row x/L of—					$p/p_{t,j}$ for right row x/L of—			
NPR	0.178	0.330	0.500	0.669	0.839	0.178	0.331	0.490	0.827
1.995	0.682	0.464	0.466	0.466	0.470	0.761	0.704	0.637	0.485
4.010	.670	.123	.276	.285	.241	.747	.685	.623	.171
6.001	.668	.122	.262	.286	.240	.740	.679	.620	.116
8.013	.665	.122	.254	.285	.240	.735	.675	.617	.115
9.011	.663	.123	.250	.284	.240	.733	.673	.617	.114
9.908	.662	.123	.249	.284	.239	.730	.671	.615	.114
10.996	.660	.124	.246	.283	.240	.728	.669	.614	.114
11.412	.659	.124	.245	.283	.240	.727	.668	.613	.114

Table 3. Continued

(w) Concluded

[Sidewalls]

NPR	$p/p_{t,j}$ for left sidewall centerline x/L of—					
	0.131	0.262	0.394	0.525	0.656	0.788
1.995	0.616	0.523	0.495	0.488	0.490	0.511
4.010	.587	.427	.356	.316	.278	.261
6.001	.585	.426	.352	.312	.276	.259
8.013	.584	.425	.349	.309	.274	.257
9.011	.584	.424	.347	.308	.274	.256
9.908	.583	.424	.345	.307	.273	.254
10.996	.583	.424	.345	.306	.272	.254
11.412	.582	.423	.344	.305	.272	.254
NPR	$p/p_{t,j}$ for right sidewall centerline x/L of—					
	0.131	0.262	0.394	0.525	0.656	0.788
1.995	0.757	0.717	0.675	0.626	0.572	0.496
4.010	.749	.709	.666	.615	.557	.465
6.001	.745	.706	.663	.613	.556	.467
8.013	.740	.702	.660	.610	.555	.467
9.011	.738	.700	.658	.609	.554	.467
9.908	.736	.699	.657	.607	.553	.466
10.996	.733	.697	.655	.606	.552	.465
11.412	.734	.696	.655	.606	.551	.465

Table 3. Continued

(x) $\delta_{v,p} = 0°$, $\delta_{v,s} = 35°$, $\theta_{\text{skew}} = 35°$, AR = 3.500, supersonic expansion ratio

[Upper flap]

NPR	$p/p_{t,j}$ for center row x/L of—							
	0.086	0.140	0.227	0.320	0.610	0.707	0.805	0.903
2.004	0.646	0.685	0.658	0.613	0.428	0.468	0.507	0.467
4.007	.631	.677	.646	.601	.378	.285	.207	.152
6.008	.619	.672	.642	.599	.378	.286	.208	.153
8.009	.612	.667	.638	.596	.379	.288	.210	.155
8.953	.609	.665	.636	.594	.379	.289	.211	.156

NPR	$p/p_{t,j}$ for left row x/L of—				$p/p_{t,j}$ for right row x/L of—			
	0.128	0.464	0.642	0.821		0.289	0.464	0.821
2.004	0.632	0.394	0.541	0.498		0.677	0.608	0.484
4.007	.614	.344	.205	.123		.670	.602	.324
6.008	.610	.343	.204	.121		.665	.599	.325
8.009	.607	.343	.204	.122		.660	.595	.327
8.953	.606	.343	.205	.122		.657	.593	.328

[Lower flap]

NPR	$p/p_{t,j}$ for center row x/L of—								
	0.117	0.192	0.275	0.360	0.540	0.633	0.725	0.818	0.910
2.004	0.747	0.707	0.664	0.620	0.445	0.442	0.447	0.441	0.443
4.007	.738	.696	.659	.612	.113	.127	.132	.133	.234
6.008	.733	.691	.653	.609	.114	.125	.130	.130	.123
8.009	.728	.686	.649	.605	.114	.123	.128	.128	.122
8.953	.726	.683	.647	.603	.114	.123	.127	.127	.122

NPR	$p/p_{t,j}$ for left row x/L of—					$p/p_{t,j}$ for right row x/L of—			
	0.178	0.330	0.500	0.669	0.839	0.178	0.331	0.490	0.827
2.004	0.654	0.254	0.302	0.522	0.506	0.742	0.683	0.620	0.481
4.007	.644	.113	.134	.194	.197	.733	.671	.613	.114
6.008	.641	.112	.131	.123	.104	.726	.665	.609	.113
8.009	.637	.113	.129	.121	.103	.720	.661	.605	.112
8.953	.635	.113	.128	.120	.102	.718	.657	.603	.112

Table 3. Continued

(x) Concluded

[Sidewalls]

NPR	$p/p_{t,j}$ for left sidewall centerline x/L of—					
	0.108	0.215	0.323	0.430	0.538	0.645
2.004	0.497	0.499	0.499	0.498	0.499	0.499
4.007	.099	.313	.262	.255	.252	.252
6.008	.099	.120	.214	.172	.172	.172
8.009	.100	.115	.125	.139	.126	.133
8.953	.100	.114	.099	.119	.108	.112
NPR	$p/p_{t,j}$ for right sidewall centerline x/L of—					
	0.131	0.262	0.394	0.525	0.656	0.788
2.004	0.741	0.705	0.661	0.613	0.561	0.483
4.007	.737	.698	.654	.606	.552	.454
6.008	.730	.693	.649	.603	.548	.458
8.009	.723	.687	.645	.600	.546	.452
8.953	.719	.684	.642	.598	.544	.451

Table 3. Continued

(y) $\delta_{v,p} = 25°$, $\delta_{v,s} = 35°$, $\theta_{\text{skew}} = 35°$, AR = 3.500, supersonic expansion ratio

[Upper flap]

	$p/p_{t,j}$ for center row x/L of—									
NPR	0.080	0.132	0.213	0.301	0.391	0.482	0.573	0.664	0.756	0.848
2.000	0.827	0.797	0.742	0.697	0.661	0.623	0.574	0.526	0.500	0.498
4.010	.819	.785	.725	.679	.641	.603	.548	.473	.365	.262
6.006	.814	.779	.718	.672	.634	.598	.544	.472	.367	.264
7.029	.810	.773	.713	.668	.630	.595	.542	.472	.368	.265

	$p/p_{t,j}$ for left row x/L of—					$p/p_{t,j}$ for right row x/L of—			
NPR	0.120	0.271	0.436	0.603	0.772	0.271	0.436	0.603	0.772
2.000	0.766	0.643	0.558	0.504	0.501	0.745	0.689	0.626	0.542
4.010	.753	.610	.504	.348	.192	.732	.674	.610	.513
6.006	.748	.604	.500	.347	.192	.724	.667	.605	.510
7.029	.745	.600	.497	.347	.193	.718	.663	.603	.509

[Lower flap]

	$p/p_{t,j}$ for center row x/L of—									
NPR	0.116	0.190	0.273	0.357	0.443	0.534	0.616	0.698	0.780	0.862
2.000	0.698	0.689	0.660	0.623	0.556	0.491	0.490	0.492	0.492	0.492
4.010	.681	.669	.642	.604	.535	.111	.125	.128	.196	.231
6.006	.673	.660	.635	.598	.532	.112	.123	.125	.123	.113
7.029	.668	.655	.631	.595	.530	.112	.121	.124	.122	.113

	$p/p_{t,j}$ for left row x/L of—					$p/p_{t,j}$ for right row x/L of—				
NPR	0.177	0.325	0.476	0.626	0.777	0.177	0.329	0.486	0.645	0.811
2.000	0.614	0.481	0.482	0.486	0.490	0.728	0.686	0.629	0.525	0.492
4.010	.587	.109	.219	.225	.232	.710	.665	.612	.496	.114
6.006	.582	.106	.115	.111	.137	.700	.657	.607	.493	.112
7.029	.579	.106	.114	.108	.094	.695	.653	.604	.493	.111

Table 3. Concluded

(y) Concluded

[Sidewalls]

NPR	$p/p_{t,j}$ for left sidewall centerline x/L of—					
	0.108	0.215	0.323	0.430	0.538	0.645
2.000	0.406	0.491	0.497	0.498	0.499	0.500
4.010	.124	.275	.252	.256	.251	.250
6.006	.103	.169	.201	.171	.166	.174
7.029	.103	.156	.159	.175	.133	.146

NPR	$p/p_{t,j}$ for right sidewall centerline x/L of –					
	0.131	0.262	0.394			
2.000	0.776	0.736	0.698			
4.010	.764	.725	.680			
6.006	.755	.715	.679			
7.029	.749	.709	.676			

Table 4. Static Internal Performance of the Skewed-Throat Nozzle

(a) $\theta_{skew} = 35°$, AR = 1.748, subsonic expansion ratio

NPR	F_A/F_i	F_r/F_i	w_p/w_i	δ_p, deg	δ_y, deg
$\delta_{v,p} = 0°$, $\delta_{v,s} = 0°$					
2.005	0.9553	0.9575	0.8291	1.19	3.75
4.010	.9847	.9859	.8322	2.83	.39
5.006	.9830	.9842	.8343	2.82	.26
5.900	.9789	.9801	.8363	2.73	.31
7.011	.9738	.9748	.8388	2.58	.42
7.820	.9693	.9702	.8406	2.50	.50
$\delta_{v,p} = 0°$, $\delta_{v,s} = 12°$					
2.003	0.9385	0.9447	0.8724	−0.49	6.57
4.006	.9341	.9603	.8768	5.20	12.42
5.020	.9394	.9668	.8795	6.52	12.13
5.906	.9392	.9669	.8816	6.58	12.17
7.001	.9387	.9660	.8843	6.53	12.11
8.224	.9360	.9629	.8873	6.42	12.06
8.586	.9354	.9621	.8887	6.40	12.01
$\delta_{v,p} = 0°$, $\delta_{v,s} = 24°$					
2.010	0.9358	0.9416	0.8748	−0.65	6.30
4.003	.9272	.9607	.8785	4.78	14.46
5.005	.9211	.9644	.8807	6.27	16.16
5.908	.9201	.9689	.8825	6.66	17.14
7.009	.9186	.9708	.8855	6.89	17.75
8.202	.9179	.9717	.8884	6.95	18.02
$\delta_{v,p} = 0°$, $\delta_{v,s} = 35°$					
2.006	0.9448	0.9491	0.8710	−0.49	5.41
4.004	.9210	.9554	.8794	4.88	14.69
5.007	.9192	.9631	.8804	6.39	16.27
5.901	.9161	.9671	.8825	6.71	17.60
7.002	.9126	.9707	.8841	6.85	18.88
7.998	.9088	.9711	.8864	6.97	19.60
$\delta_{v,p} = 7°$, $\delta_{v,s} = 35°$					
2.004	0.9494	0.9498	0.9563	0.03	1.62
4.001	.9278	.9511	.9630	4.13	12.05
5.000	.9211	.9558	.9646	6.75	14.06
5.905	.9193	.9609	.9655	7.96	15.11
6.999	.9171	.9643	.9670	8.47	16.12
8.202	.9152	.9671	.9686	8.77	16.94
8.424	.9148	.9673	.9689	8.83	17.05

Table 4. Continued

(a) Concluded

NPR	F_A/F_i	F_r/F_i	w_p/w_i	δ_p, deg	δ_y, deg
$\delta_{v,p} = 20°$, $\delta_{v,s} = 35°$					
2.001	0.9568	0.9618	1.0679	5.61	−1.76
4.006	.9513	.9707	1.0691	8.14	8.20
5.006	.9273	.9610	1.0704	10.95	10.84
5.913	.9192	.9621	1.0712	12.40	12.27
7.011	.9110	.9625	1.0722	13.75	13.35
8.212	.9054	.9631	1.0735	14.60	14.15
9.023	.9031	.9638	1.0745	14.99	14.53
9.628	.9030	.9651	1.0748	15.14	14.74
$\delta_{v,p} = 25°$, $\delta_{v,s} = 35°$					
2.001	0.8389	0.9270	0.9329	23.59	9.89
4.001	.7924	.9521	.9529	28.71	20.76
5.003	.7747	.9570	.9570	30.64	22.72
5.901	.7759	.9629	.9593	30.48	23.75
6.793	.7744	.9672	.9633	30.68	24.50
$\delta_{v,p} = 0°$, $\delta_{v,s} = 0°$					
2.004	0.9220	0.9271	0.6710	3.74	4.72
4.006	.9733	.9755	.6892	1.14	−3.66
5.003	.9776	.9790	.7085	0.90	−2.90
5.899	.9768	.9778	.7178	.81	−2.41
7.006	.9721	.9728	.7313	.70	−2.02
8.207	.9695	.9699	.7468	.60	−1.63
8.343	.9694	.9698	.7489	.63	−1.61
$\delta_{v,p} = 0°$, $\delta_{v,s} = 35°$					
2.006	0.8679	0.8762	0.7988	1.99	7.66
3.997	.8552	.9265	.8226	7.61	21.55
5.005	.8465	.9331	.8286	9.83	23.27
5.905	.8448	.9369	.8335	11.10	23.63
7.000	.8459	.9427	.8409	10.88	24.35
7.343	.8451	.9432	.8434	10.74	24.61
$\delta_{v,p} = 25°$, $\delta_{v,s} = 35°$					
2.009	0.8050	0.9390	0.9150	21.43	24.43
3.998	.7317	.9277	.9551	27.96	29.71
5.011	.7075	.9293	.9673	31.04	31.08
5.907	.7020	.9322	.9783	32.50	30.87
7.007	.6955	.9354	.9918	34.12	30.60
7.245	.6959	.9358	.9941	34.17	30.53

Table 4. Continued

(b) $\theta_{\text{skew}} = 35°$, AR = 1.748, supersonic expansion ratio

NPR	F_A/F_i	F_r/F_i	w_p/w_i	δ_p, deg	δ_y, deg
$\delta_{v,p} = 0°$, $\delta_{v,s} = 35°$					
2.004	0.9235	0.9274	0.8652	−3.27	4.13
3.999	.9184	.9503	.8719	−.51	14.89
6.005	.9072	.9531	.8748	6.28	16.84
8.599	.9043	.9637	.8792	7.86	18.85
$\delta_{v,p} = 0°$, $\delta_{v,s} = 24°$					
2.001	0.9456	0.9676	0.8919	−6.88	10.20
3.996	.9256	.9559	.8952	−.52	14.45
6.011	.9122	.9560	.8986	6.34	16.34
7.997	.9138	.9638	.9024	8.09	16.91
9.021	.9159	.9670	.9046	8.26	16.99
$\delta_{v,p} = 0°$, $\delta_{v,s} = 12°$					
2.006	0.9614	0.9784	0.8853	−6.25	8.74
4.012	.9394	.9621	.8946	−.73	12.46
5.995	.9285	.9584	.8985	7.92	12.13
8.012	.9329	.9650	.9021	9.05	11.94
9.065	.9347	.9670	.9042	9.08	11.94
$\delta_{v,p} = 0°$, $\delta_{v,s} = 0°$					
4.004	0.9659	0.9710	0.8617	4.07	4.19
5.998	.9727	.9792	.8646	6.05	2.74
8.024	.9708	.9776	.8673	6.34	2.34
9.006	.9698	.9765	.8687	6.28	2.37
9.902	.9685	.9751	.8704	6.26	2.33
11.002	.9669	.9734	.8719	6.21	2.37
11.373	.9662	.9727	.8725	6.20	2.36
$\delta_{v,p} = 7°$, $\delta_{v,s} = 35°$					
2.002	0.9225	0.9285	0.8798	3.02	5.74
4.007	.9228	.9644	.8874	4.60	16.31
6.002	.8913	.9564	.8904	11.77	18.20
7.994	.8819	.9602	.8943	13.80	19.48
$\delta_{v,p} = 20°$, $\delta_{v,s} = 35°$					
2.006	0.9317	0.9684	0.9043	11.48	11.17
3.999	.8887	.9727	.9208	15.53	19.17
6.020	.8207	.9517	.9259	23.92	21.02
7.394	.8116	.9558	.9296	25.55	21.71

Table 4. Continued

(b) Concluded

NPR	F_A/F_i	F_r/F_i	w_p/w_i	δ_p, deg	δ_y, deg
$\delta_{v,p} = 25°$, $\delta_{v,s} = 35°$					
1.996	0.9014	0.9613	0.9188	16.46	12.63
3.999	.8608	.9729	.9392	20.49	20.36
6.010	.7849	.9505	.9452	28.61	22.34
7.110	.7757	.9557	.9489	30.19	22.95
$\delta_{v,p} = 0°$, $\delta_{v,s} = 35°$					
2.001	0.8503	0.8551	0.7977	2.38	5.57
4.008	.8502	.9163	.8222	5.32	21.36
6.004	.8392	.9262	.8325	11.62	22.76
7.430	.8425	.9372	.8426	10.72	24.18
$\delta_{v,p} = 0°$, $\delta_{v,s} = 0°$					
2.005	0.9161	0.9203	0.6832	4.23	3.50
3.993	.9669	.9689	.6961	2.38	−2.78
6.002	.9766	.9777	.7236	0.97	−2.55
8.009	.9727	.9732	.7480	.78	−1.75
8.754	.9714	.9718	.7569	.71	−1.51
$\delta_{v,p} = 0°$, $\delta_{v,s} = 0°$, short sidewalls					
2.007	0.9467	0.9519	0.6910	4.12	4.31
4.030	.9576	.9605	.7048	3.30	3.06
6.011	.9548	.9604	.7261	3.24	5.33
8.004	.9474	.9556	.7491	2.98	6.90
8.814	.9450	.9542	.7597	2.92	7.38
$\delta_{v,p} = 0°$, $\delta_{v,s} = 0°$, left short sidewall					
2.005	0.9130	0.9153	0.6997	4.03	0.69
3.994	.9448	.9474	.7193	3.75	2.05
6.016	.9422	.9509	.7533	3.90	6.74
8.010	.9440	.9595	.7860	4.04	9.53
9.008	.9460	.9634	.8030	3.74	10.29
9.216	.9451	.9631	.8070	3.80	10.45
$\delta_{v,p} = 25°$, $\delta_{v,s} = 35°$					
2.013	0.7571	0.8804	0.8982	24.90	20.28
4.004	.7553	.9396	.9416	24.83	30.00
6.007	.7041	.9343	.9641	32.37	30.93
7.251	.6914	.9364	.9814	34.83	30.61

Table 4. Concluded

(c) $\theta_{\text{skew}} = 35°$, AR = 3.500, supersonic expansion ratio

NPR	F_A/F_i	F_r/F_i	w_p/w_i	δ_p, deg	δ_y, deg
$\delta_{v,p} = 25°$, $\delta_{v,s} = 35°$					
2.000	0.8776	0.9483	0.9172	19.86	10.91
4.010	.7858	.9371	.9326	29.46	17.79
6.006	.7649	.9520	.9446	32.82	20.02
7.029	.7651	.9600	.9507	33.32	20.66
$\delta_{v,p} = 0°$, $\delta_{v,s} = 0°$					
1.995	0.9555	0.9619	0.8621	−1.97	6.34
4.010	.9423	.9584	.8713	6.68	8.19
6.001	.9586	.9741	.8771	7.39	7.15
8.013	.9621	.9768	.8830	7.16	7.00
9.011	.9616	.9760	.8858	7.07	6.93
9.908	.9611	.9754	.8888	7.01	6.90
10.996	.9619	.9757	.8920	6.87	6.80
11.412	.9615	.9751	.8926	6.83	6.79
$\delta_{v,p} = 0°$, $\delta_{v,s} = 35°$					
2.004	0.9325	0.9381	0.8821	−2.04	5.90
4.007	.9073	.9378	.8895	6.41	13.29
6.008	.9126	.9594	.8967	9.19	15.72
8.009	.9168	.9706	.9041	9.39	16.99
8.953	.9166	.9722	.9080	9.35	17.37

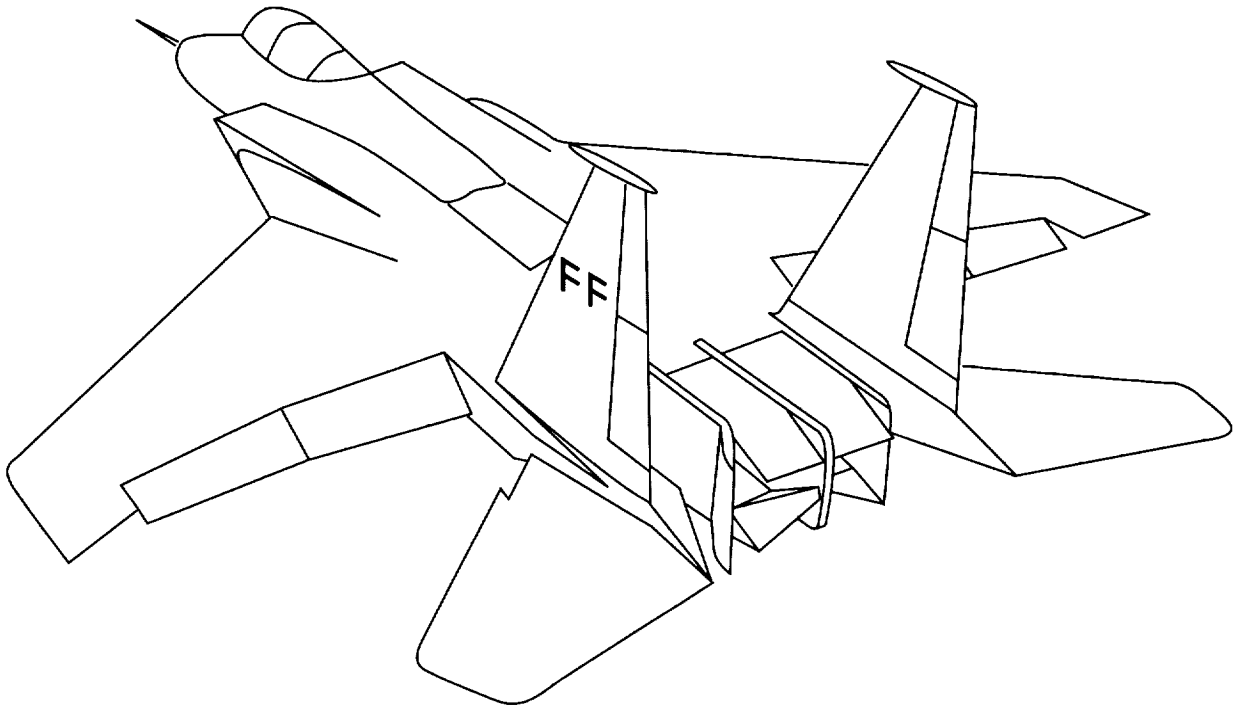

Figure 1. Skewed-throat nozzles installed on typical fighter airplane.

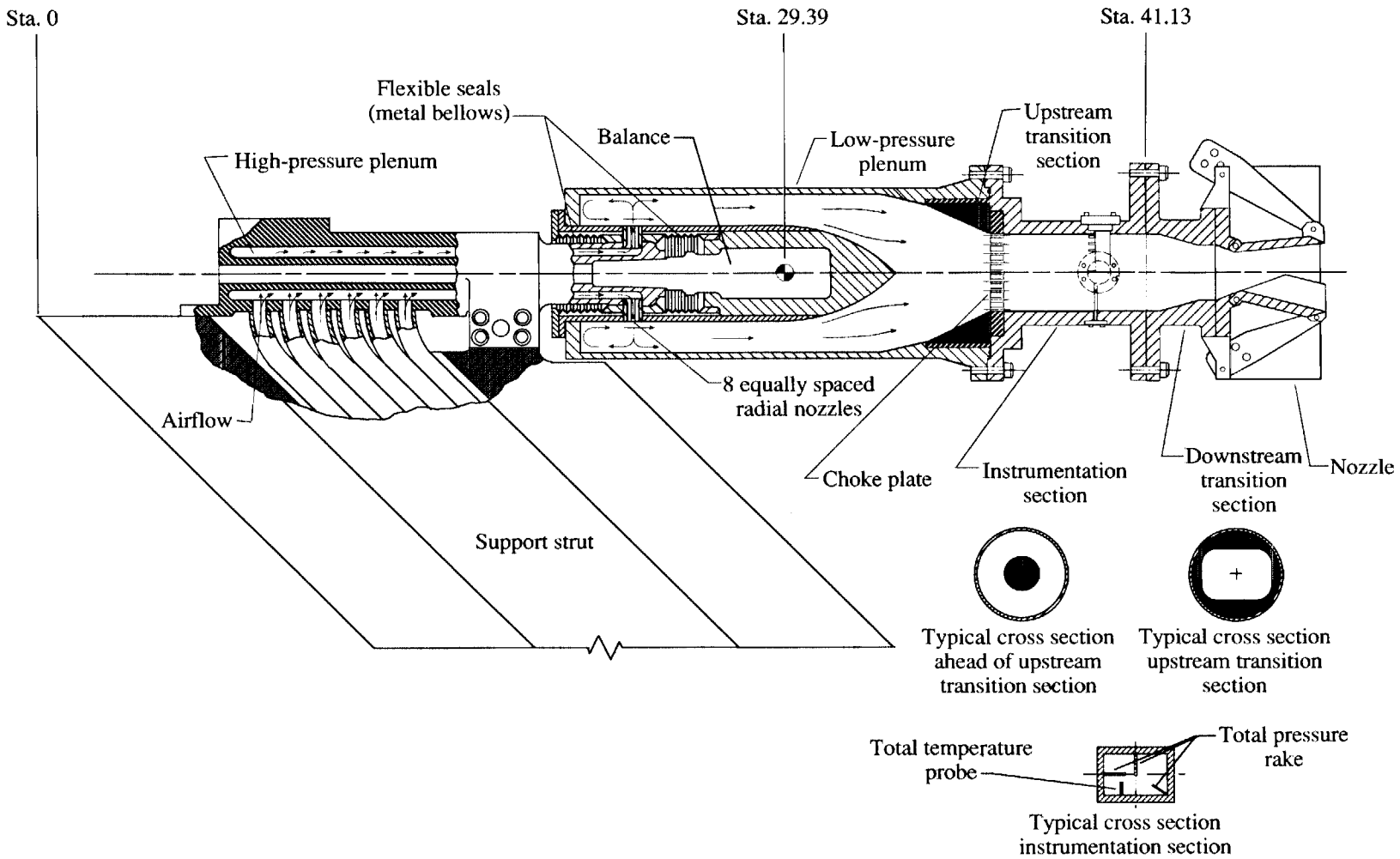

Figure 2. Single engine propulsion simulation system with typical nozzle configuration installed. All dimensions are in inches.

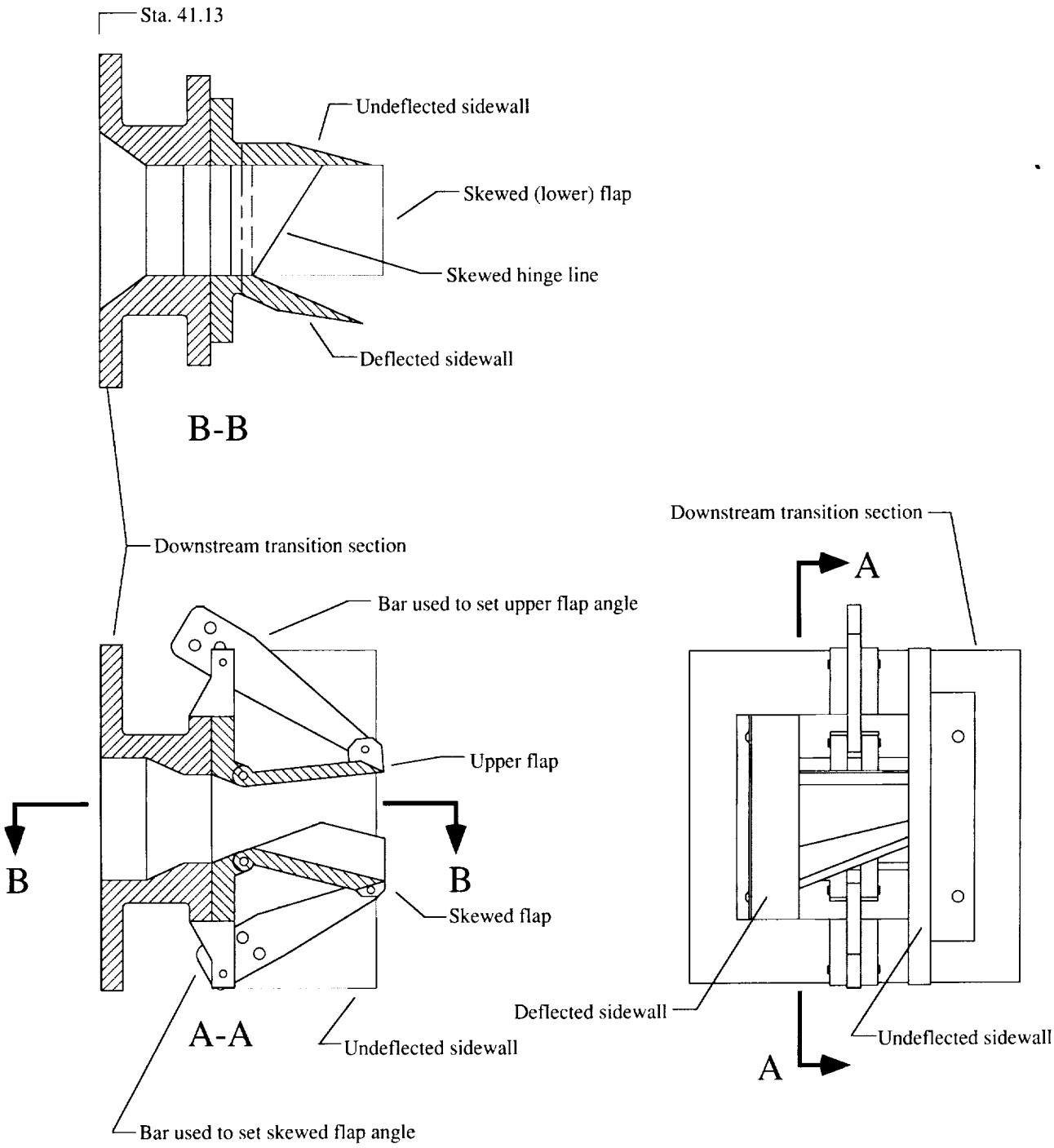

(a) $\theta_{\text{skew}} = 35°$, AR = 1.748, supersonic expansion ratio, $\delta_{v,p} = 0°$.

Figure 3. Typical skewed-throat nozzle configurations. Some surfaces shaded for clarity.

$\theta_{skew} = 35°$ $\theta_{skew} = 50°$

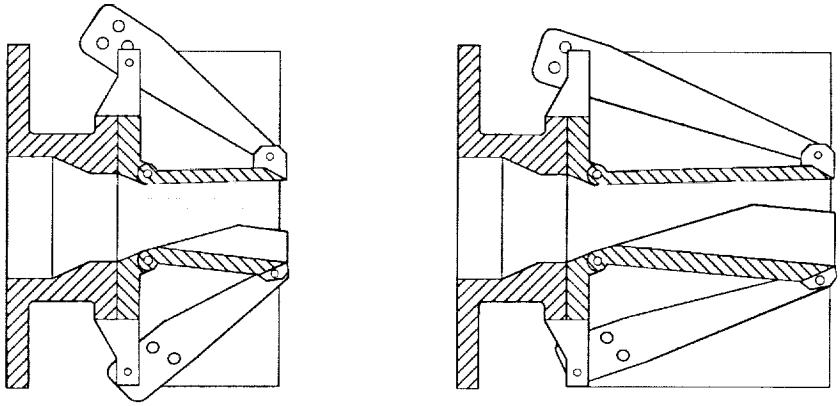

Subsonic (low) expansion ratio, $\delta_{v,p} = 0°$

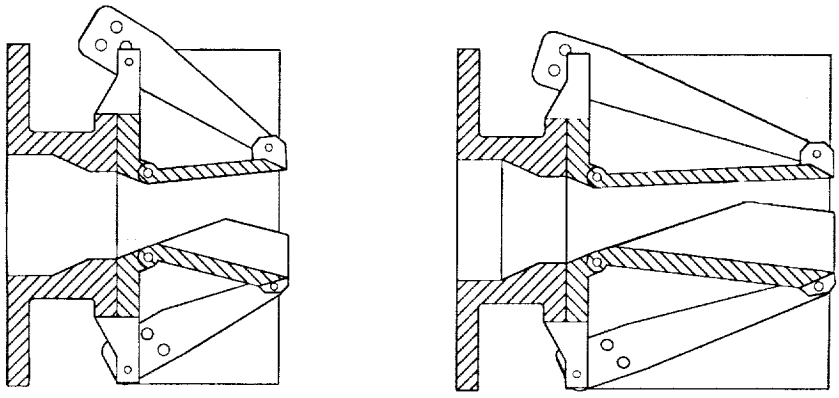

Supersonic (high) expansion ratio, $\delta_{v,p} = 0°$

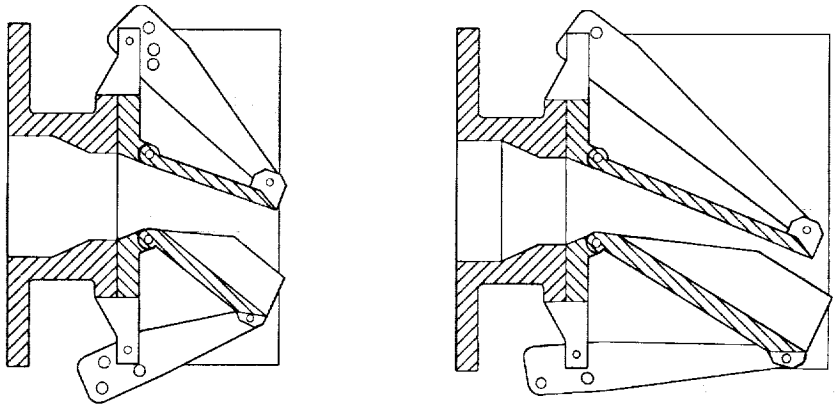

Supersonic (high) expansion ratio, $\delta_{v,p} = 25°$

(b) Variations of hinge line skew angle, expansion ratio, and pitch flap deflection.

Figure 3. Continued.

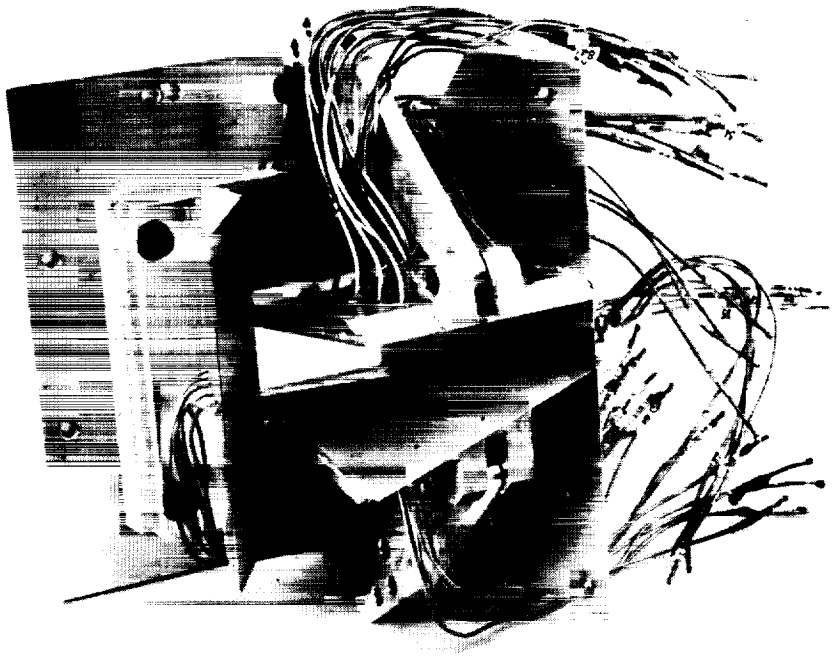

L-88-6835

Yaw thrust-vectoring configuration.

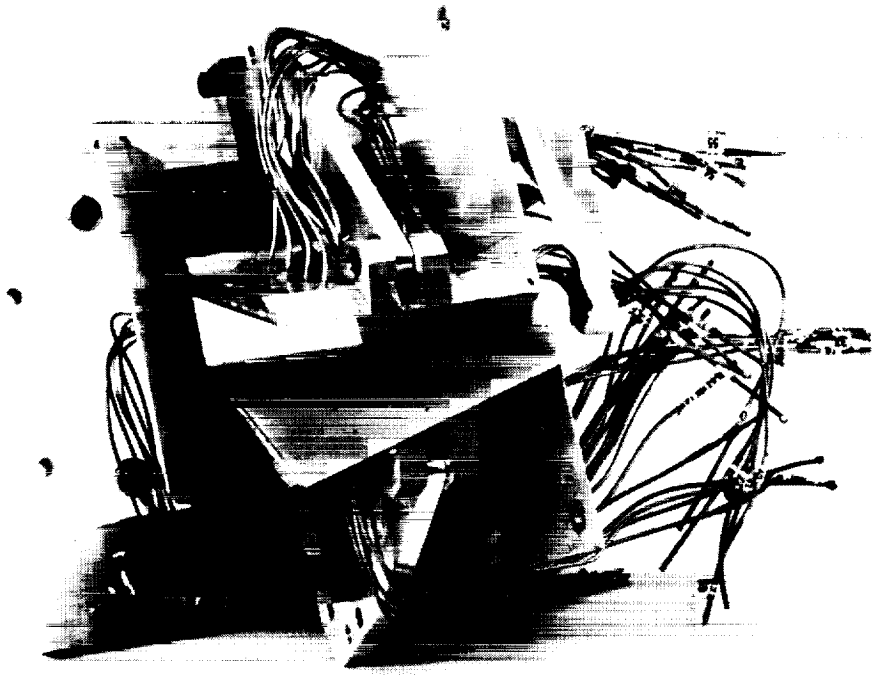

L-88-6832

Multiaxis thrust-vectoring configuration.

(c) Skewed-throat nozzle.

Figure 3. Concluded.

θ_{skew}	AR	Expansion ratio	A	B	C	D
35°	1.748	Supersonic	3.200	2.475	5.10°	0.312
35°	1.748	Subsonic	3.200	2.475	1.50°	.312
35°	3.500	Supersonic	3.200	3.500	4.53°	.520
50°	1.748	Supersonic	5.450	2.475	1.97°	.312
50°	1.748	Subsonic	5.450	2.475	1.02°	.312

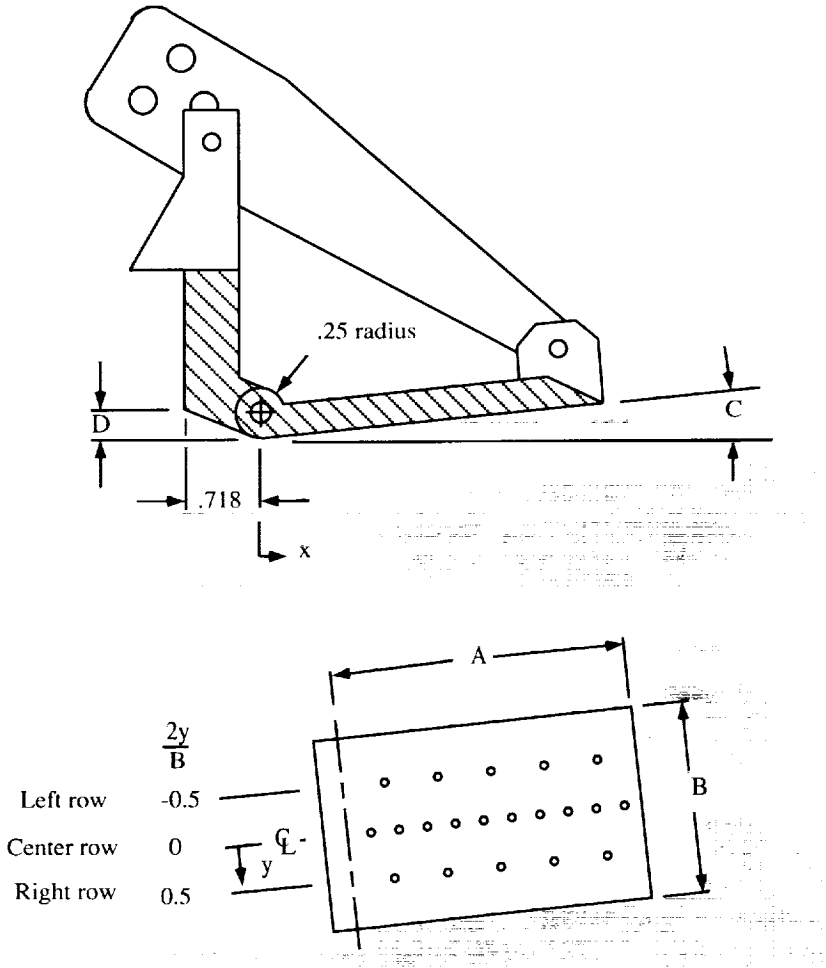

(a) Upper flap assembly details.

Figure 4. Dimensions of skewed-throat nozzle. All dimensions are in inches unless otherwise noted.

θ_{skew}	AR	Expansion ratio	E	F	G	J	K	L
35°	1.748	Supersonic	0.062	18.55°	13.09°	0.230	2.475	3.200
35°	1.748	Subsonic	.062	15.35°	7.15°	.230	2.475	3.200
35°	3.500	Supersonic	.270	11.55°	13.99°	.230	3.500	3.200
50°	1.748	Supersonic	.062	18.15°	6.69°	.370	2.475	5.450
50°	1.748	Subsonic	.062	17.23°	5.30°	.370	2.475	5.450

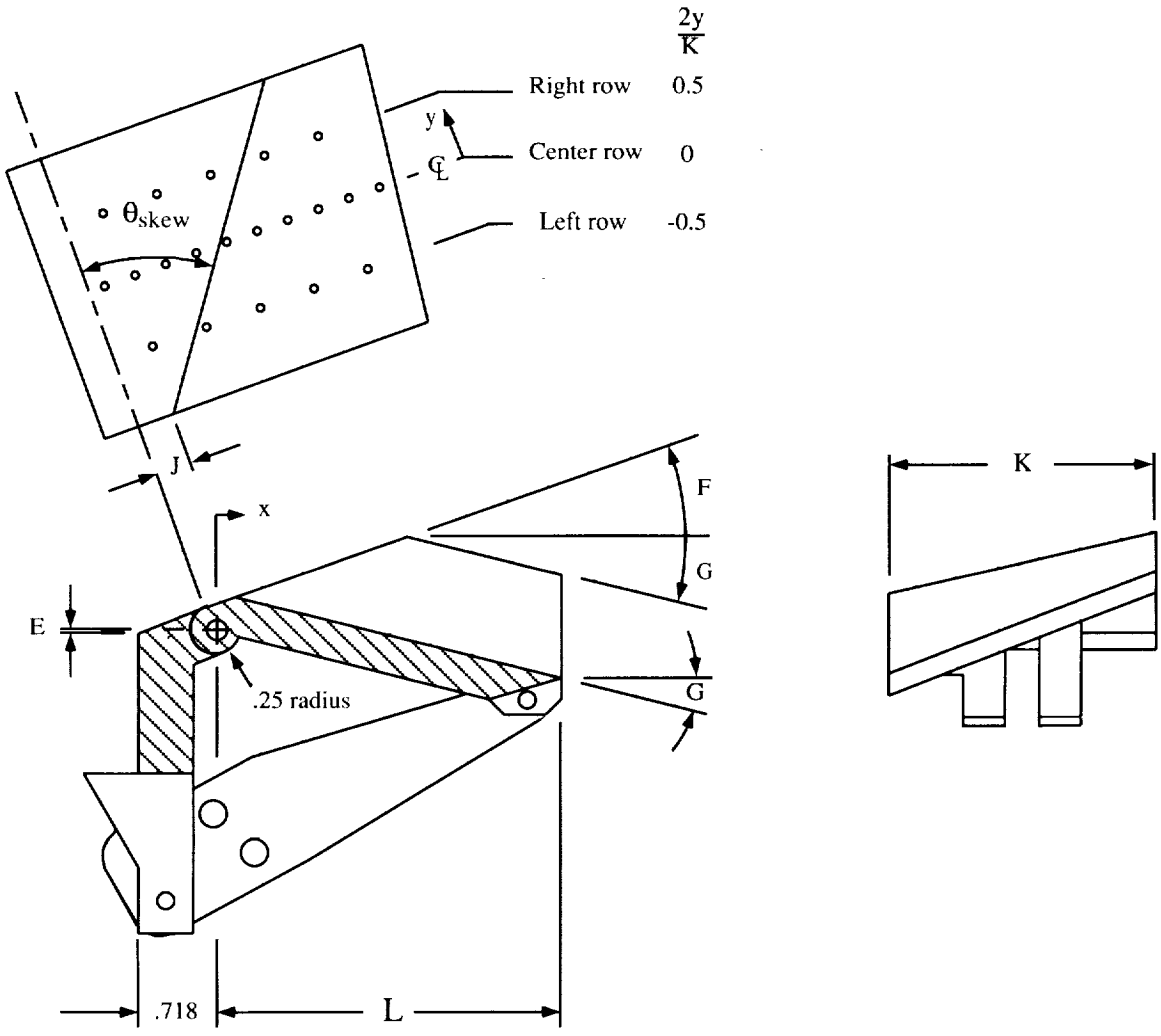

(b) Skewed flap assembly details.

Figure 4. Continued.

θ_{skew}	$\delta_{v,s}$	M	N	P
35°	12°	3.658	7.625	2.70
35°	24°	3.658	7.625	2.70
35°	35°	3.658	7.625	2.66
50°	12°	5.718	8.500	4.76
50°	24°	5.718	8.500	4.75
50°	35°	5.718	8.500	4.72

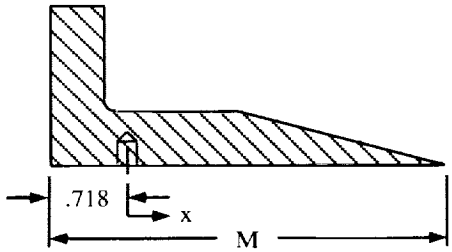

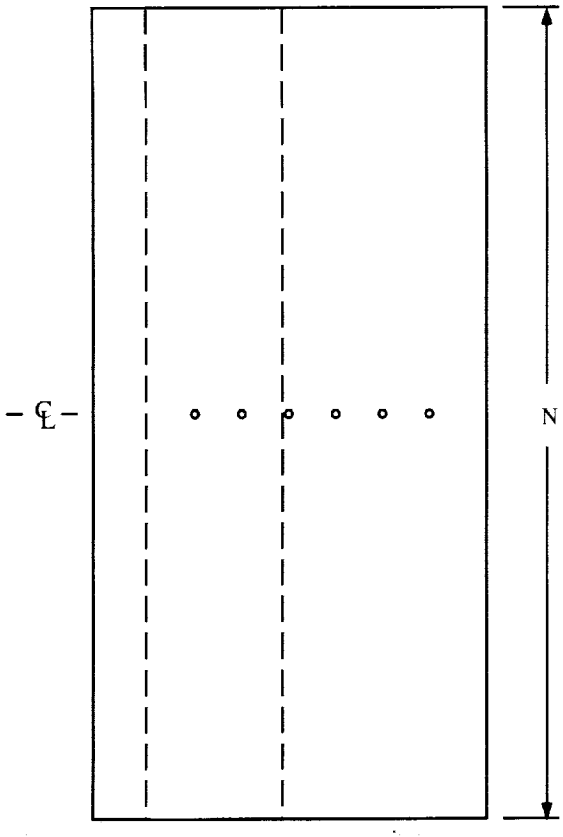

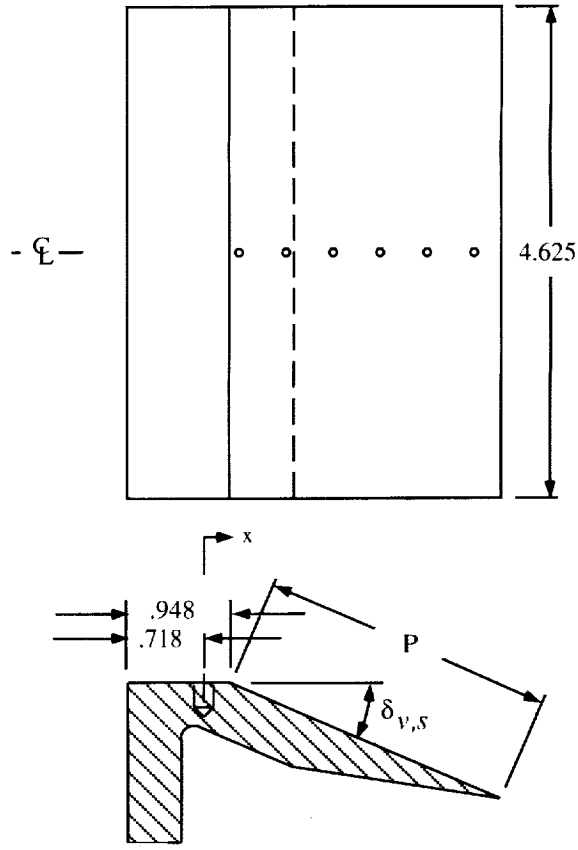

Undeflected sidewall

Deflected sidewall

(c) Undeflected and deflected sidewall details.

Figure 4. Continued.

AR	Q	R
1.748	37.5°	2.475
3.500	26.6°	3.500

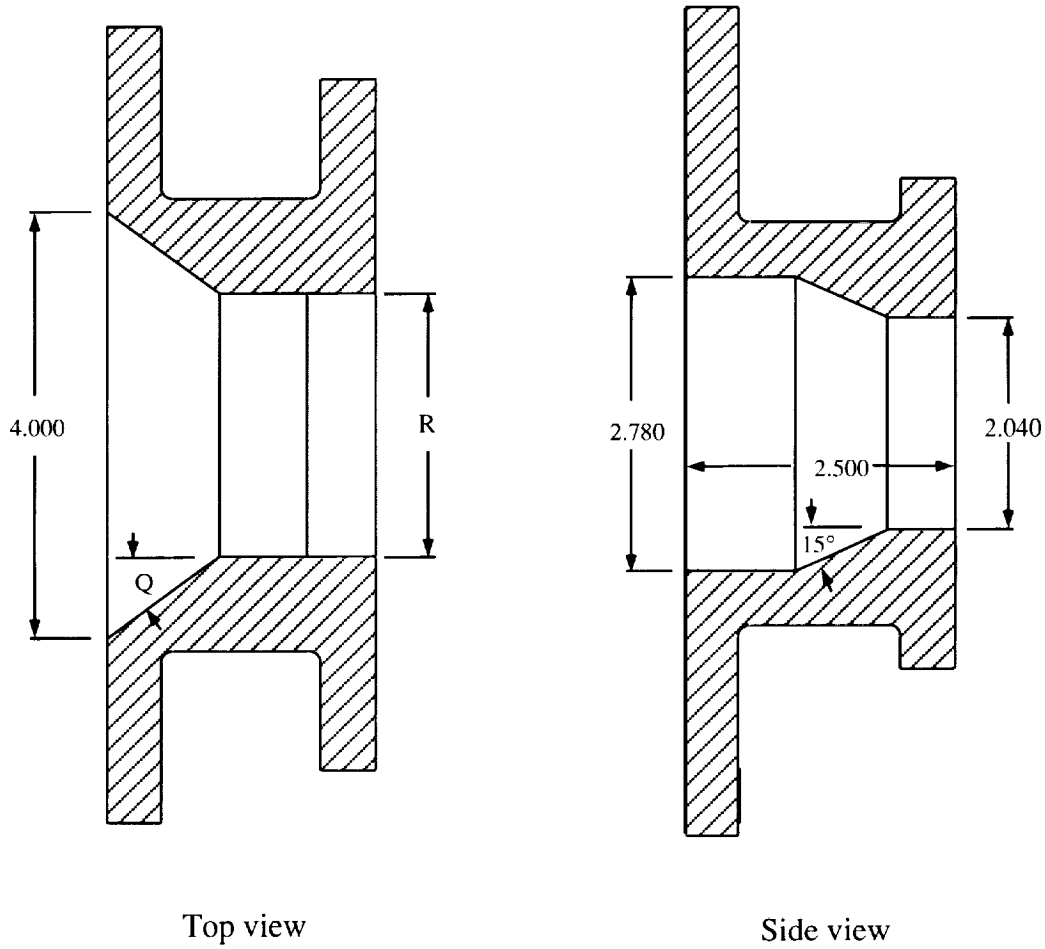

(d) Transition section details.

Figure 4. Concluded.

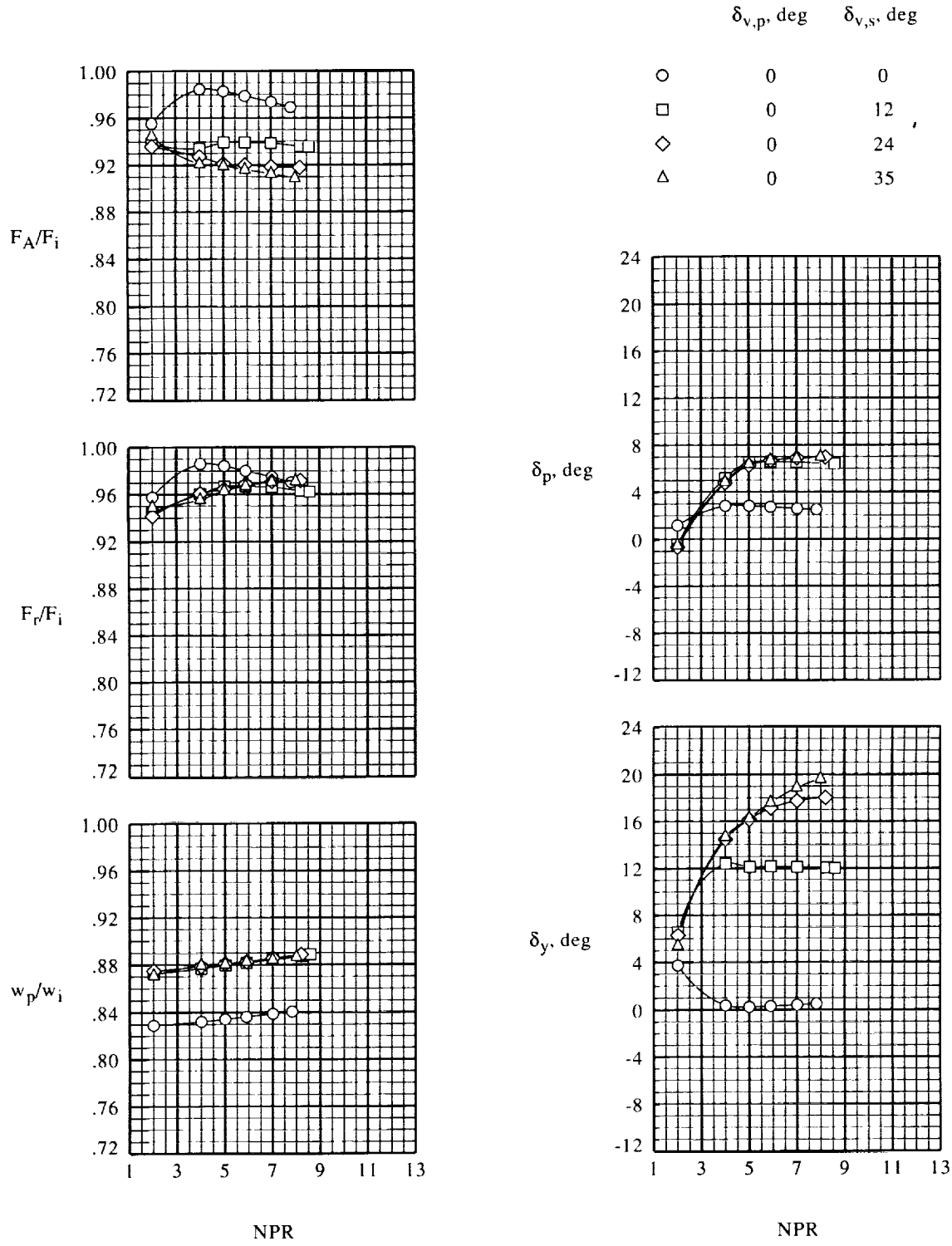

(a) $\delta_{v,p} = 0°$.

Figure 5. Sidewall and pitch flap angles effect on internal performance. $\theta_{skew} = 35°$; AR = 1.748; subsonic expansion ratio.

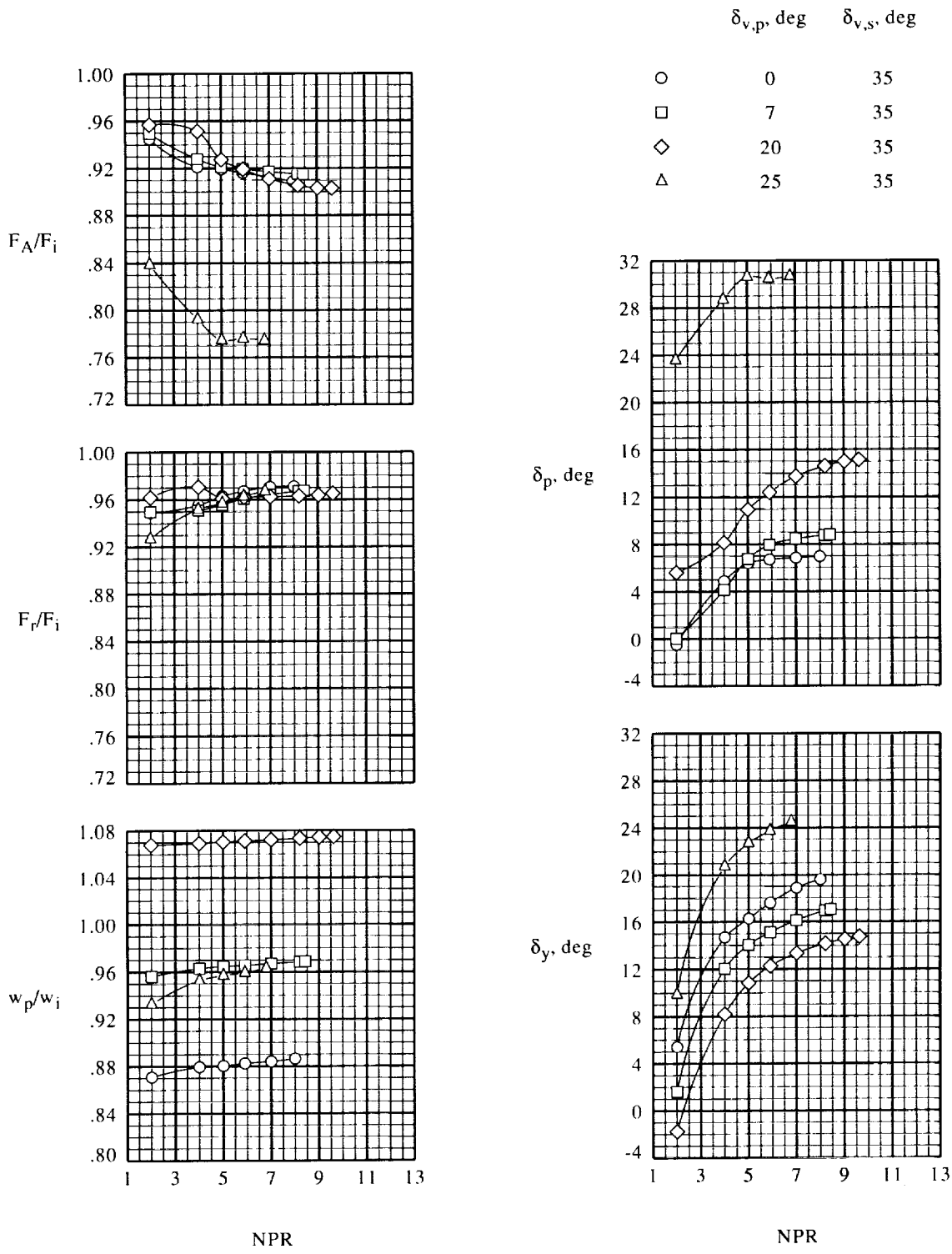

(b) $\delta_{v,s} = 35°$.

Figure 5. Concluded.

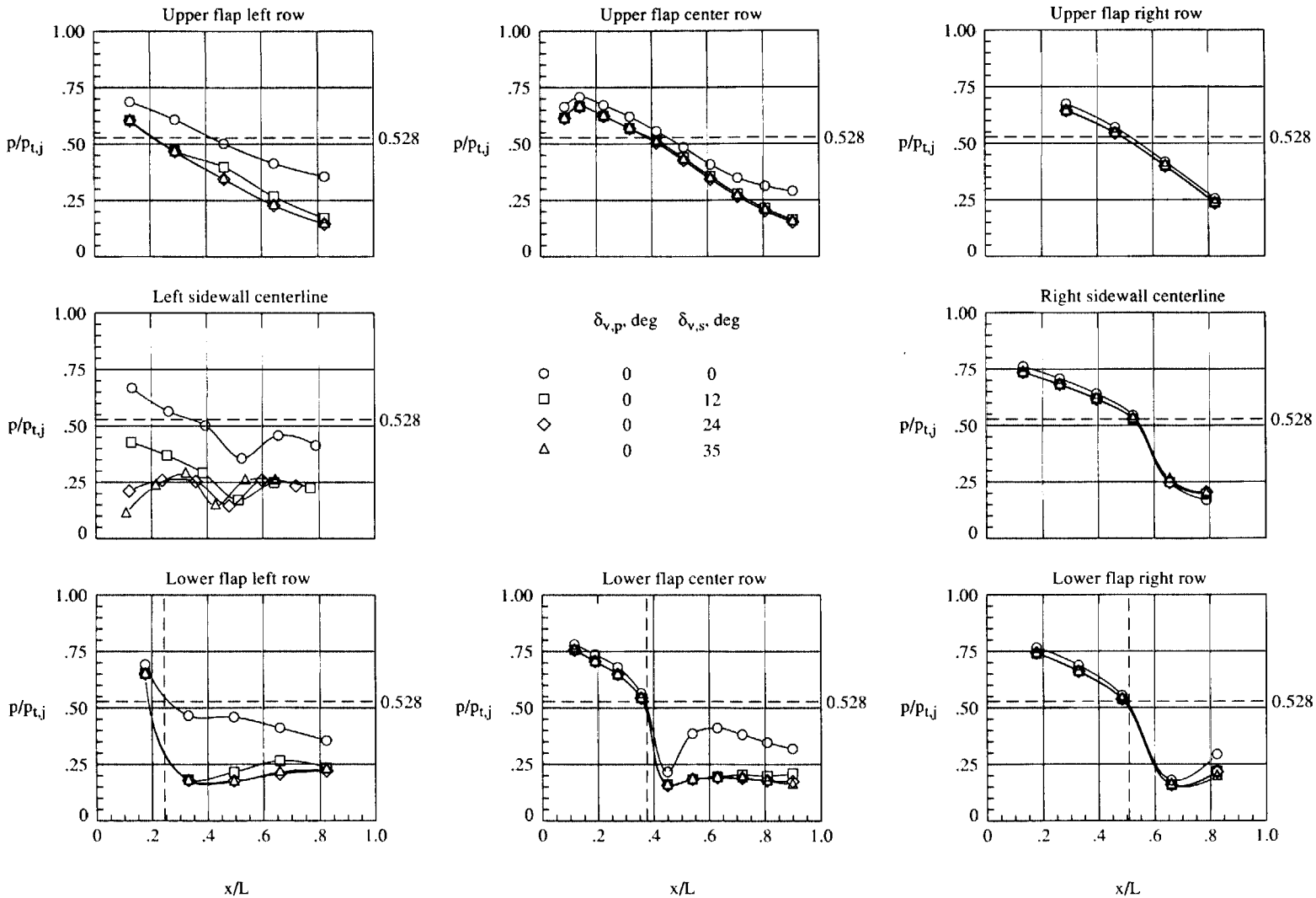

Figure 6. Skewed-throat static pressure distributions. θ_{skew} = 35°; AR = 1.748; subsonic expansion ratio at NPR = 4.005. Vertical dashed lines represent locations of skewed hinge line.

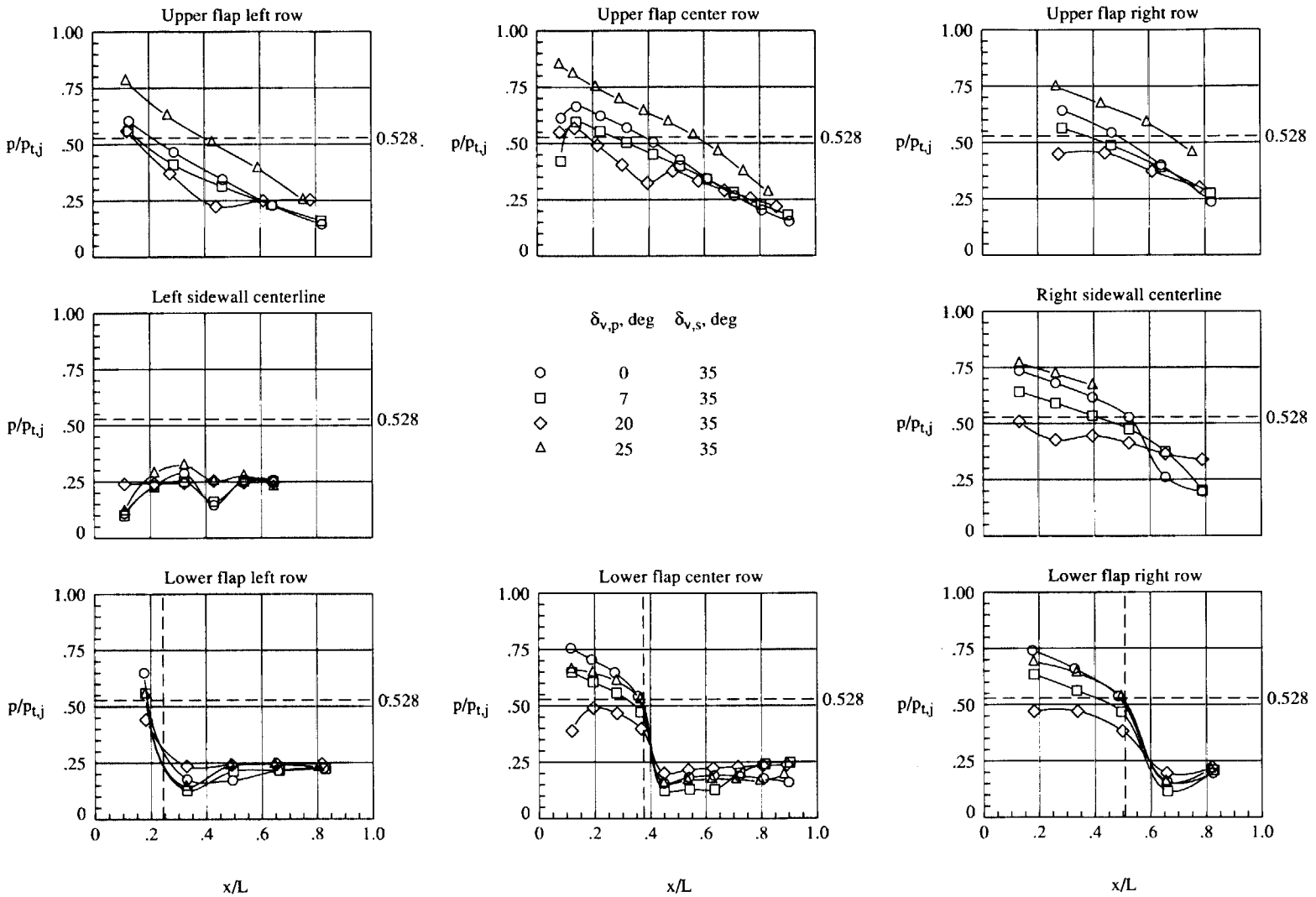

Figure 7. Skewed-throat static pressure distributions. θ_{skew} = 35°; AR = 1.748; subsonic expansion ratio at NPR = 4.003. Vertical dashed lines represent locations of skewed hinge line.

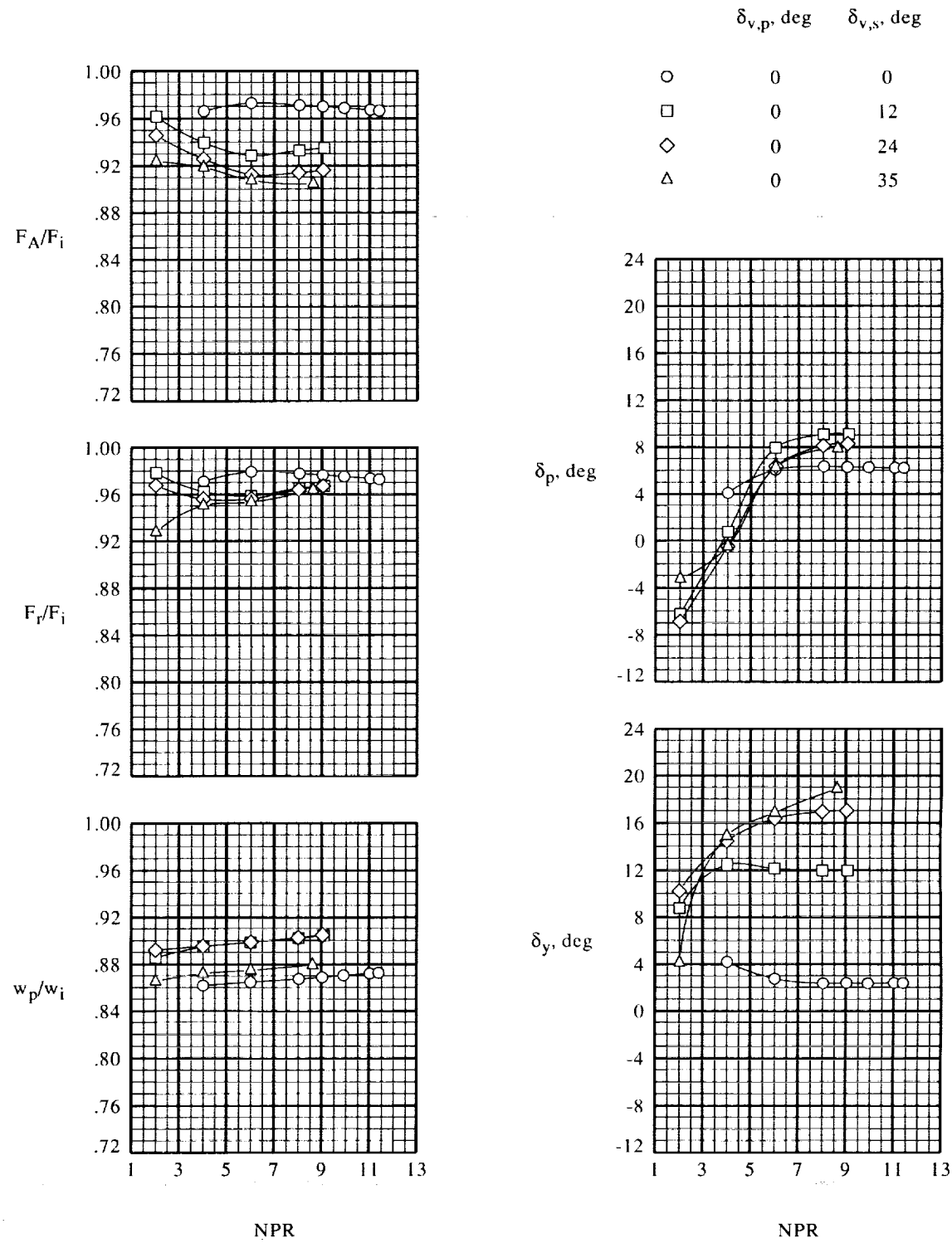

(a) $\delta_{v,p} = 0°$.

Figure 8. Sidewall and pitch flap angles effect on internal performance. $\theta_{skew} = 35°$; AR = 1.748; supersonic expansion ratio.

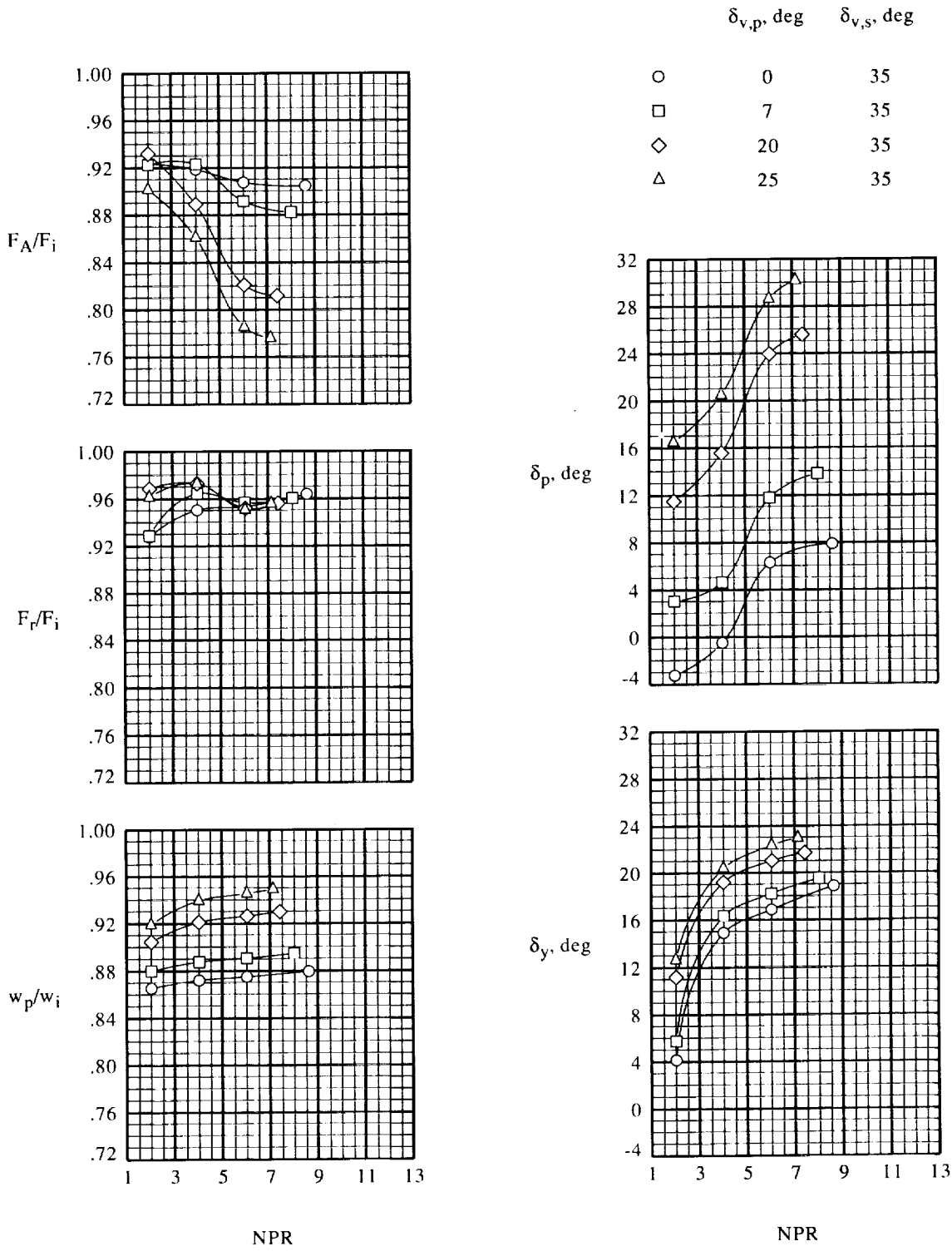

(b) $\delta_{v,s} = 35°$.

Figure 8. Concluded.

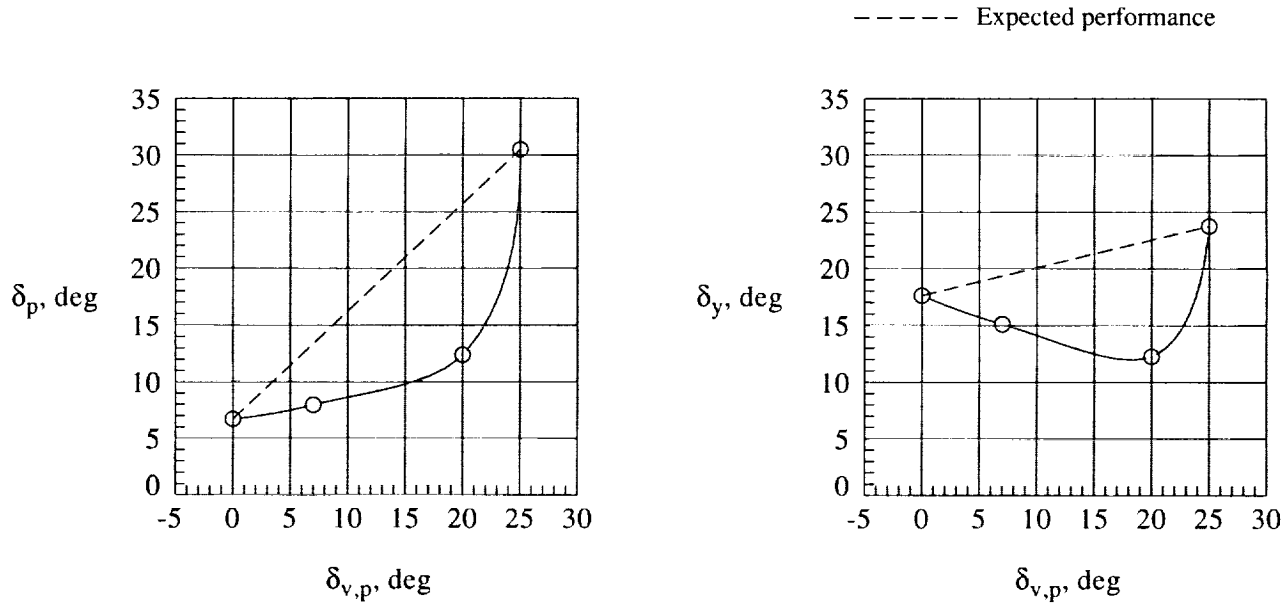

(a) Subsonic expansion ratio.

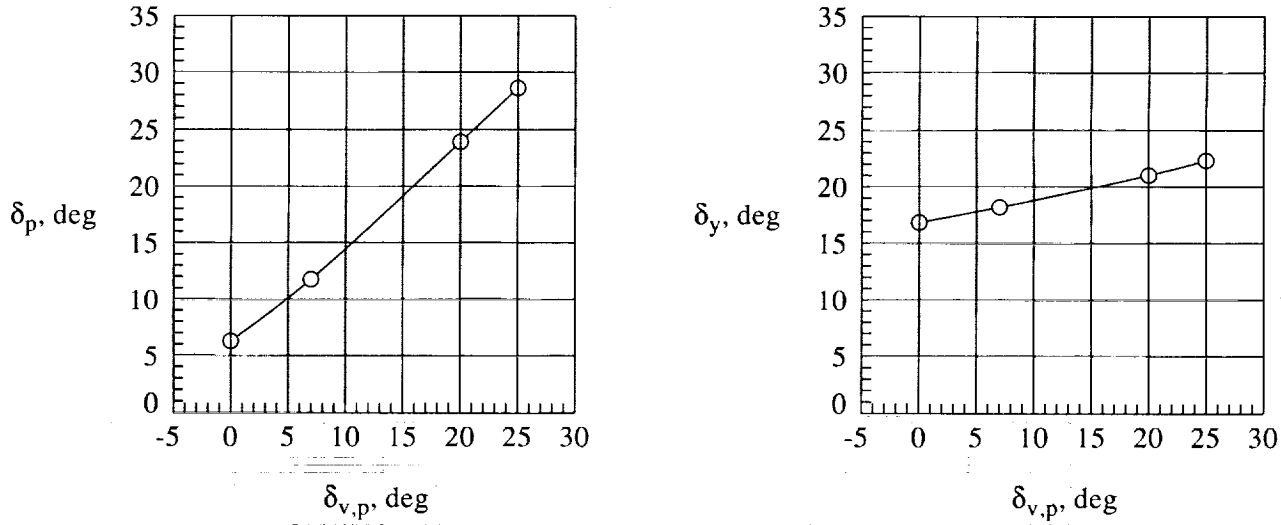

(b) Supersonic expansion ratio.

Figure 9. Pitch flap deflection angle effect on pitch and yaw thrust-vector angles. $\theta_{\text{skew}} = 35°$; AR = 1.748; $\delta_{v,s} = 35°$; NPR = 6.

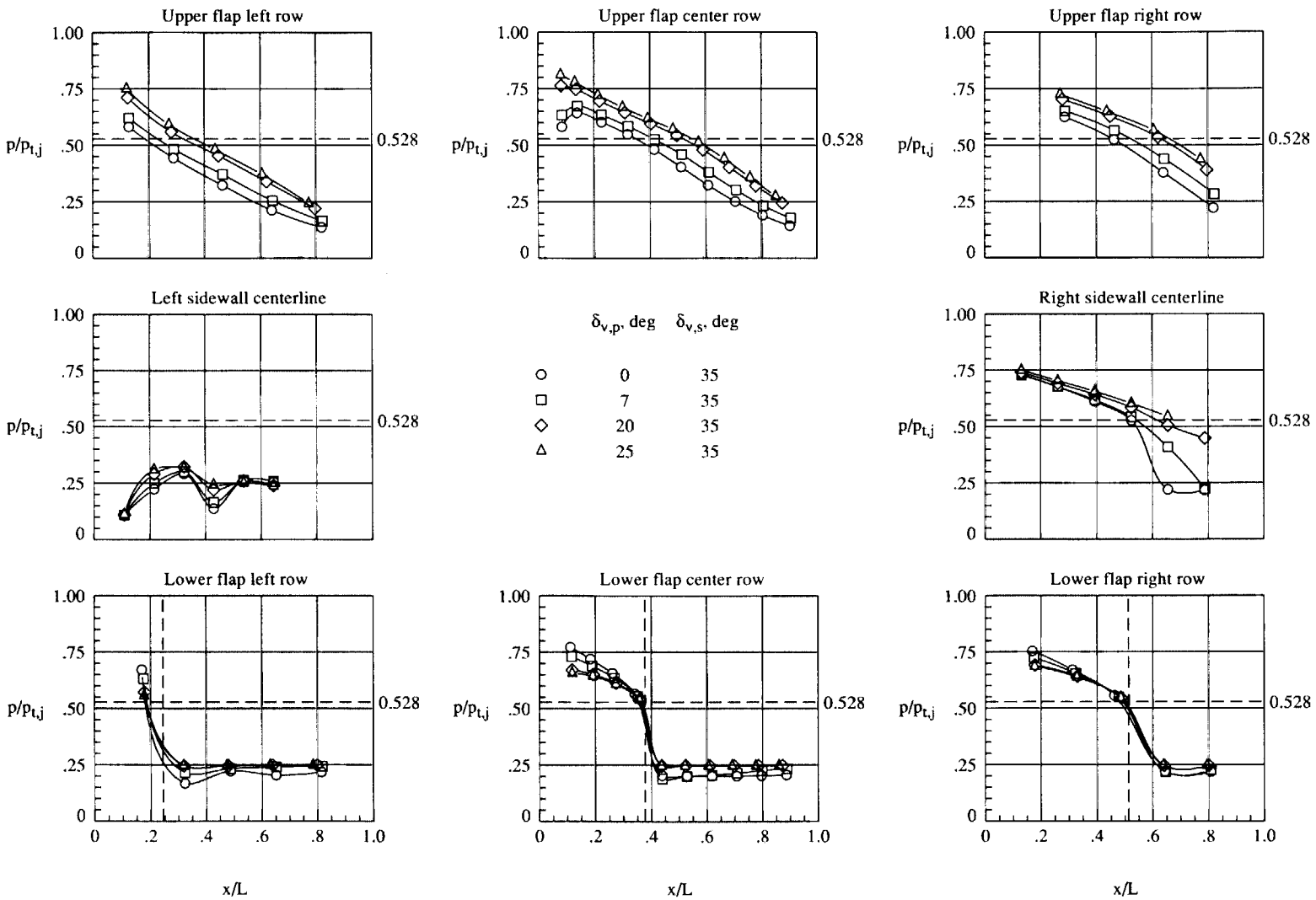

Figure 10. Skewed-throat static pressure distributions. θ_{skew} = 35°; AR = 1.748; supersonic expansion ratio at NPR = 4.001. Vertical dashed lines represent locations of skewed hinge line.

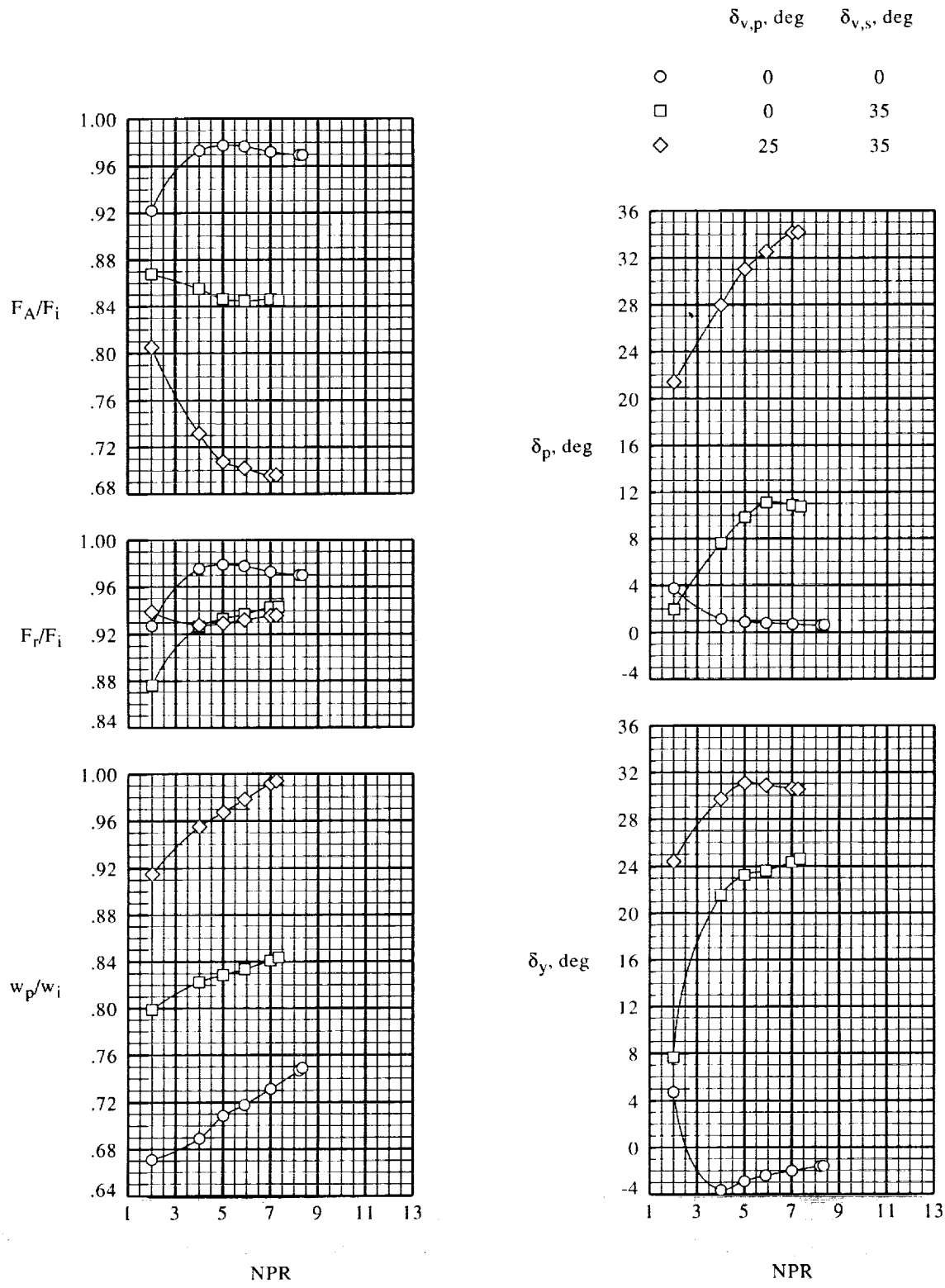

(a) Subsonic expansion ratio.

Figure 11. Sidewall and pitch flap angles effect on internal performance. $\theta_{skew} = 50°$; AR = 1.748.

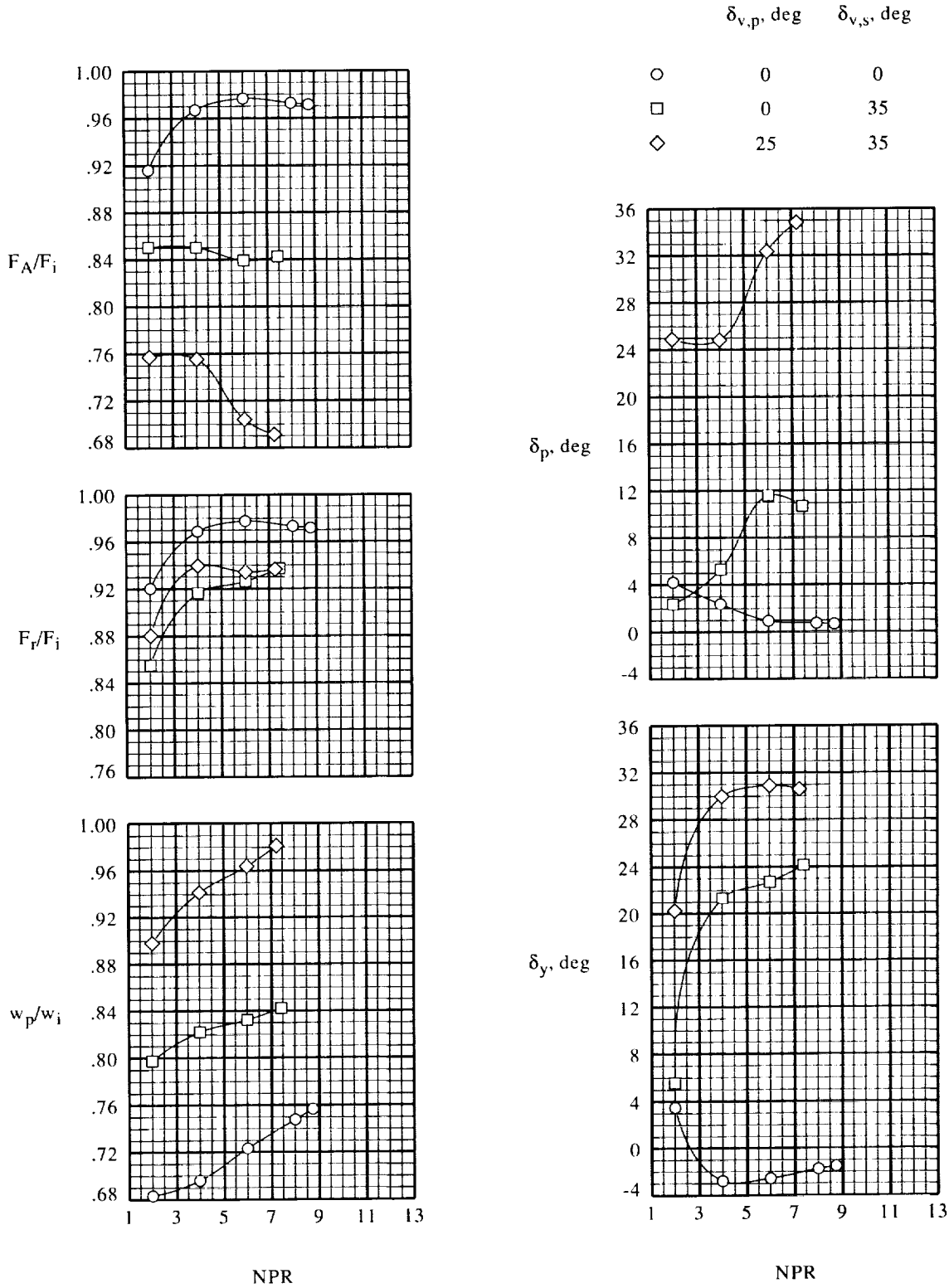

(b) Supersonic expansion ratio.

Figure 11. Concluded.

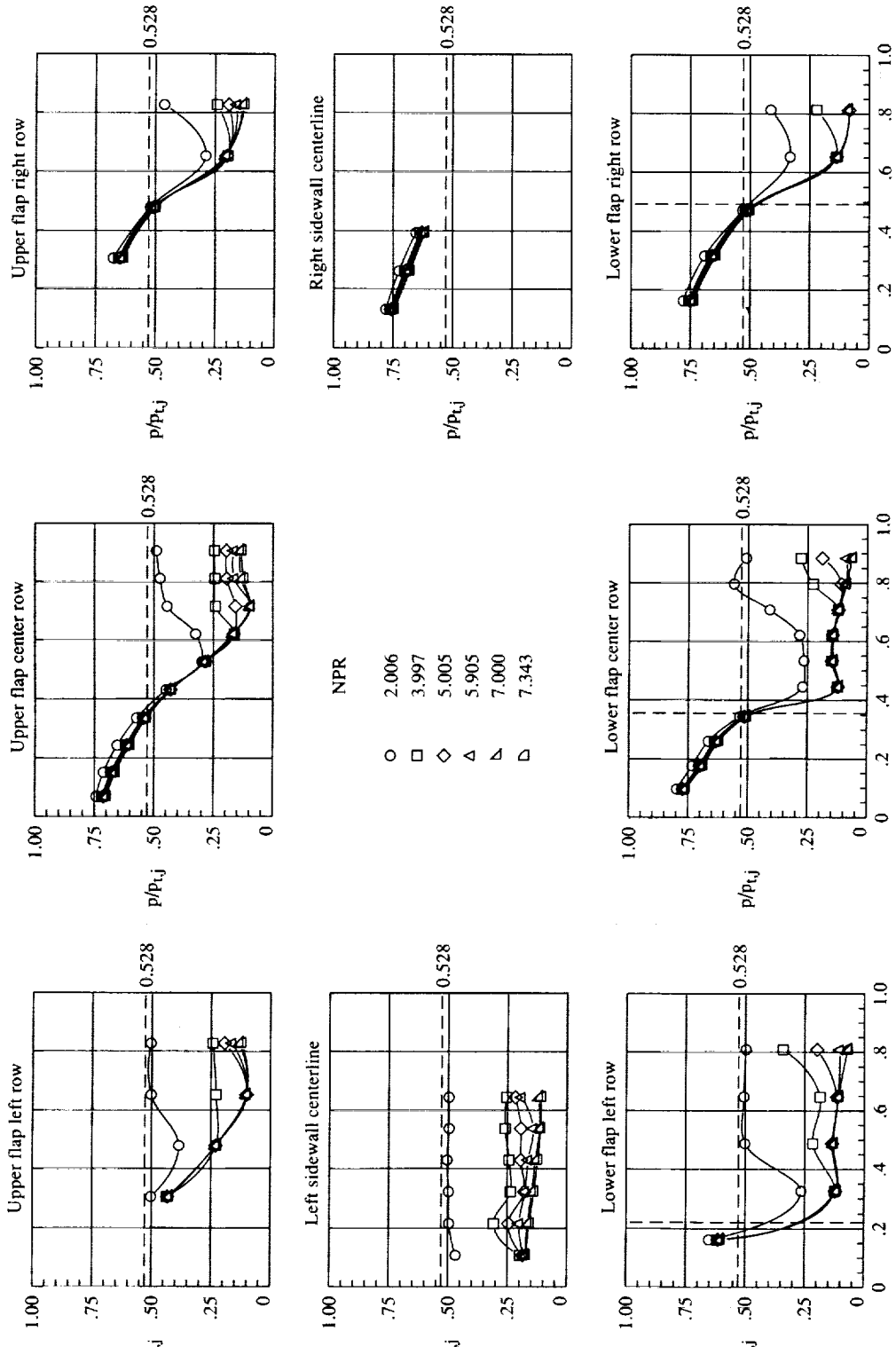

Figure 12. Skewed-throat static pressure distributions. $\theta_{skew} = 50°$; AR = 1.748; subsonic expansion ratio with $\delta_{v,p} = 0°$ and $\delta_{v,s} = 35°$. Vertical dashed lines represent locations of skewed hinge line.

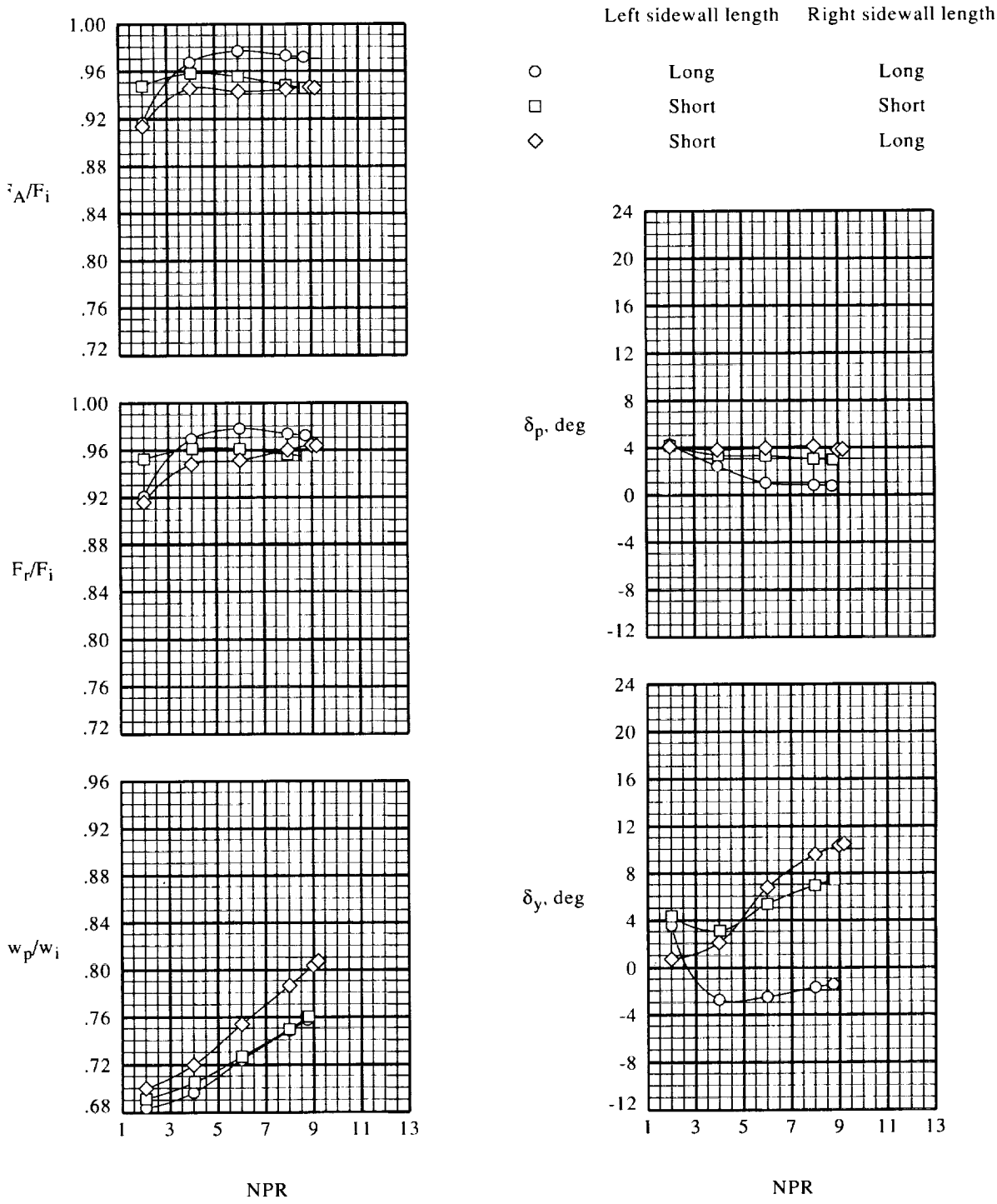

Figure 13. Sidewall length effect on internal performance. $\theta_{skew} = 50°$; AR = 1.748; supersonic expansion ratio with $\delta_{v,p} = 0°$ and $\delta_{v,s} = 0°$.

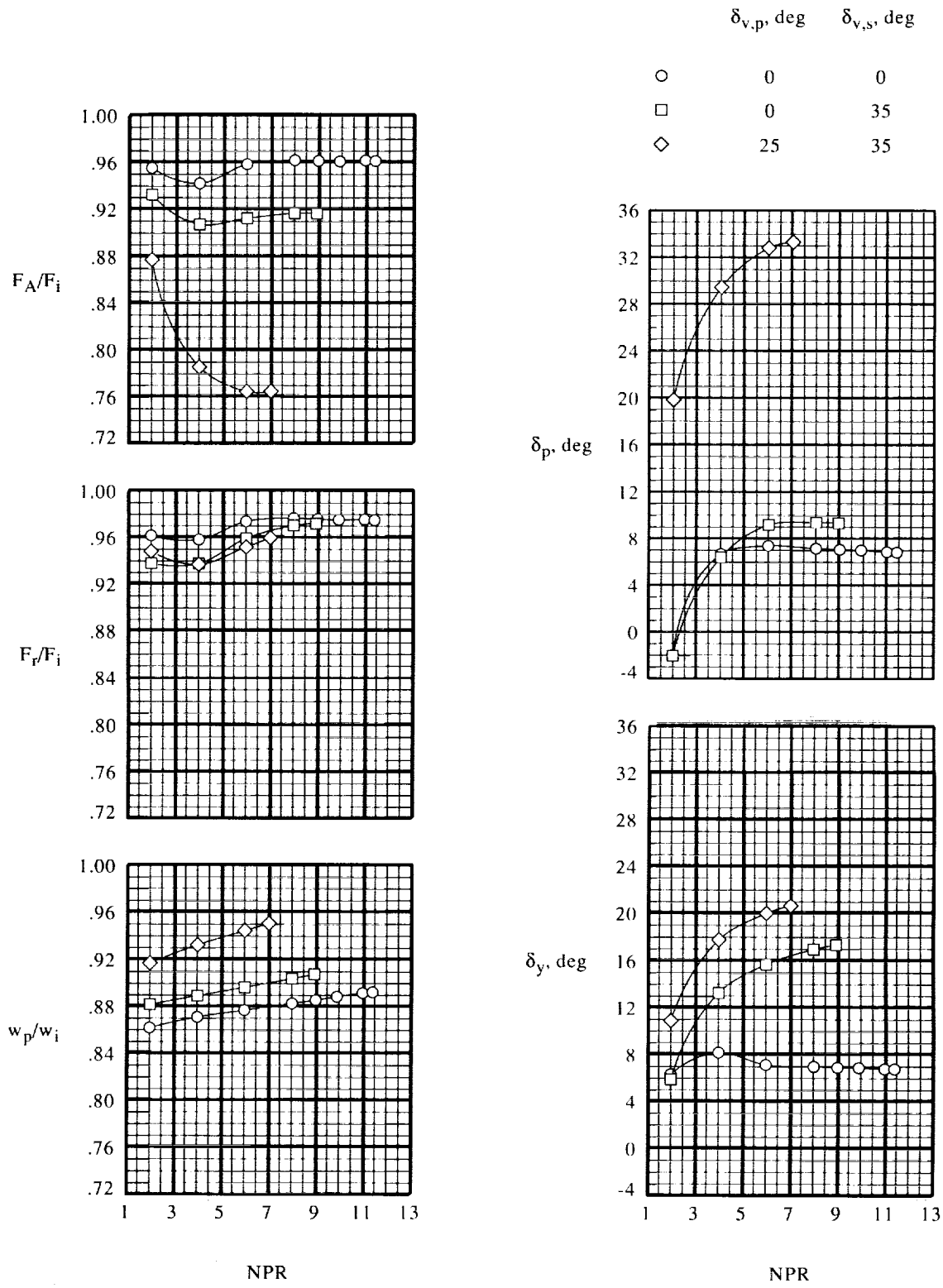

Figure 14. Sidewall and pitch flap angles effect on internal performance. $\theta_{skew} = 35°$; AR = 3.500; supersonic expansion ratio.

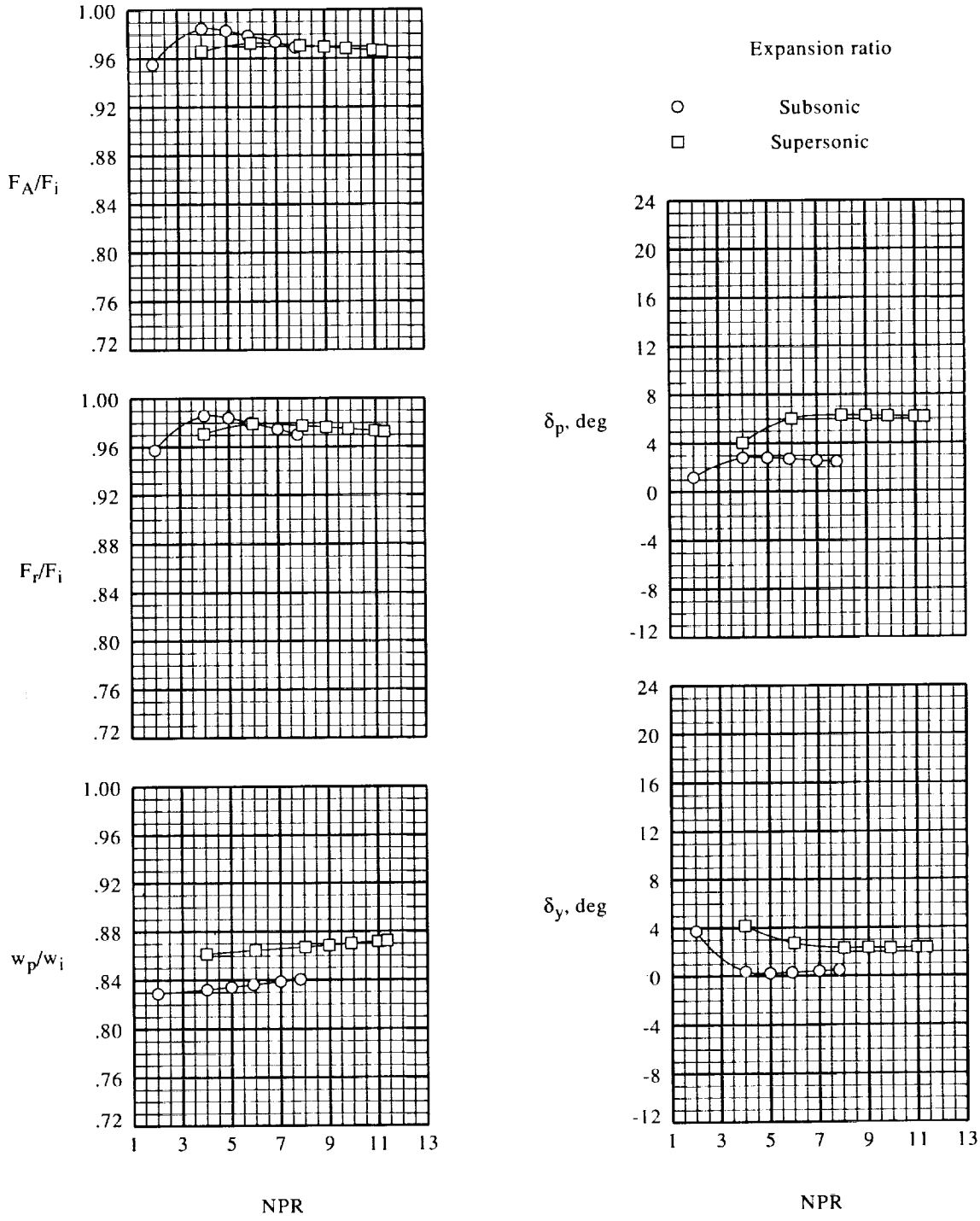

(a) $\delta_{v,p} = 0°$ and $\delta_{v,s} = 0°$.

Figure 15. Expansion ratio effect on internal performance. $\theta_{\text{skew}} = 35°$; AR = 1.748.

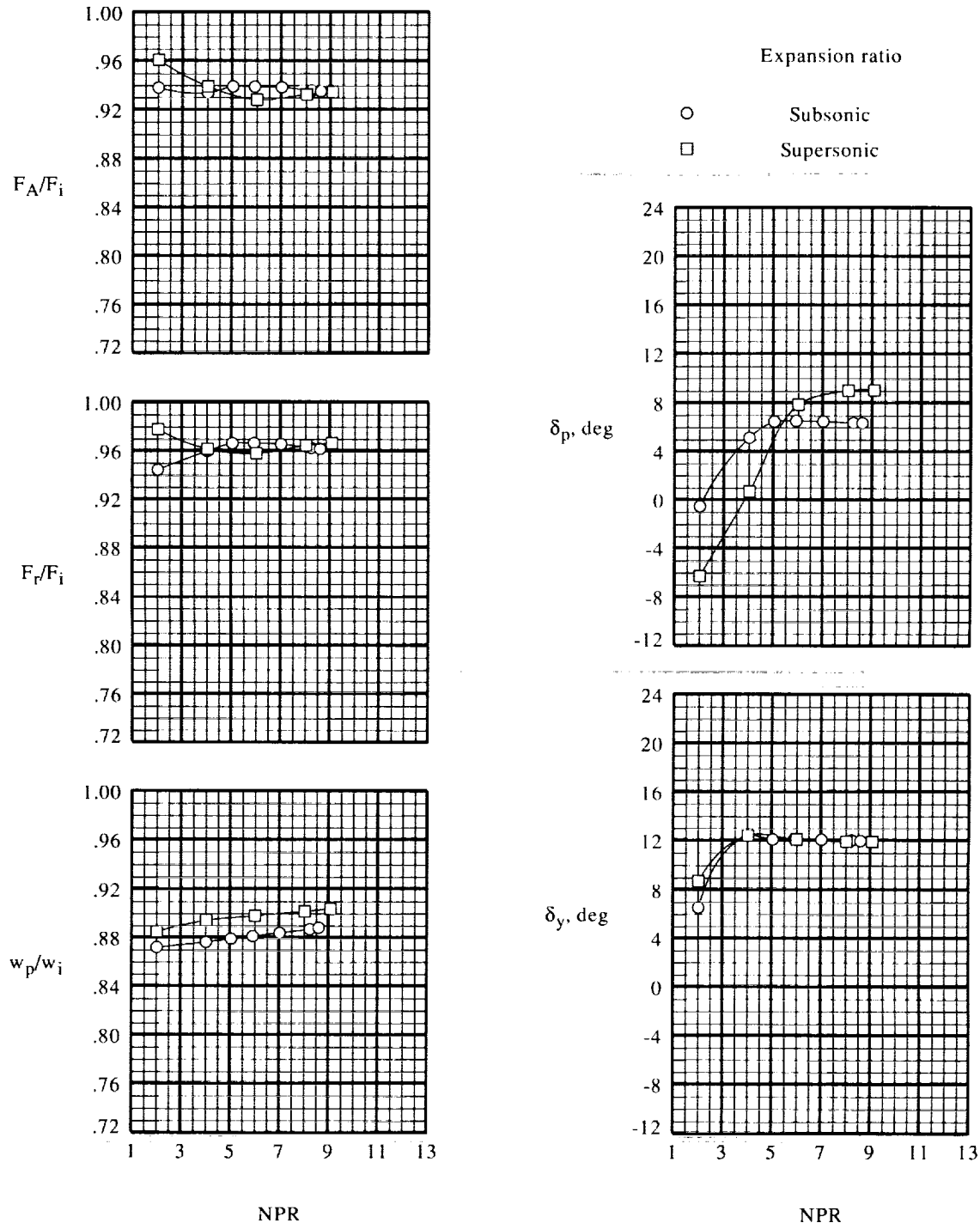

(b) $\delta_{v,p} = 0°$ and $\delta_{v,s} = 12°$.

Figure 15. Continued.

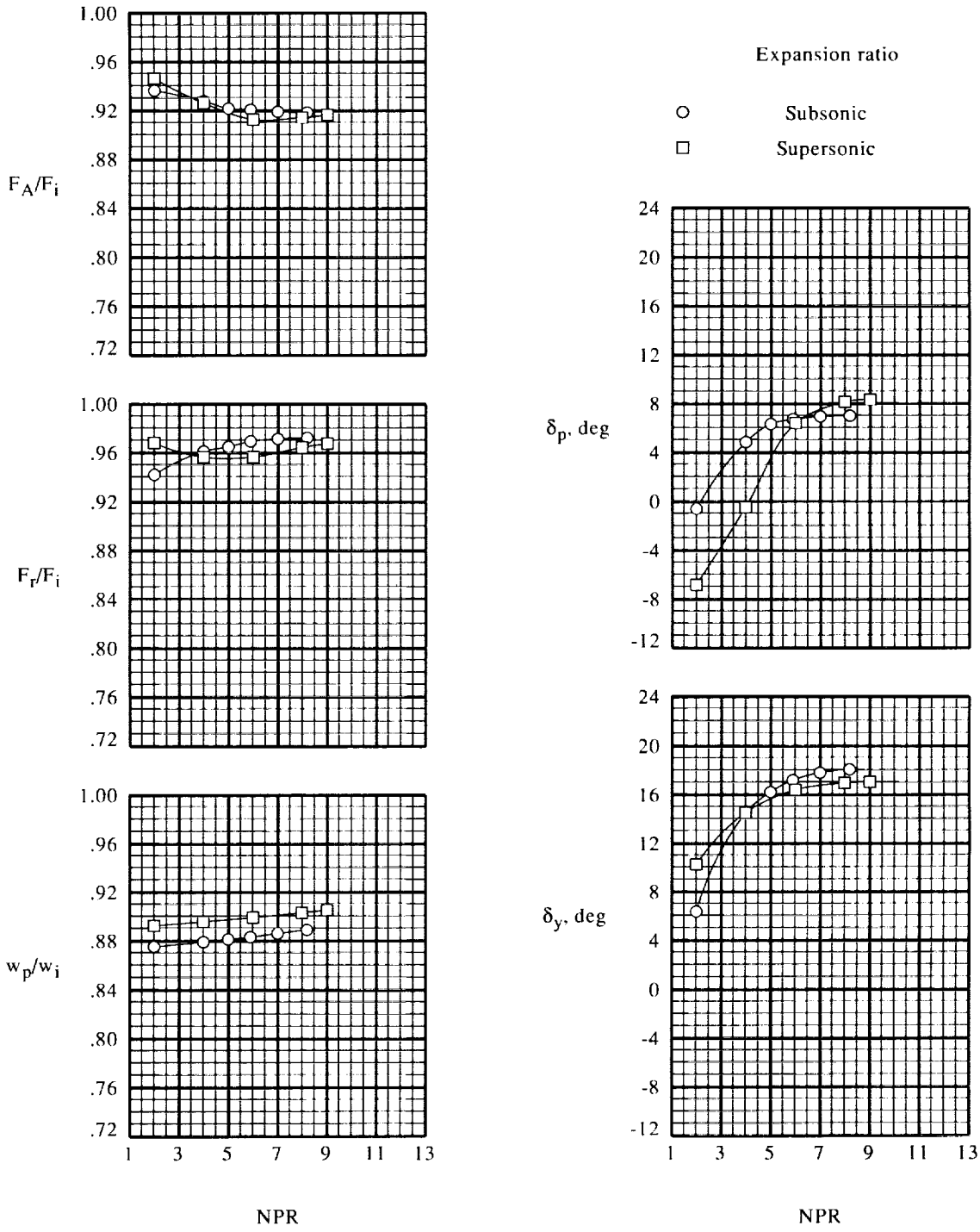

(c) $\delta_{v,p} = 0°$ and $\delta_{v,s} = 24°$.

Figure 15. Continued.

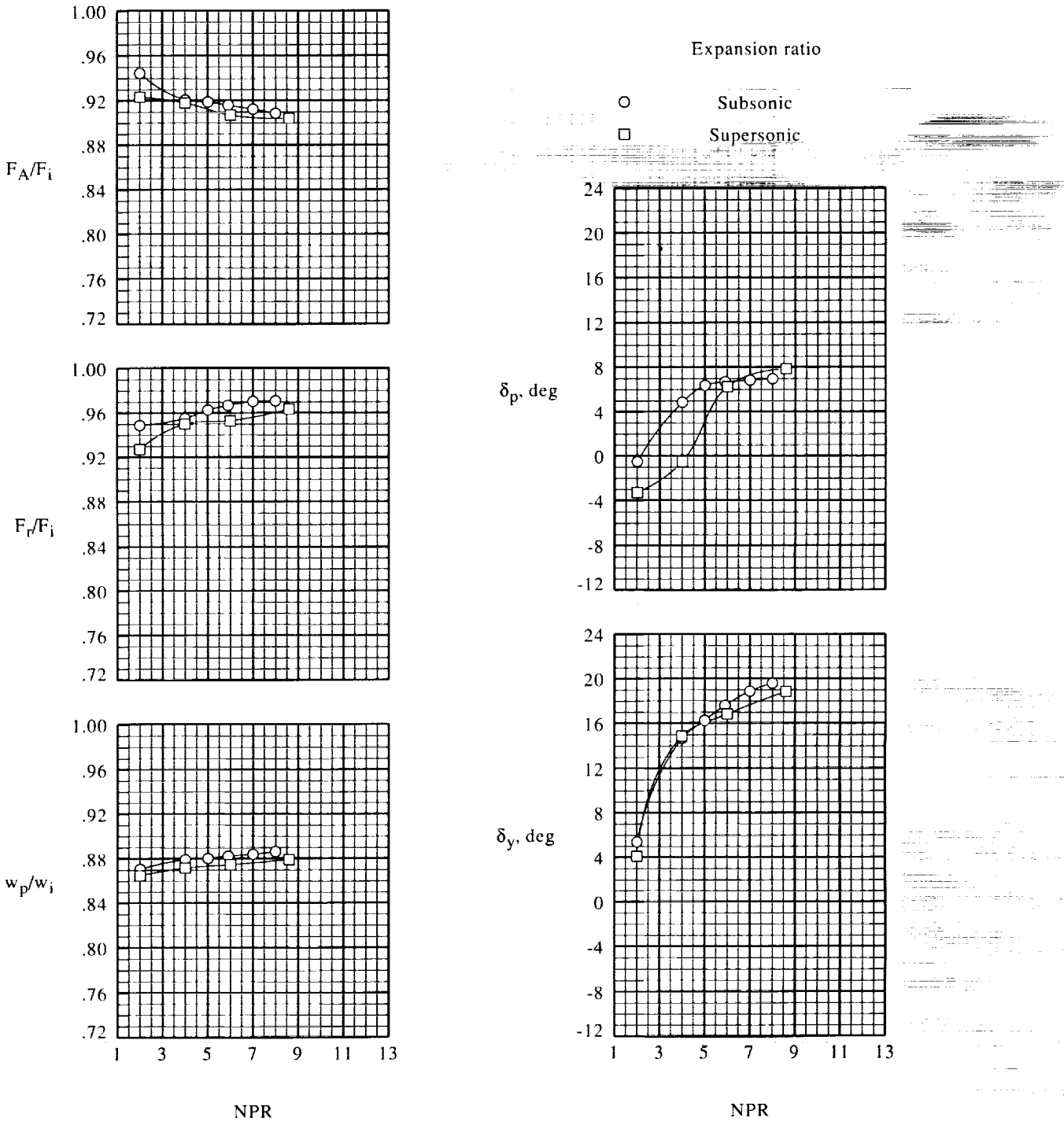

(d) $\delta_{v,p} = 0°$ and $\delta_{v,s} = 35°$.

Figure 15. Continued.

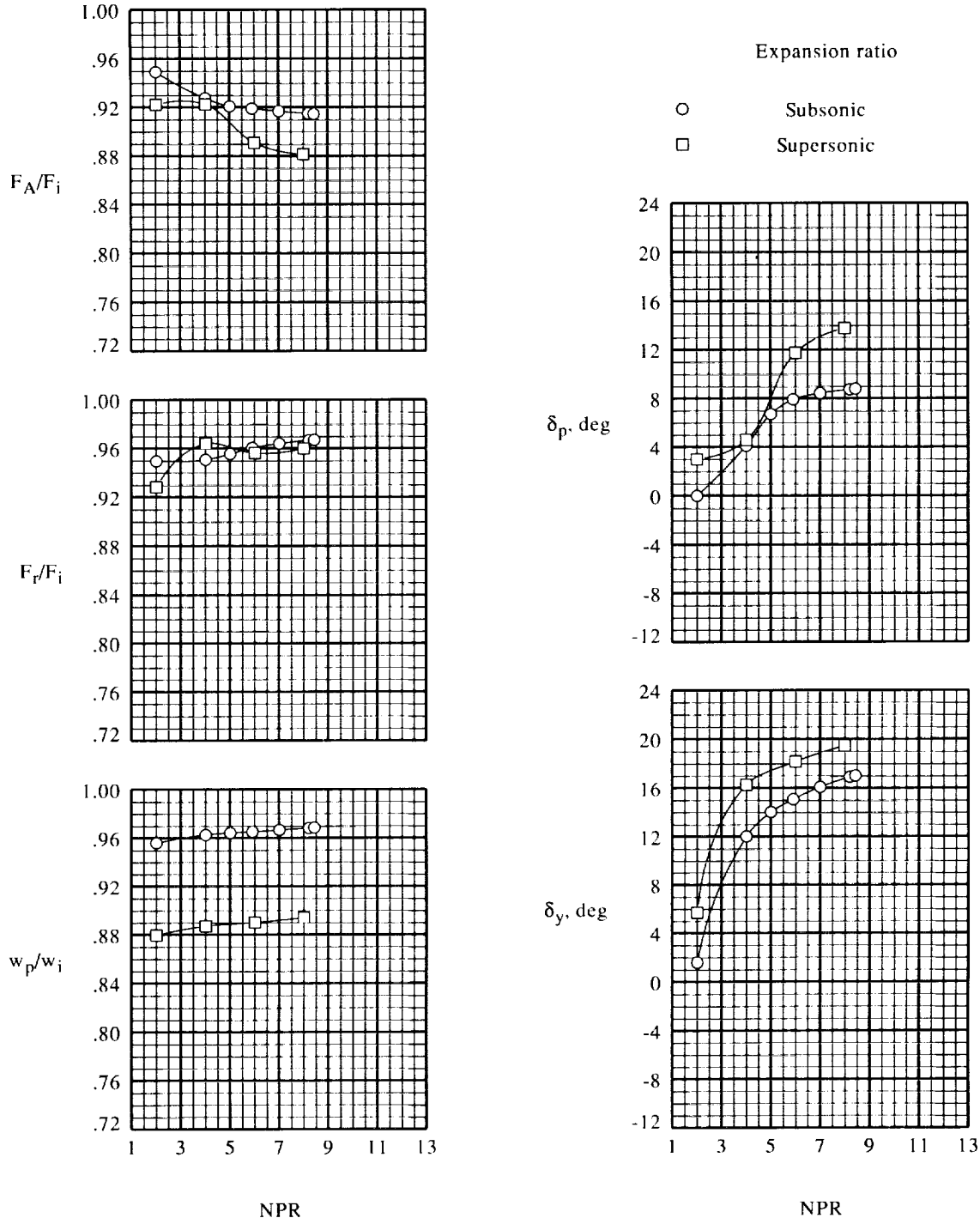

(e) $\delta_{v,p} = 7°$ and $\delta_{v,s} = 35°$.

Figure 15. Continued.

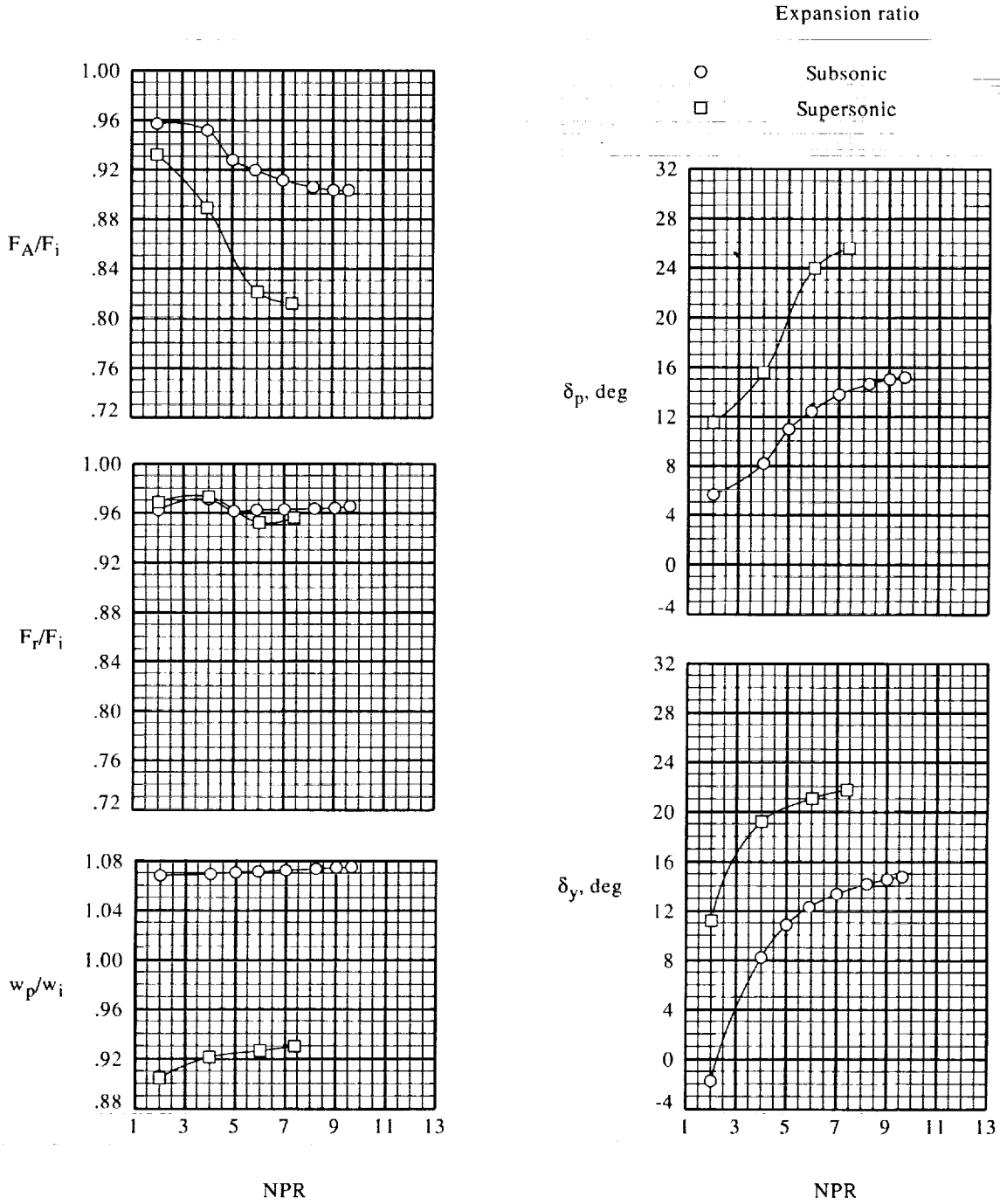

(f) $\delta_{v,p} = 20°$ and $\delta_{v,s} = 35°$.

Figure 15. Continued.

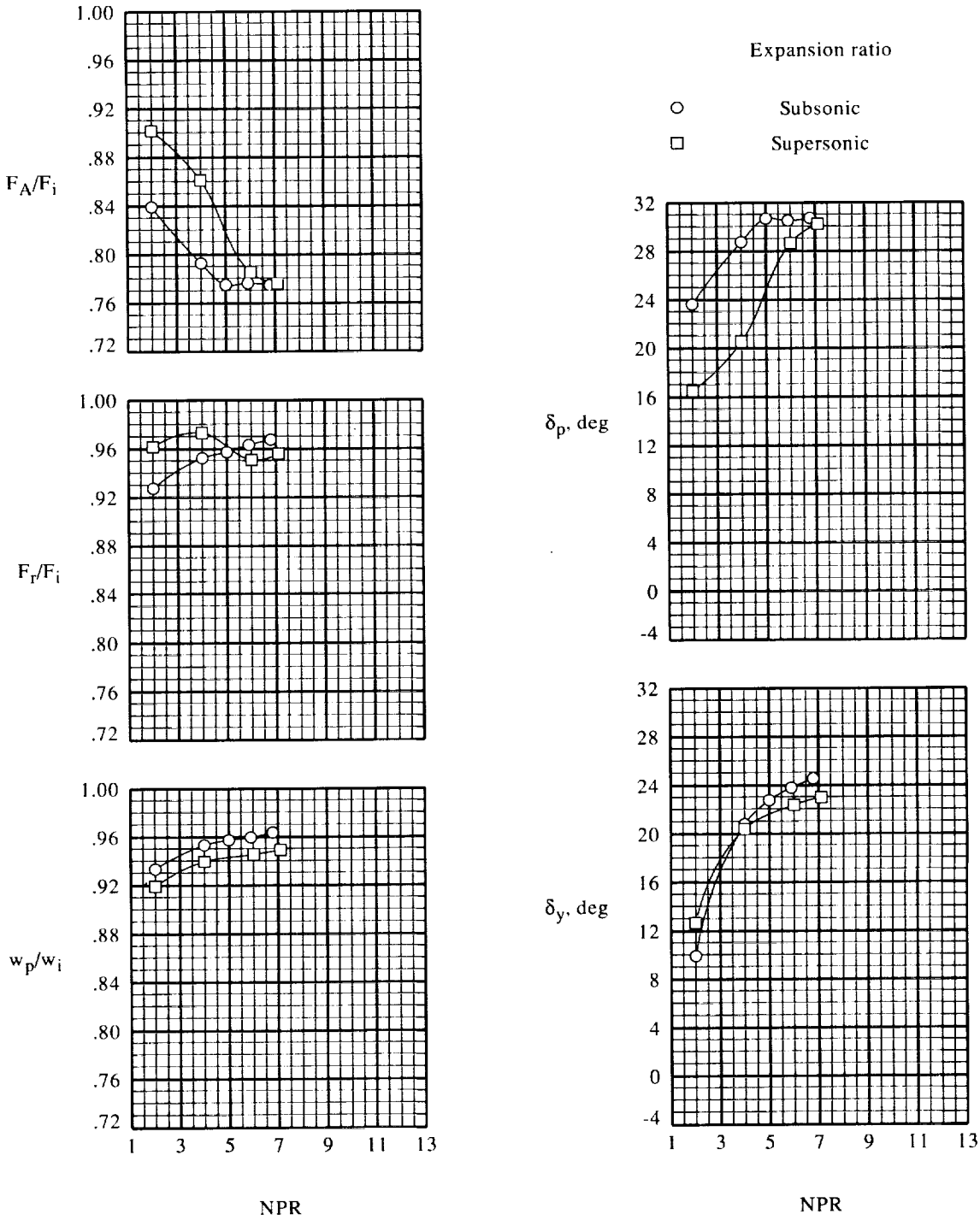

(g) $\delta_{v,p} = 25°$ and $\delta_{v,s} = 35°$.

Figure 15. Concluded.

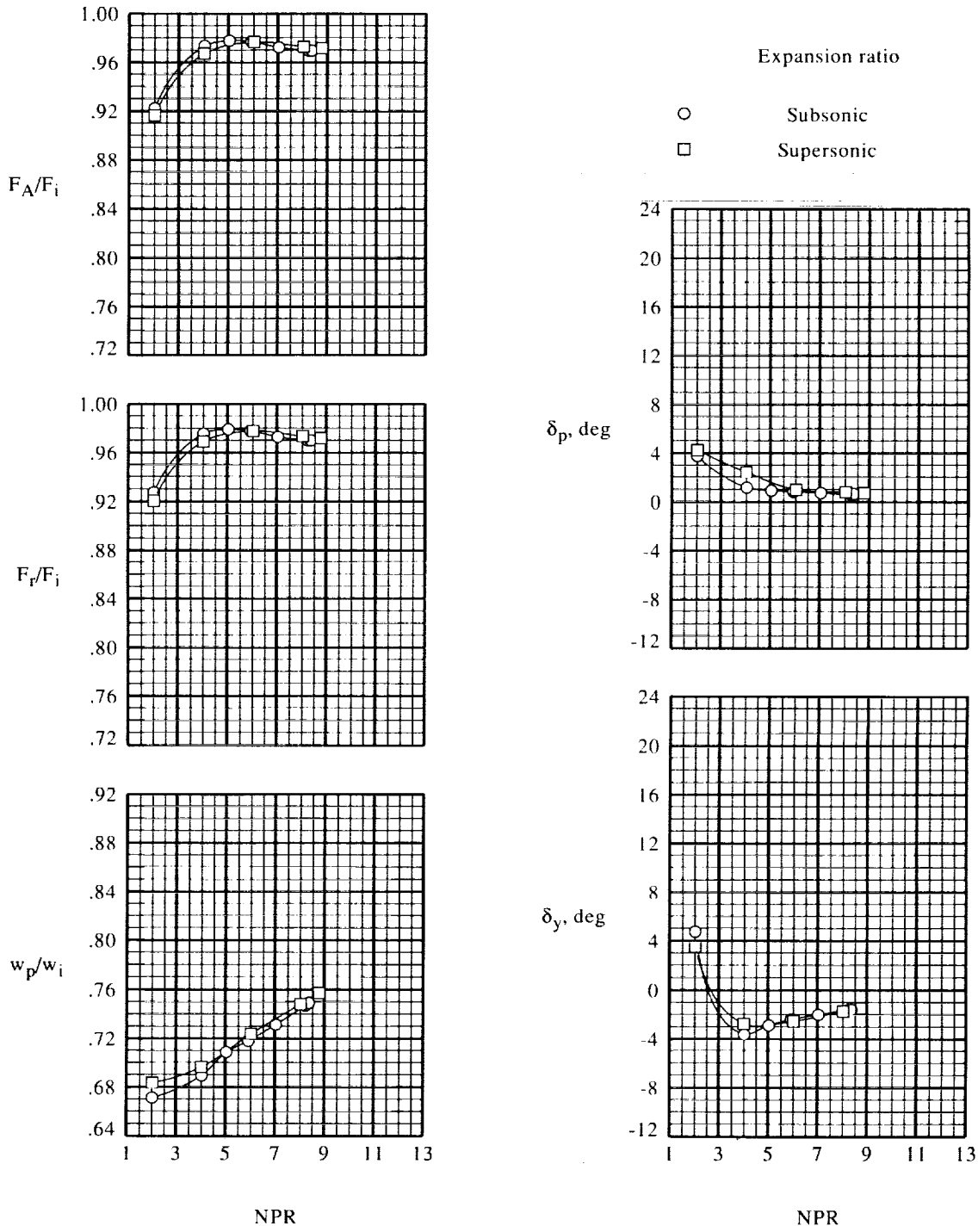

(a) $\delta_{v,p} = 0°$ and $\delta_{v,s} = 0°$.

Figure 16. Expansion ratio effect on internal performance. $\theta_{skew} = 50°$; AR = 1.748.

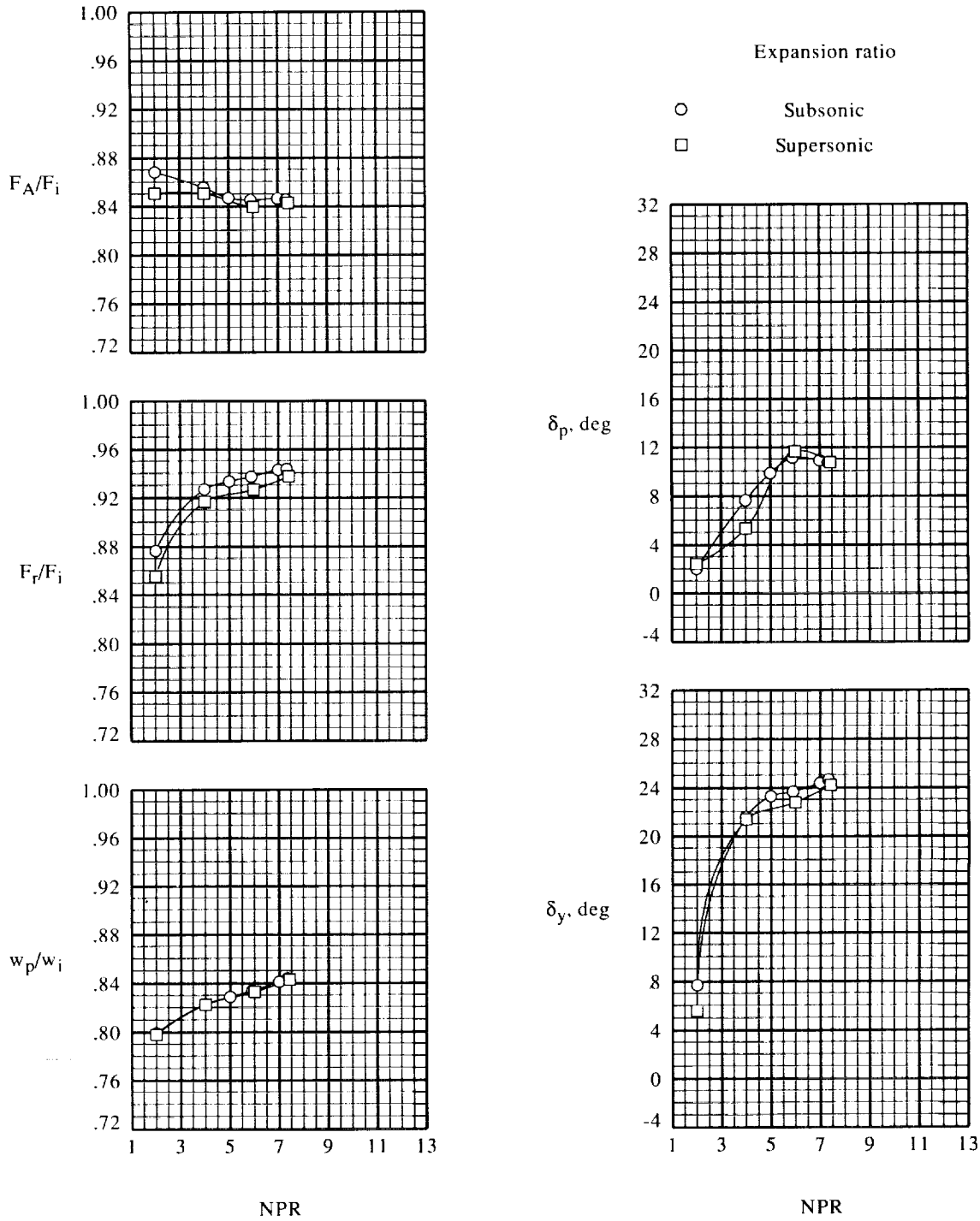

(b) $\delta_{v,p} = 0°$ and $\delta_{v,s} = 35°$.

Figure 16. Continued.

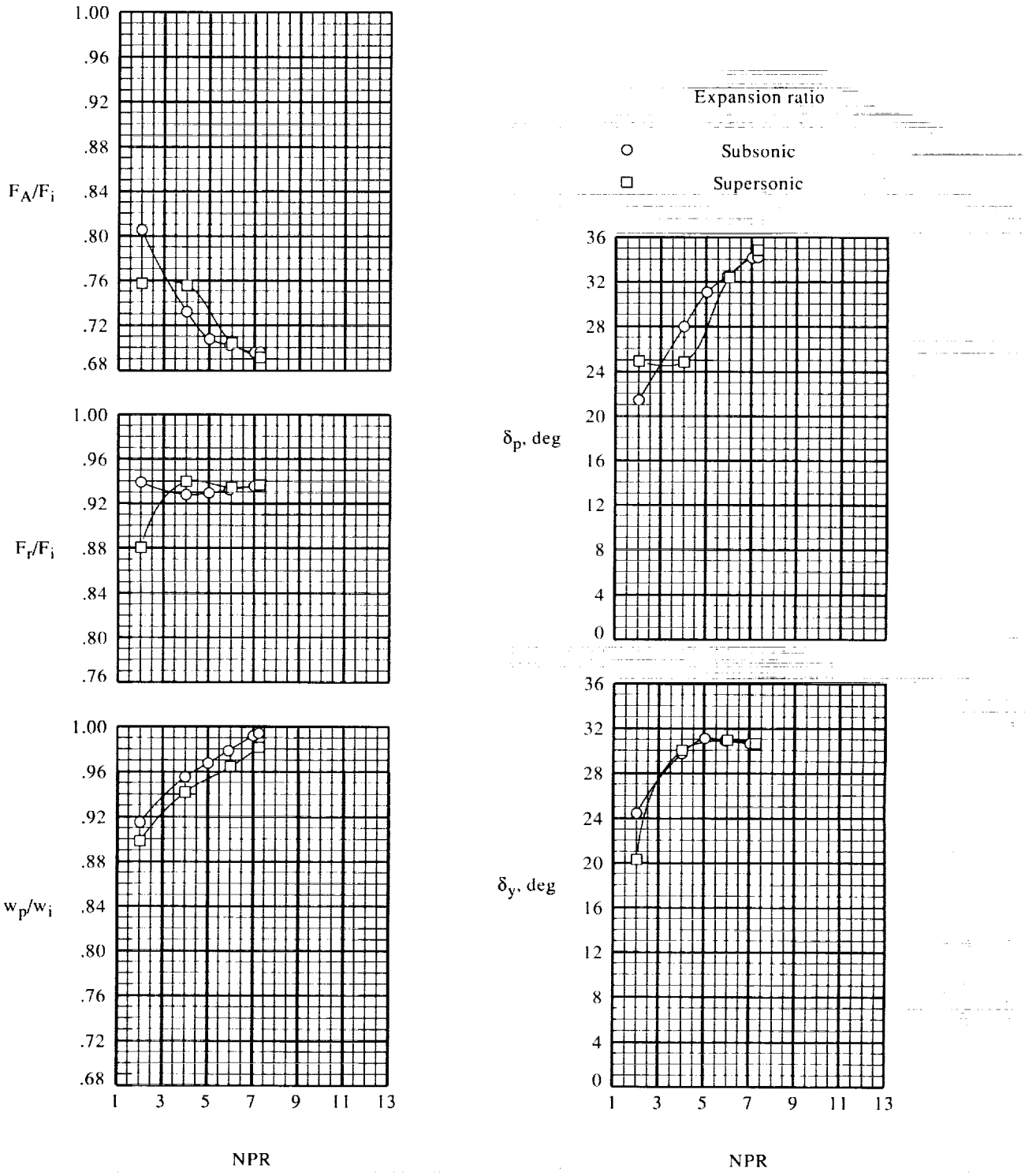

(c) $\delta_{v,p} = 25°$ and $\delta_{v,s} = 35°$.

Figure 16. Concluded.

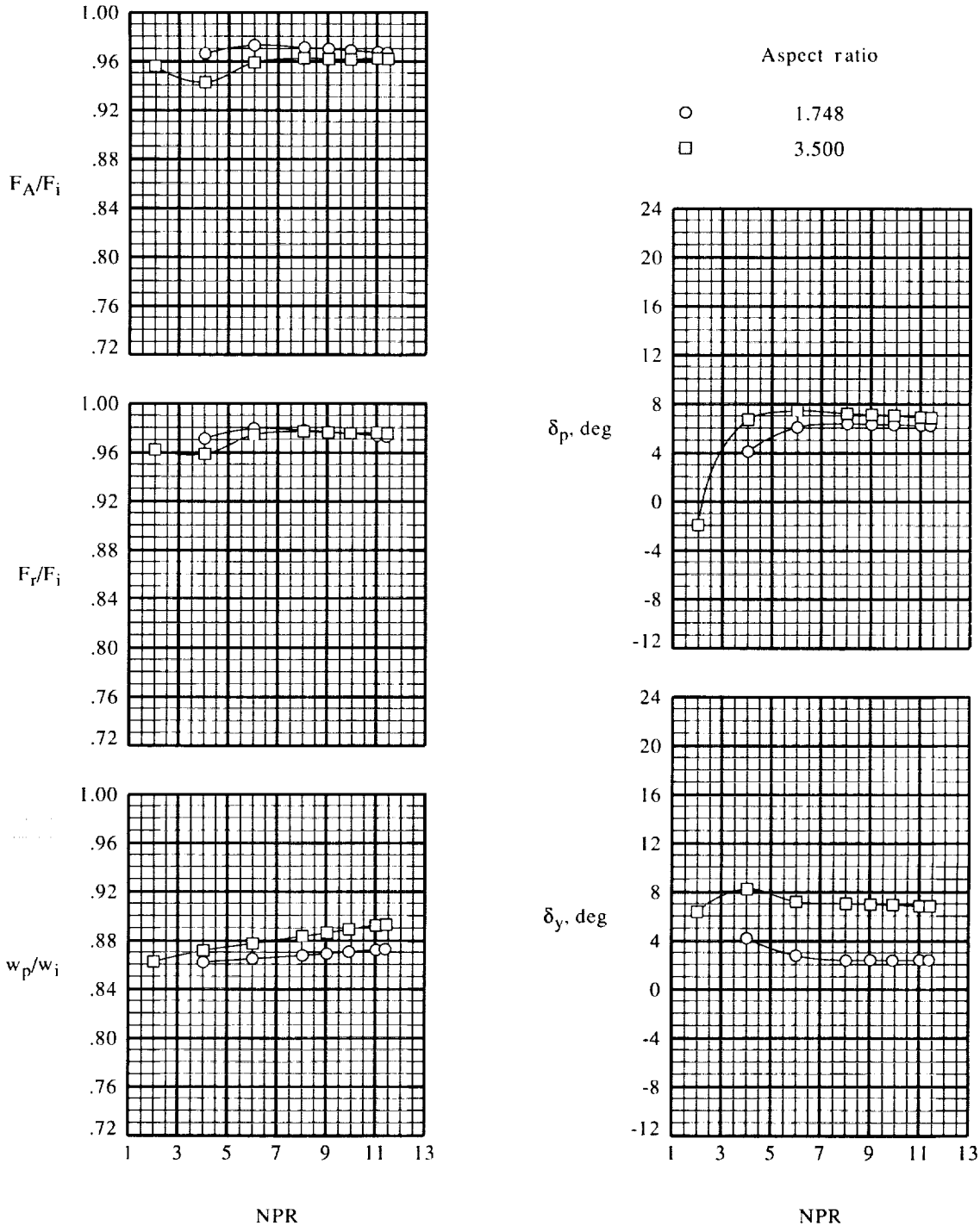

(a) $\delta_{v,p} = 0°$ and $\delta_{v,s} = 0°$.

Figure 17. Aspect ratio effect on internal performance. $\theta_{skew} = 35°$; supersonic expansion ratio.

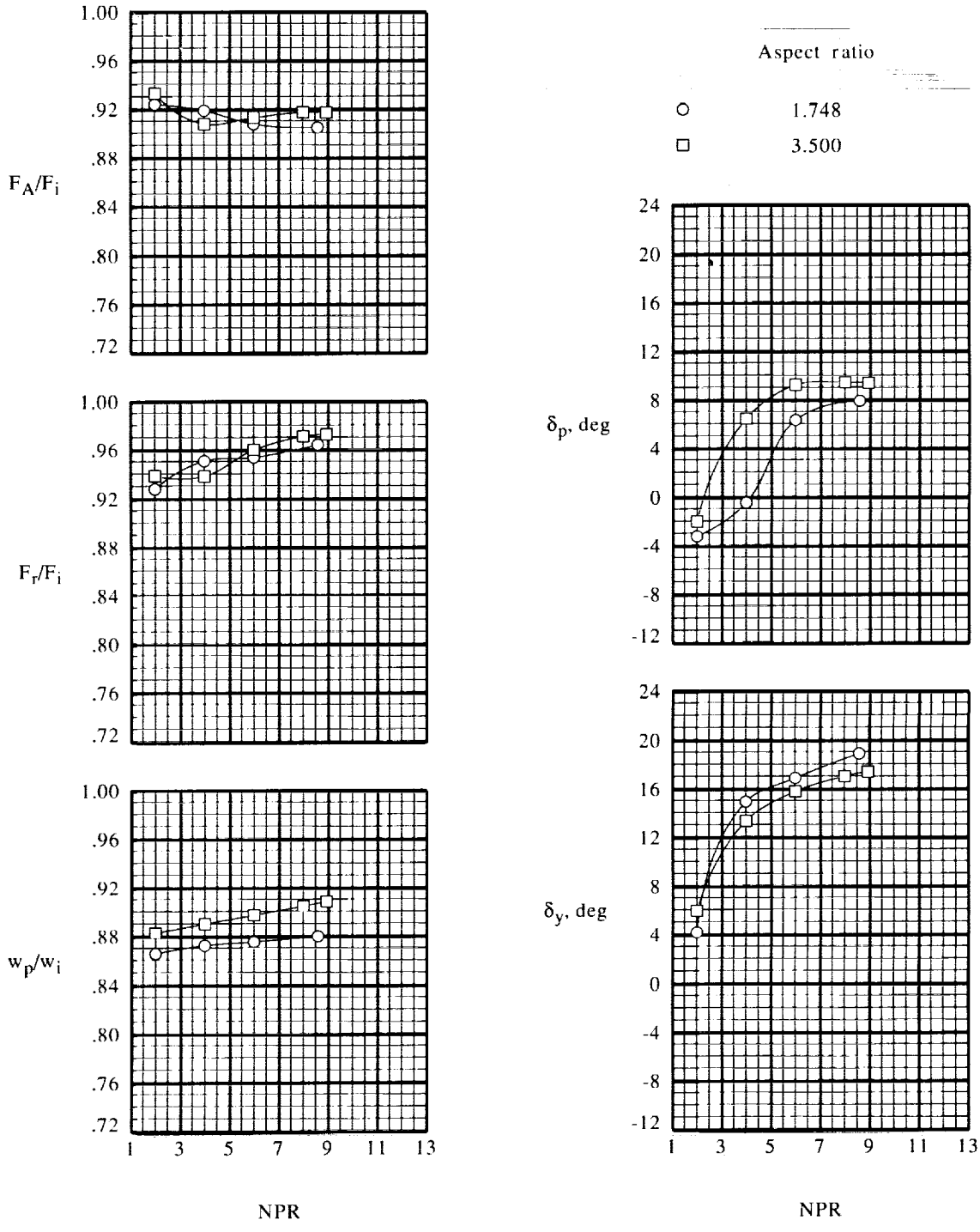

(b) $\delta_{v,p} = 0°$ and $\delta_{v,s} = 35°$.

Figure 17. Continued.

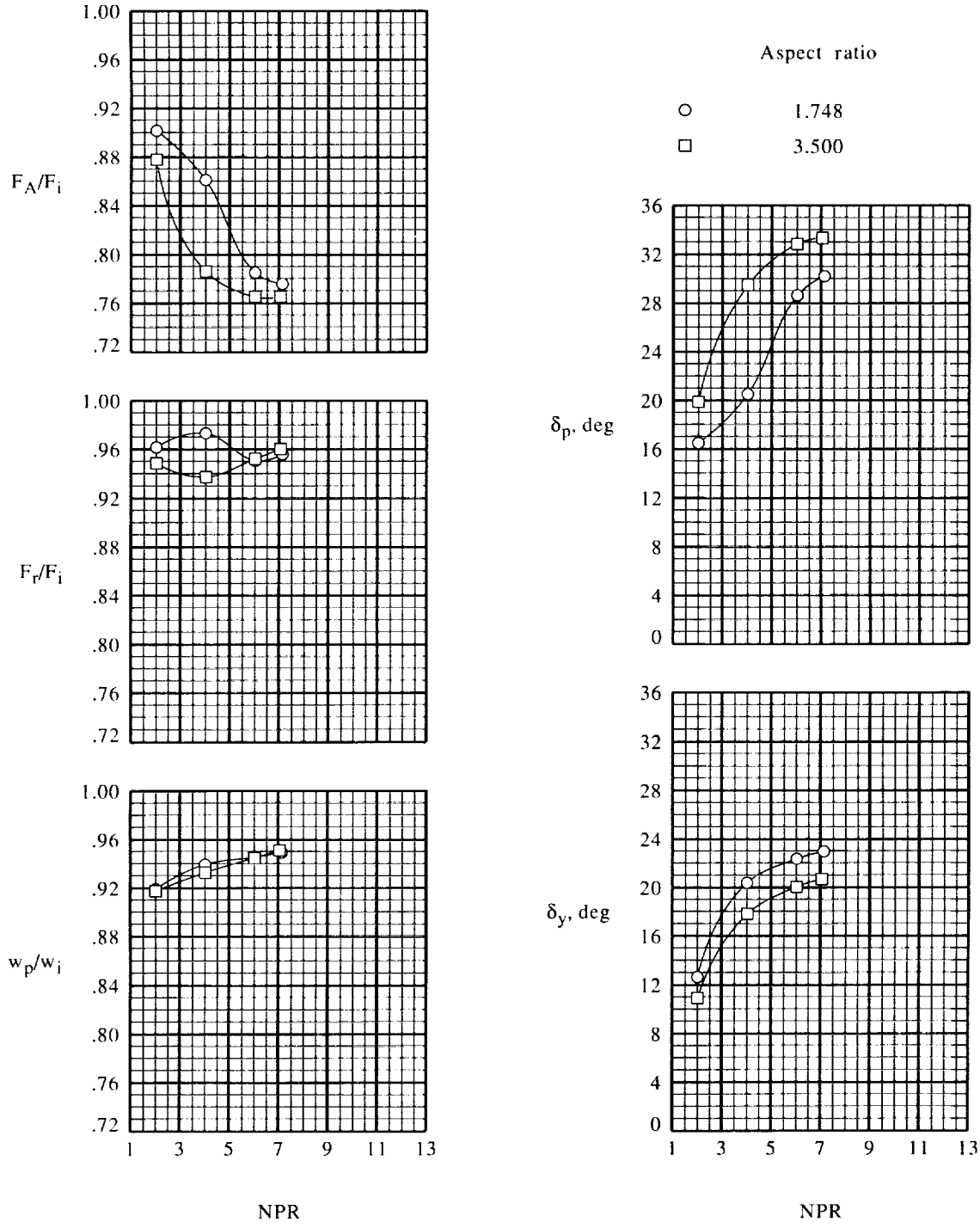

(c) $\delta_{v,p} = 25°$ and $\delta_{v,s} = 35°$.

Figure 17. Concluded.

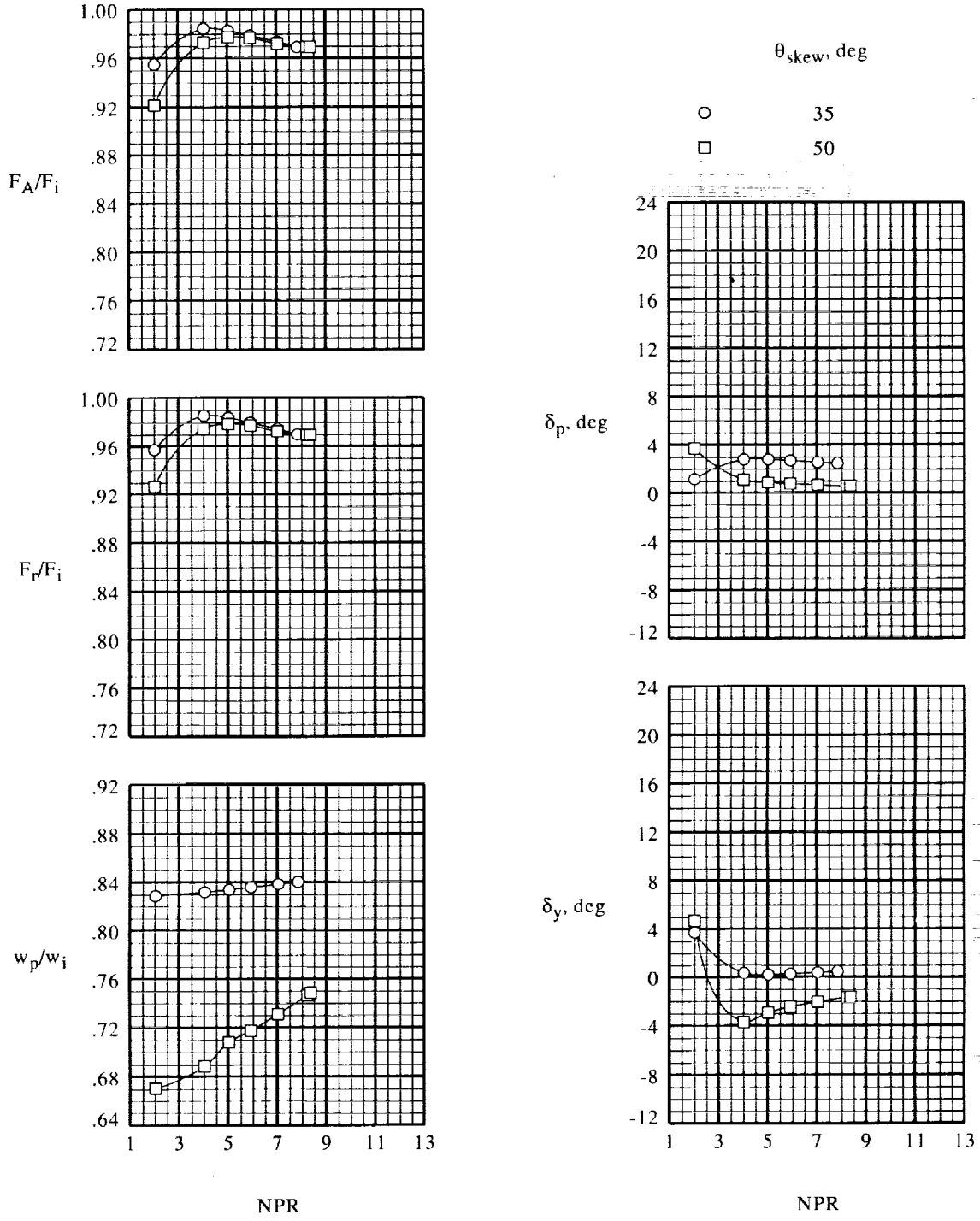

(a) $\delta_{v,p} = 0°$ and $\delta_{v,s} = 0°$.

Figure 18. Throat skew angle effect on internal performance. Subsonic expansion ratio; AR = 1.748.

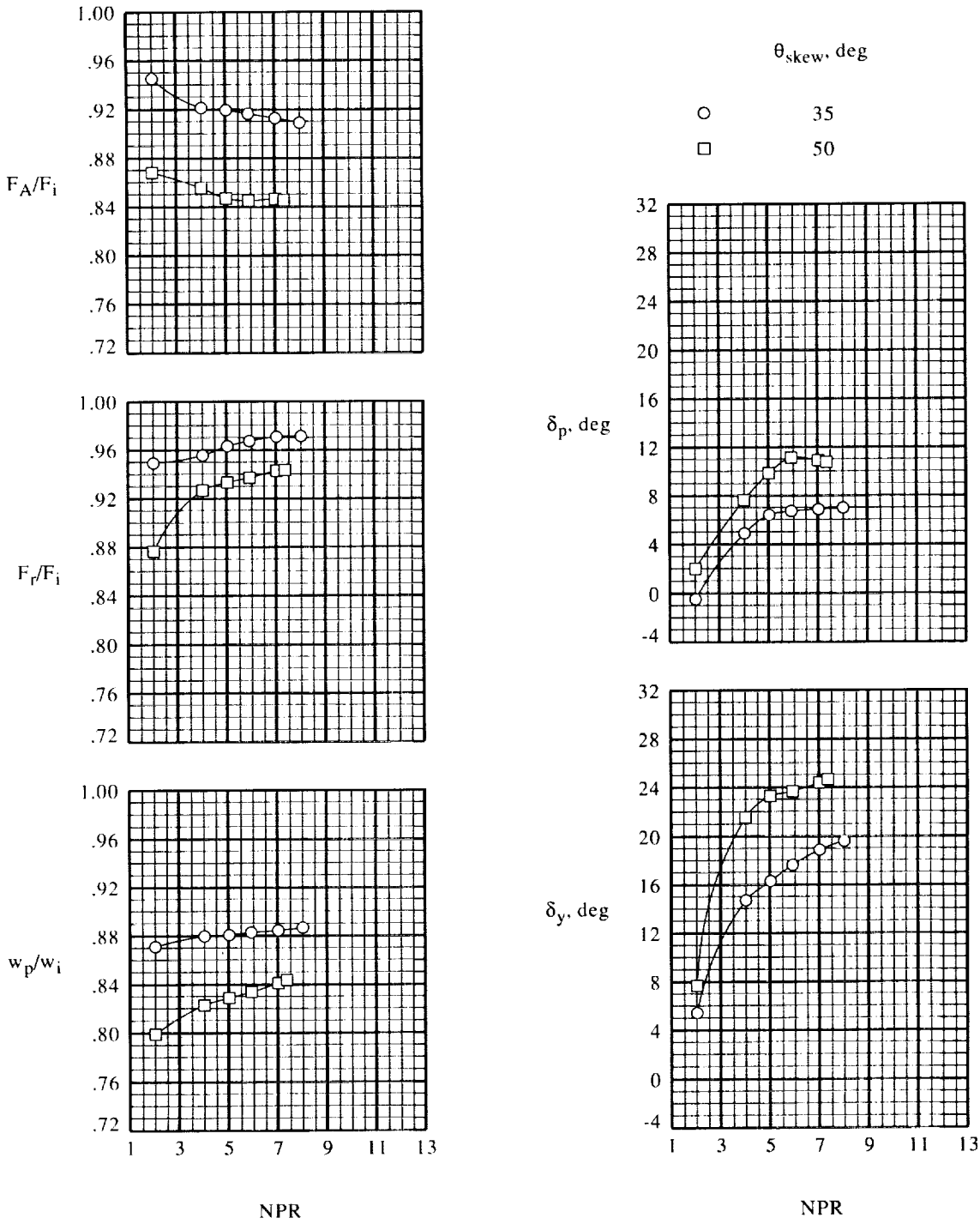

(b) $\delta_{v,p} = 0°$ and $\delta_{v,s} = 35°$.

Figure 18. Continued.

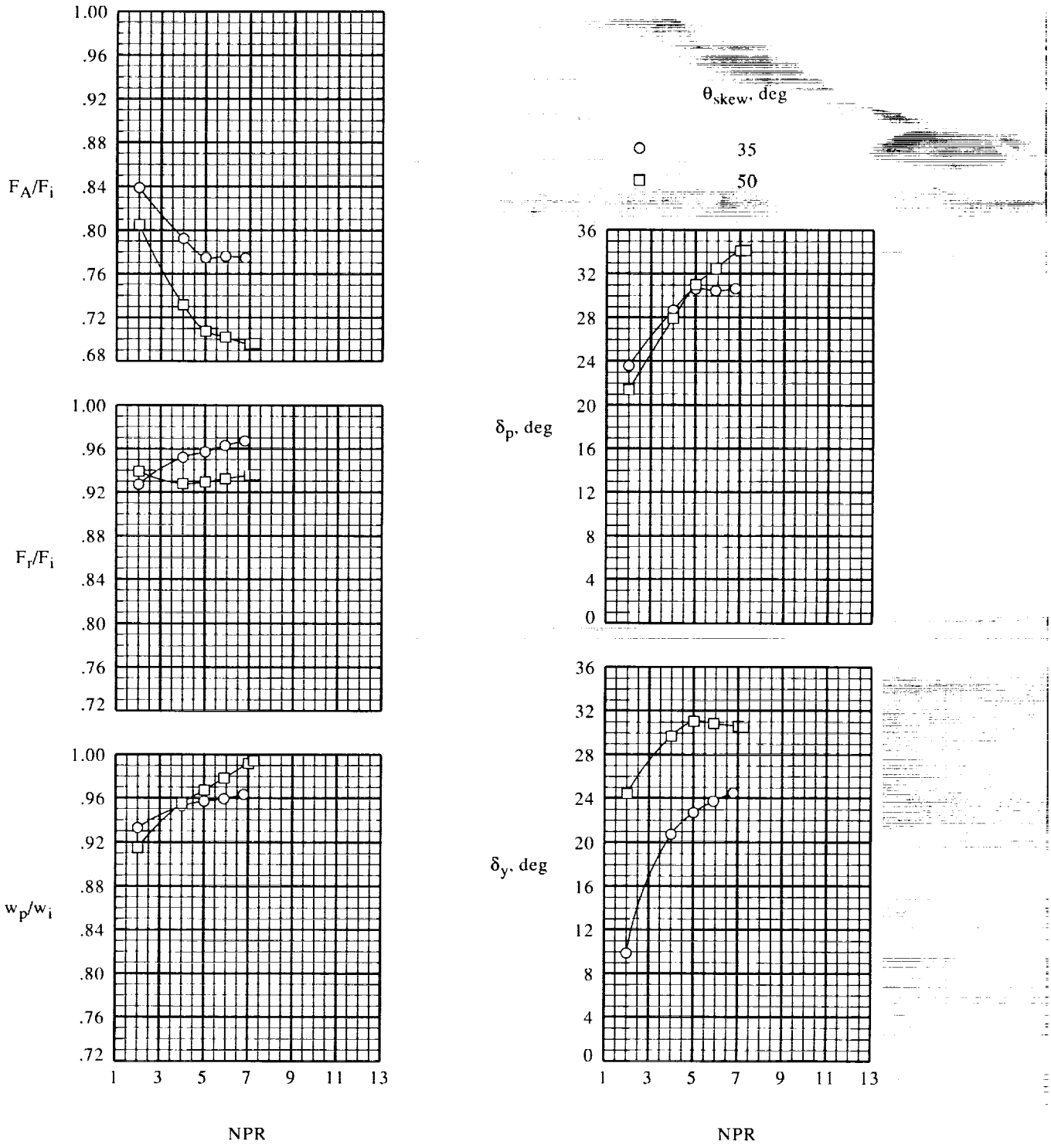

(c) $\delta_{v,p} = 25°$ and $\delta_{v,s} = 35°$.

Figure 18. Concluded.

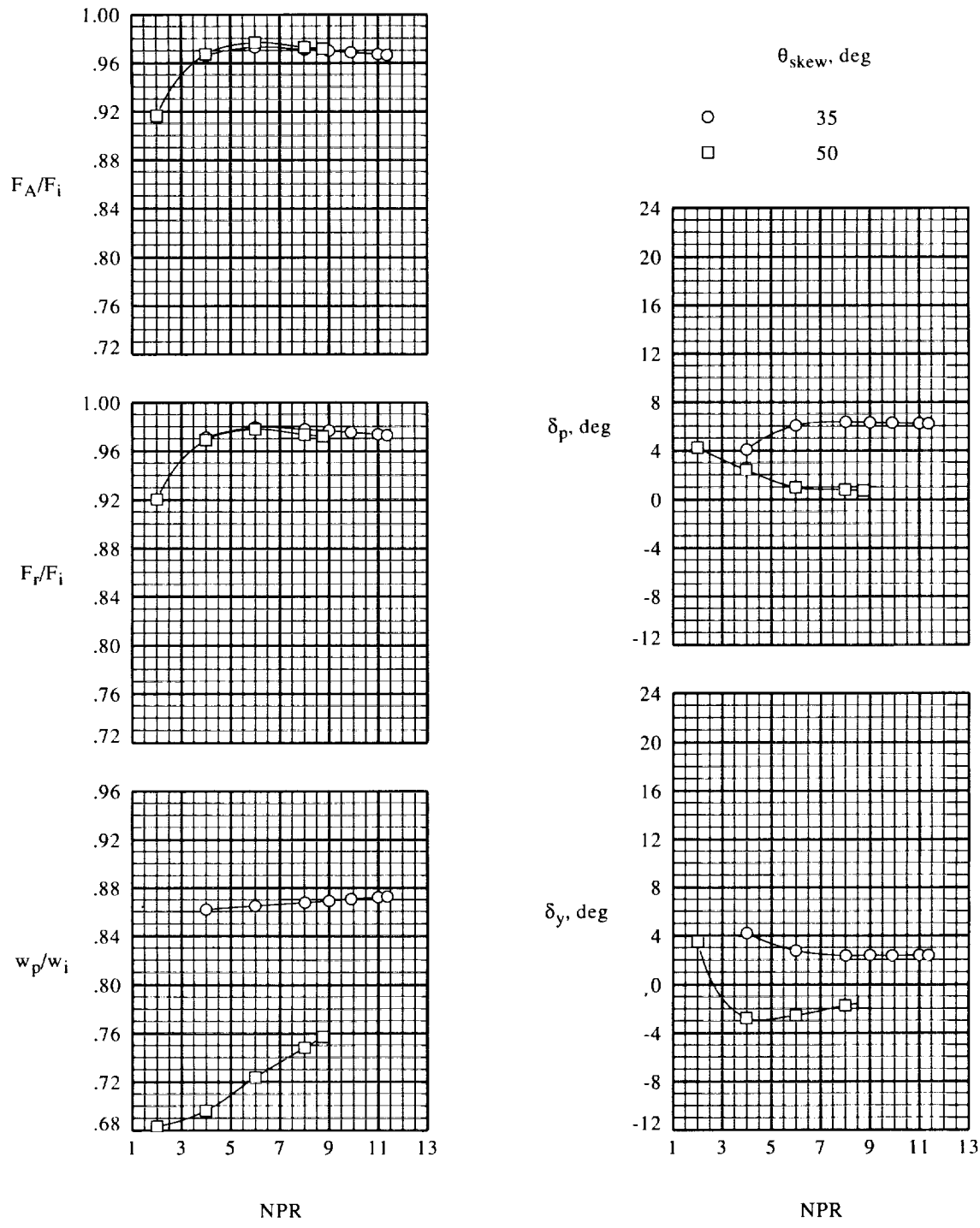

(a) $\delta_{v,p} = 0°$ and $\delta_{v,s} = 0°$.

Figure 19. Throat skew angle effect on internal performance. Supersonic expansion ratio; AR = 1.748.

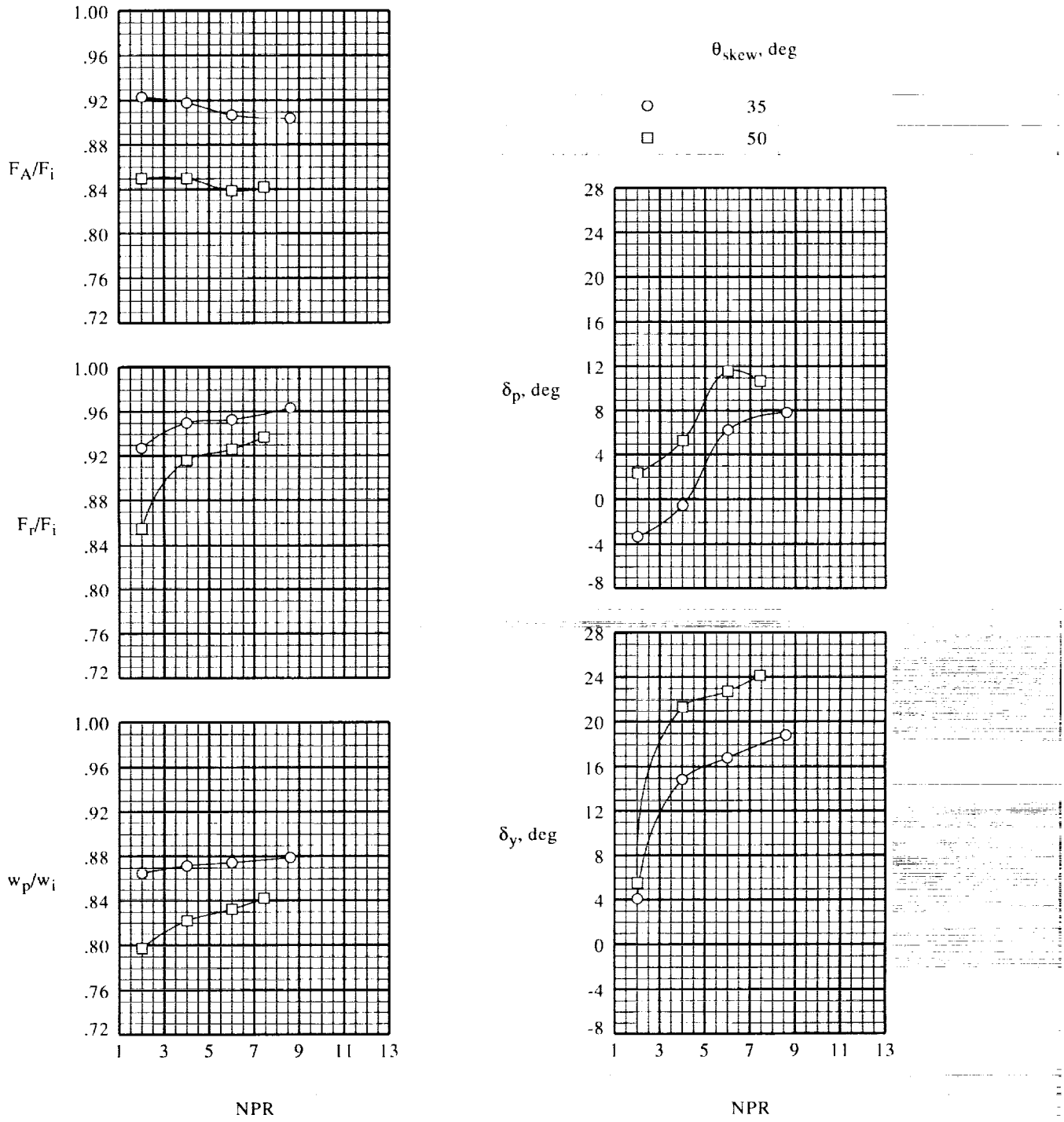

(b) $\delta_{v,p} = 0°$ and $\delta_{v,s} = 35°$.

Figure 19. Continued.

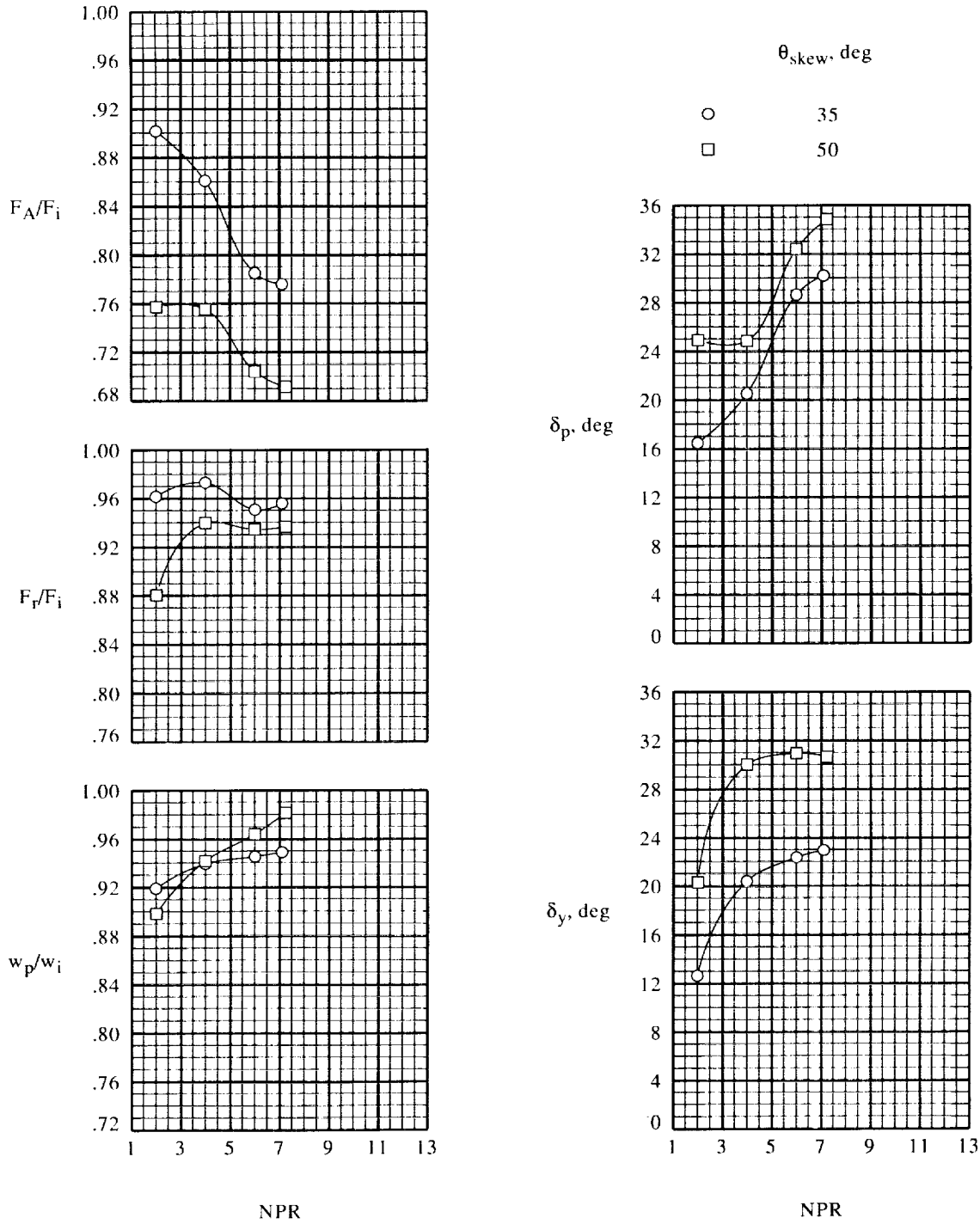

(c) $\delta_{v,p} = 25°$ and $\delta_{v,s} = 35°$.

Figure 19. Concluded.

REPORT DOCUMENTATION PAGE

Form Approved
OMB No. 0704-0188

1. AGENCY USE ONLY *(Leave blank)*	2. REPORT DATE	3. REPORT TYPE AND DATES COVERED
	April 1994	Technical Paper

4. TITLE AND SUBTITLE
Static Performance Investigation of a Skewed-Throat Multiaxis Thrust-Vectoring Nozzle Concept

5. FUNDING NUMBERS
WU 505-62-30-01

6. AUTHOR(S)
David J. Wing

7. PERFORMING ORGANIZATION NAME(S) AND ADDRESS(ES)
NASA Langley Research Center
Hampton, VA 23681-0001

8. PERFORMING ORGANIZATION REPORT NUMBER
L-17271

9. SPONSORING/MONITORING AGENCY NAME(S) AND ADDRESS(ES)
National Aeronautics and Space Administration
Washington, DC 20546-0001

10. SPONSORING/MONITORING AGENCY REPORT NUMBER
NASA TP-3411

11. SUPPLEMENTARY NOTES

12a. DISTRIBUTION/AVAILABILITY STATEMENT
Unclassified Unlimited

Subject Category 02

12b. DISTRIBUTION CODE

13. ABSTRACT *(Maximum 200 words)*

The static performance of a jet exhaust nozzle which achieves multiaxis thrust vectoring by physically skewing the geometric throat has been characterized in the static test facility of the 16-Foot Transonic Tunnel at NASA Langley Research Center. The nozzle has an asymmetric internal geometry defined by four surfaces: a convergent-divergent upper surface with its ridge perpendicular to the nozzle centerline, a convergent-divergent lower surface with its ridge skewed relative to the nozzle centerline, an outwardly deflected sidewall, and a straight sidewall. The primary goal of the concept is to provide efficient yaw thrust vectoring by forcing the sonic plane (nozzle throat) to form at a yaw angle defined by the skewed ridge of the lower surface contour. A secondary goal is to provide multiaxis thrust vectoring by combining the skewed-throat yaw-vectoring concept with upper and lower pitch flap deflections. The geometric parameters varied in this investigation included lower surface ridge skew angle, nozzle expansion ratio (divergence angle), aspect ratio, pitch flap deflection angle, and sidewall deflection angle. Nozzle pressure ratio was varied from 2 to a high of 11.5 for some configurations. The results of the investigation indicate that efficient, substantial multiaxis thrust vectoring was achieved by the skewed-throat nozzle concept. However, certain control surface deflections destabilized the internal flow field, which resulted in substantial shifts in the position and orientation of the sonic plane and had an adverse effect on thrust-vectoring and weight flow characteristics. By increasing the expansion ratio, the location of the sonic plane was stabilized. The asymmetric design resulted in interdependent pitch and yaw thrust vectoring as well as nonzero thrust-vector angles with undeflected control surfaces. By skewing the ridges of both the upper and lower surface contours, the interdependency between pitch and yaw thrust vectoring may be eliminated and the location of the sonic plane may be further stabilized.

14. SUBJECT TERMS	15. NUMBER OF PAGES
Nozzle; Thrust vectoring; Multiaxis thrust vectoring; Skewed throat	124
	16. PRICE CODE: A06

17. SECURITY CLASSIFICATION OF REPORT	18. SECURITY CLASSIFICATION OF THIS PAGE	19. SECURITY CLASSIFICATION OF ABSTRACT	20. LIMITATION OF ABSTRACT
Unclassified	Unclassified	Unclassified	

NSN 7540-01-280-5500

Standard Form 298(Rev. 2-89)
Prescribed by ANSI Std. Z39-18
298-102

National Aeronautics and
Space Administration
Langley Research Center
Mail Code 180
Hampton, VA 23681-00001

SPECIAL FOURTH-CLASS RATE
POSTAGE & FEES PAID
NASA
Permit No. G-27